

UNCLASSIFIED

AD NUMBER
AD839480
NEW LIMITATION CHANGE
TO Approved for public release, distribution unlimited
FROM Distribution authorized to U.S. Gov't. agencies and their contractors; Administrative/Operational Use; May 1968. Other requests shall be referred to Air Force Materials Laboratory, Attn: MAAE, Wright-Patterson AFB, OH 45433.
AUTHORITY
AFSC/USAF ltr, 2 Mar 1972

THIS PAGE IS UNCLASSIFIED

AD 339480

AFML-TR-68-126

DEVELOPMENT OF THICK-WALL, FILAMENT-WOUND,  
HIGH-PRESSURE CONTAINERS

Ralph Molho and Robert E. Landes

Aerojet-General Corporation

TECHNICAL REPORT AFML-TR-68-126

May 1968

This document is subject to special export controls and each transmittal to foreign governments or foreign nationals may be made only with prior approval of the Air Force Materials Laboratory (MAAE), Wright-Patterson Air Force Base, Ohio 45433.

Air Force Materials Laboratory  
Air Force Systems Command  
Wright-Patterson Air Force Base, Ohio

001

157

## NOTICES

When Government drawings, specifications, or other data are used for any purpose other than in connection with a definitely related Government procurement operation, the United States Government thereby incurs no responsibility nor any obligation whatsoever; and the fact that the Government may have formulated, furnished, or in any way supplied the said drawings, specifications, or other data, is not to be regarded by implication or otherwise as in any manner licensing the holder or any other person or corporation, or conveying any rights or permission to manufacture, use, or sell any patented invention that may in any way be related thereto.

This document is subject to special export controls and each transmittal to foreign governments or foreign nationals may be made only with prior approval of the Air Force Materials Laboratory (MAAE), Wright-Patterson Air Force Base, Ohio 45433.

Copies of this report should not be returned unless return is required by security considerations, contractual obligations, or notice on a specific document.

J

2

AFML-TR-68-126

DEVELOPMENT OF THICK-WALL, FILAMENT-WOUND,  
HIGH-PRESSURE CONTAINERS

Ralph Molho and Robert E. Landes

This document is subject to special export controls and each transmittal to foreign governments or foreign nationals may be made only with prior approval of the Air Force Materials Laboratory (MAAE), Wright-Patterson Air Force Base, Ohio 45433.

## FOREWORD

This report was prepared by the Structural Products Department, Electronics Division of the Aerojet-General Corporation, Azusa, California, under USAF Contract No. AF 33(615)-3995. The contract was initiated under Project No. 7381 (Materials Evaluation), Task No. 738101 (Exploratory Design and Prototype Development), and BPSN No. 66 (687381-738101-62405514). The work was administered under the direction of the Air Force Materials Laboratory, with Mr. T. J. Reinhart, Jr. (MAAF). as Project Engineer.

This report is submitted in fulfillment of the contract and covers all work conducted between June 1966 and March 1968. The report was submitted by the authors in April 1968 for publication as a technical report and is catalogued by Aerojet-General as Report No. 3532.

W. T. Cox, Manager of the Structural Products Department, provided technical direction. The program was conducted by personnel from the Composites Engineering Section - initiated under S. B. Fabeck, and concluded under D. F. Fernandez, Section Managers. Assisting in the program were F. J. Darms and E. E. Morris, heads of the Advanced Composites and Composite Tankage Groups, respectively. Phases I and II, and the initial work of Phase III, were managed by R. D. Saunders. The latter portion of Phase III was managed by R. Molho. R. E. Landes and F. J. Darms performed the analytical study. R. D. Saunders and F. J. Darms conducted the structural design of the thick-wall composite vessel.

Special acknowledgment is due to N. R. Dunavant, P. B. Guhl, A. Taoyama, and P. A. McDonald for their assistance in the areas of fabrication and test. The technical illustrations were prepared by R. J. Hilgaertner.

This technical report has been reviewed and is approved.

*Albert Olevitch*  
ALBERT OLEVITCH, Chief  
Materials Engineering Branch  
Materials Application Division  
Air Force Materials Laboratory

## ABSTRACT

Thick-wall, glass-filament-wound, high-pressure containers with thin-metal liners were investigated analytically and experimentally. An analysis adapting thin-wall theory to a multilayered thick-wall vessel was developed and programmed on the computer. Comparisons to select the most efficient configuration, and evaluation of materials and processing techniques preceded the sequential fabrication and testing of sixteen 12-in.-dia prototype vessels designed to operate at a working pressure of 15,000 psi. Results indicate that mismatch of strains, and relative movement between the rigid thick-metal boss and the overwrapped composite, caused strain magnification in the transition area between the boss and liner. This condition developed because of the need to maintain overall strain compatibility between the filaments and metal structure and was the principal factor contributing to premature vessel failure. Tests indicated that improvements in the structure could be achieved by (a) applying the fibers at high winding tensions, (b) increasing the payoff tape width, and (c) using glass-reinforcement tapes to optimize the contour. Studies were also conducted on improving the internal supporting mandrel material and increasing the adhesive bond strength between the liner and composite structure. Continued studies are recommended in these areas and in thick-wall composite structures with load-bearing, non-buckling liners.

TABLE OF CONTENTS

	PAGE
I. INTRODUCTION . . . . .	1
1. Background . . . . .	1
2. Program Plan . . . . .	3
II. SUMMARY . . . . .	5
III. ANALYTICAL METHODS (PHASE I) . . . . .	6
1. Analysis . . . . .	6
2. Computer Program . . . . .	6
3. Parametric Study . . . . .	7
IV. PRESSURE-VESSEL DESIGN (PHASE II) . . . . .	20
1. Criteria . . . . .	20
2. Configuration . . . . .	20
3. Materials . . . . .	20
V. PRESSURE-VESSEL FABRICATION AND TESTING (PHASE III) . . . . .	33
1. Metal Liner . . . . .	33
2. Filament Winding . . . . .	38
a. Fabrication Over Wood Mandrel . . . . .	47
b. Vessels TW-1 Through TW-9 . . . . .	47
c. Vessels TW-10 Through TW-12 . . . . .	69
d. Vessels TW-13 Through TW-16 . . . . .	76
3. Test Results . . . . .	77
a. TW-1 . . . . .	80
b. TW-2 . . . . .	80
c. TW-3 . . . . .	80
d. TW-4 . . . . .	88
e. TW-5 . . . . .	88
f. TW-6 . . . . .	88
g. TW-7 . . . . .	96
h. TW-8 . . . . .	96
i. TW-9 . . . . .	96
j. TW-10 . . . . .	96
k. TW-11 . . . . .	101
l. TW-12 . . . . .	101
m. TW-13 . . . . .	101
n. TW-14 . . . . .	101
o. TW-15 . . . . .	104
p. TW-16 . . . . .	104
VI. CONCLUSIONS . . . . .	109
VII. RECOMMENDATIONS . . . . .	107
Appendix I - Thick-Wall, Filament-Wound, Pressure-Vessel Analysis . . . . .	109
Appendix II - Structural Design - Thick-Wall, Filament-Wound, Pressure Vessel . . . . .	129
Appendix III - Fabrication Procedure for 12-in.-dia Thick-Wall, Filament-Wound, High-Pressure Containers . . . . .	132
Appendix IV - Test Procedure for 12-in.-dia Thick-Wall, Filament-Wound, High-Pressure Containers . . . . .	142
References . . . . .	147

LIST OF ILLUSTRATIONS

FIGURE		PAGE
1	Effect of Number of Elements on Weight of Structure . . . . .	8
2	Effect of Number of Elements on Winding Stress Distribution . . . . .	9
3	Variation of Filament Stress Over Contour . . . . .	10
4	Effect of Wrap Tension Program on Weight of Structure . . . . .	12
5	Wall Stresses in Oblate Spheroid at Equator . . . . .	13
6	Effect of Design Pressure on Weight of Structure . . . . .	14
7	Wall Stress in Oblate Spheroid at $R/A = 0.43$ , Wrap Angle ( $\alpha$ ) = $45^\circ$ . . . . .	16
8	Effect of Variation in Modulus on Weight of Structure . . . . .	17
9	Combination of Tension Programs and Modulus Variations to Achieve a Constant Design Stress in All Layers of Composite . . . . .	18
10	Thick-Wall, Filament-Wound, High-Pressure Container . . . . .	21
11	Welded Liner for Thick-Wall, Filament-Wound, High- Pressure Container . . . . .	25
12	Forward Boss for Welded Liner . . . . .	26
13	Aft Boss for Welded Liner . . . . .	27
14	Forward and Aft Heads for Welded Liner . . . . .	28
15	Hydrotest Closure for Thick-Wall, Filament-Wound, High- Pressure Container . . . . .	29
16	Head Sections of Liner . . . . .	34
17	Forward Boss . . . . .	35
18	Aft Boss . . . . .	36
19	Seam-Welded Specimens . . . . .	37
20	Boss-to-Head Weld . . . . .	39
21	Head Section Weld . . . . .	40
22	Completed Liner . . . . .	41
23	Completed Liners in Shipping Crate . . . . .	42
24	Hydrotest Closure . . . . .	43
25	Electron-Beam Weld Section . . . . .	44
26	Electron-Beam Closure Weld . . . . .	45
27	Closure Weld After Hydrotest . . . . .	46
28	Wood Mandrel . . . . .	48
29	Winding Shaft . . . . .	49
30	Wood Mandrel Being Wrapped . . . . .	50
31	Sectioned Overwrapped Wood Mandrel . . . . .	51
32	Sectioned Overwrapped Wood Mandrel with Overlay . . . . .	52
33	Winding of Container TW-1 . . . . .	53
34	Container TW-1 Before Closure Welding . . . . .	55
35	Roving Buildup . . . . .	61
36	Roving Buildup for Various Tape Widths and Boss Sizes . . . . .	62
37	Vessel Length for Various Tape Widths and Boss Sizes . . . . .	63
38	Thickness at Equator for Various Tape Widths and Boss Sizes . . . . .	64
39	Wrap Angle for Various Tape Widths and Boss Sizes . . . . .	65
40	Strain Distribution in Metal Structure . . . . .	67
41	Liner Section at Equator . . . . .	70
42	Seam-Weld Cross Section at Equator (40X) . . . . .	71
43	Weld Nugget No. 1 at Equator (150X) . . . . .	72
44	Grain Boundary of Weld Nugget No. 1 at Equator (500X) . . . . .	73

LIST OF ILLUSTRATIONS (cont.)

FIGURE		PAGE
45	Weld Nugget No. 2 at Equator (150X) . . . . .	74
46	Weld Nugget No. 3 at Equator (150X) . . . . .	75
47	Container TW-1 After Hydrotest . . . . .	83
48	Sectioned Container TW-1 After Hydrotest . . . . .	84
49	Strain-Gage Curves for Container TW-1 (First Cycle) . . . . .	85
50	Strain-Gage Curves for Container TW-2 (Second Cycle) . . . . .	86
51	Location of Strain Gages . . . . .	87
52	Container TW-3 Liner After Removing Laminate . . . . .	89
53	Liner-to-Boss Weld Section of TW-3 Liner After Removing Laminate . . . . .	90
54	Crimping of Liner Adjacent to the Liner-to-Boss Weld (Container TW-3) . . . . .	91
55	Rubber Bladder for Thick-Wall Container . . . . .	92
56	Instrumentation Layout . . . . .	93
57	Pressure/Deflection Curves for TW-4 . . . . .	94
58	Vessel Growth During Pressurization (TW-4) . . . . .	95
59	Container TW-7 After Burst . . . . .	97
60	Container TW-7 After Sectioning . . . . .	98
61	Pressure/Deflection Curves for TW-8 . . . . .	99
62	Vessel Growth During Pressurization (TW-8) . . . . .	100
63	Containers TW-11 and TW-12 After Burst . . . . .	102
64	Vessel Growth During Pressurization (TW-12) . . . . .	103
65	Element of Shell of Revolution . . . . .	110
66	Diagram of Strain Compatibility . . . . .	112
67	Geometry of General Winding Pattern . . . . .	120
68	Geometry of In-Plane Winding Pattern . . . . .	122
69	Hydraulic Test Facility Schematic . . . . .	143
70	Burst Pressurization Schematic . . . . .	145

LIST OF TABLES

TABLE		PAGE
I	Design Criteria for 12-in.-dia, Thick-Wall, Filament-Wound, High-Pressure Vessel . . . . .	22
II	Candidate Liner Materials . . . . .	23
III	Materials Available for Filament Winding . . . . .	30
IV	Candidate Resin Systems . . . . .	31
V	Mechanical Properties of Adhesives (Metal-to-Metal Bonds) . . . . .	59
VI	Fabrication Summary, 12-in.-Diameter, Thick-Wall, Filament-Wound, High-Pressure Vessel . . . . .	78
VII	Test Summary, 12-in.-Diameter, Thick-Wall, Filament-Wound, High-Pressure Vessel . . . . .	81

## SECTION I

### INTRODUCTION

#### 1. BACKGROUND

Primary emphasis to date in applying filament winding technology has been in the area of pressure vessels - particularly thin-wall structures that have a radius 10 times greater than the wall thickness. Filament-wound, glass-reinforced resin construction adapted to thick-wall, high-pressure gas containers [30,000 psi (30.00 ksi) and higher] suggests a method in which the inherent characteristics, including high performance, dimensional stability, structural reliability, and ease and low cost of fabrication, are particularly attractive. Techniques have been advanced and empirically validated for use in optimizing design and fabrication concepts for thin-wall, filament-wound vessels. Far less effort has been expended on thick-wall, filament-wound tanks and their associated problems. Principal areas of investigation on the filament-wound, thick-wall vessels may be grouped into the composite shell and sealant-liner structures. Analytical methods, design approaches, and fabrication processes can be established for both structures to assure optimum performance.

Design and analysis efforts on thin-wall vessels have been based principally on membrane theory and - in the case of filament-wound structures - on a netting analysis that takes into account fiber properties and orientations. The thick-wall composite shell required to react high internal pressures introduces discontinuity stresses that must be minimized to achieve a uniform stress field throughout. These stresses result principally from the head-contour difference between the inner and outer layers, and from uncontrolled filament tensioning during winding. The stress distributions in a pressurized thick-walled structure, calculated by equations developed by Lamé, are such that the outer surface is subjected to low stresses and is therefore inefficient. Several methods have been recommended for the construction of thick-walled, filament-wound, high-pressure vessels that will elastically resist relatively high internal pressures and will make effective use of the material near the outer surface. Basically, they create pre-stresses of different magnitudes throughout the vessel wall, so that the resultant stress distribution will approach a constant value for each structural element when internal pressure is applied. The more practicable methods to accomplish this condition include the following:

- Varying winding tensions of discrete layers of glass filaments during fabrication.
- Application of discrete layers of pre-stressed glass filaments with different elastic moduli.
- Addition of an outer overwrap of a pre-stressed metal filament layer in order to achieve greater elastic restraint.
- A combination of the above methods.

Liner impermeability becomes a primary consideration in selecting the best combination of materials and processes to ensure a successful filament-wound, high-pressure gas container. Molded elastomers, polymeric films, metal coatings, and various other materials have been investigated as sealant liners and generally found to be functionally inadequate for the stringent leakage requirements of high-pressure gas-storage applications. Previous investigations conducted by Aerojet (References 1, 2, and 3) have shown that a filament-wound vessel incorporating a metal liner meets the impermeability requirements, withstands wide temperature variations, and is capable of repeated operating strains while providing higher performance levels than are attainable with homogeneous-metal structures.

The performance efficiency of a filament-wound, metal-lined pressure container indicates that a minimum weight (thinnest gage thickness) liner is to be preferred. The principal problems associated with thin-metal liners are availability of the material, fabrication formability, biaxial plastic deformation in loading the filaments to optimum stress levels, and ability to sustain cyclic pressurization in conjunction with the plastic deformation.

Various stainless-steel and aluminum alloy thin-metal liners (0.003 and 0.006 in. thick) have been designed and successfully fabricated by Aerojet. The design and fabrication approaches used there were utilized in the current vessels. The head sections of the thin-metal foil liners were constructed by hydroforming - a process in which the foil was cut to the required size, placed between thin mild-steel plates, and positioned on a work table. A male punch, machined to the desired configuration, formed the heads by forcing the steel plates against a rubber diaphragm which was backed by hydraulic fluid. Each formed metal-foil head section was stress-relieved, trimmed to the required dimension, and joined to a cylindrical section - or to each other for oblate-spheroid vessels - by means of resistance-roll-seam welding. The weld consisted of a series of overlapping spot welds made progressively along a lapped joint with roller-type electrodes.

A reliable adhesive bond should be maintained between the liner and composite shell if a filament-wound container having a thin-metal liner strained in the plastic range is to perform properly under cyclic pressurization. Failure or lack of an adequate adhesive bond can induce compressive buckling in the liner. In the absence of an adequate bond, buckling can occur as a result of external compression of the liner by the overwrapped filaments (a) after the supporting mandrel is removed, or (b) after the proof pressurization cycle (in which the elastic limit is exceeded) as the vessel pressure is relieved. Subsequent fatigue failure in the buckled area of the metal is caused by cyclic pressurization of the vessel.

Another way to prevent cyclic fatigue of the metal liner is to utilize high-modulus fibers such as boron or graphite. The high-modulus filaments will reduce the high biaxial strains otherwise encountered in liners. Under such circumstances the metal liner of a high-modulus, filament-reinforced tank can sustain fatigue cycling without failure by operating efficiently at strains below the elastic limit.

Compressive buckling also can be eliminated through the utilization of a thicker, load-bearing, non-buckling liner that is strained within the tensile

and compressive elastic limits at operating conditions after being subjected to an initial plastic deformation during the vessel's first proof test. A filament-wound composite combined with a load-bearing, non-buckling, metal shell provides the necessary sealant liner and utilizes the maximum fiber strength. Also, it does not require an adhesive bond between the metal liner and composite wall to prevent buckling from cyclic pressurization loading. After the proof test is completed and the tank is at zero internal pressure, the liner is in maximum compression due to the external forces produced by the overwrapped filaments. If the liner is sufficiently thick, then the compressive buckling strength is not exceeded. Unfortunately, the greater thickness required for metal liners serving in non-buckling capacities substantially decreases the glass filament-wound vessel performance level. These low-modulus glass filaments require greater wall thickness for non-buckling applications than do the advanced high-modulus filaments. However, the advanced materials are not currently available for purchase in production quantities and furthermore they do not exhibit the strength-to-density ratios available in glass composites. Detailed results of prior Aerojet work in the area of filament-wound vessels with non-buckling metal liners are presented in References 4 and 5.

The present report provides a detailed summary of all work performed during the investigation of thick-wall, filament-wound, high-pressure containers. Included along with the data obtained are conclusions and recommendations. Fabrication procedures, test methods, specimen configurations, analyses, and vessel design calculations are covered in the appendixes. This work will help establish design theory, provide useful data, select the most applicable materials, and improve processing techniques for the continuing development of thick-wall, filament-wound, high-pressure gas containers.

## 2. PROGRAM PLAN

The work under Contract AF 33(615)-3995 was directed toward the development of analytical methods and fabrication techniques for thick-wall, filament-wound, metal-lined, high-pressure gas containers. The basic objectives were to theoretically establish, and experimentally confirm, the design theory, selected materials, and fabrication procedures for reliable, high-performance containers.

The program originally consisted of a three-phase, 22-month technical effort that involved (a) review of thick-wall theory for homogeneous materials and development of a new analytical method for filament-wound anisotropic composite walls with varying radii of curvature, (b) analysis and evaluation of various methods to obtain a high-performance structure (including filament-tensioning programs and the use of layers of materials of graduated moduli), (c) design of thick-wall pressure vessels to achieve optimum performance, and (d) prototype fabrication and testing to validate or modify the design procedures.

The principal problems under investigation were in the areas of design and analysis. The most significant undertaking was the determination of a filament-wound, high-pressure, vessel design that assured a uniform distribution of fiber stresses in each layer of material, thereby achieving maximum performance. Additional design problems - factors that generally do not materially influence stress distribution in a thin-wall pressure vessel -

included: (a) difference in head contour at the inner and outer layers, (b) the radial strain within the composite, and (c) bearing stress distributions in the area of the bosses.

Specific processing areas of investigation included liner integrity, liner-to-laminate adhesive bond, mandrel support for the overwrapped thin liner, and filament bridging and composite buildup in the areas adjacent to the bosses.

Phase I was to be directed toward review and revision of existing thick-wall theory to take into account the variable radii of curvature, effects of winding tensions, properties of the fibers in the shell, and a changing tensile modulus through the wall. Shell shapes and metal liners were also to be investigated.

The work in Phase II was to be based on information generated in Phase I. A design configuration was to be established for a pressure vessel with a volume of approximately 500 cu in., a working pressure of 15.00 ksi (15,000 psi), and a burst pressure of 33.00 ksi. The first detailed design of this configuration was to be developed using the theoretical analysis of Phase I. Subsequent design iterations to optimize the configuration were to be made on the basis of the experimental data from Phase III.

Phase III was to be devoted to the fabrication and test of the designs generated in Phase II. These vessels were to be fabricated and tested in sequential lots, in accordance with the initial and subsequent iterative designs. Contractual requirements for Phase III were to include the fabrication and evaluation of 25 vessels, and the subsequent delivery of three prototype vessels which were to be fabricated to a design modified on the basis of test information fed back in order to structurally optimize the design.

Technical and processing problems described in greater detail in the body of the report made it imperative that major steps be taken, and funding utilized, to effect improvements in the container structure prior to continuing fabrication. As a result, a total of 16 vessels were fabricated and evaluated in Phase III in separate lots of 9, 3, and 4 vessels each.

## SECTION II

### SUMMARY

Thick-wall, glass-filament-wound, high-pressure gas containers with thin-metal liners were analytically and empirically investigated in a three-phase development program consisting of (1) analytical studies, (2) design, and (3) fabrication and test. An analysis was developed to adapt thin-wall theory to a multi-layered thick-wall vessel. The analysis was programed on the computer. It provided for the variation in fiber properties from layer to layer, as well as a means of defining winding tensions, for optimum pressure vessel performance.

An oblate spheroid was selected as the vessel configuration offering the best performance efficiency. The vessel was designed and analyzed with the aid of the computer program by inputting specific dimensional criteria and material properties based upon the oblate-spheroid configuration. Thin (0.006-in.), annealed, Type 347 stainless-steel material was utilized for the liner because of impermeability requirements, high biaxial ductility, previous successful experience in forming and resistance welding, and maximum performance efficiency.

A total of 16 pressure vessels, utilizing identical liners, were fabricated. Fourteen vessels were subjected to single-cycle burst tests and two were fatigue cycled. Fabrication and testing were performed in three separate lots of 9, 3, and 4 vessels each. During the course of the work, designs and processes were modified in attempts to improve structural performance. The principal problem encountered through the program was the integrity of the thin-metal liners. Of the 16 vessels tested, 13 failed as a direct result of liner leakage. Additional studies were conducted concurrently to resolve this problem. (Such leakage was attributed to localized strain incompatibility between the metal liner and the glass-reinforced composite structure due to certain features of the configuration.) These investigative studies included (a) providing a more reliable liner-to-composite adhesive bond, (b) ensuring adequate mandrel support for the overwrapped metal liner, and (c) minimizing strain magnification in the transition area between the metal liner and metal boss.

As a result of these programs, an improved cleaning and liner-to-composite adhesive bond system and a sand-acrylic mandrel material were developed, and higher winding tensions combined with a wider band tape width were found to reduce excessive strains developed during vessel pressurization.

Two of the vessels which failed in the composite structure exhibited burst pressures which were 72% of the design values, while one of the vessels subjected to fatigue cycling attained 13 cycles from 0 to 15.00 ksi operating pressure before liner failure occurred.

Specific recommendations were made for further development work in the thick-wall vessels. These included utilizing a metal liner sufficiently thick to withstand the winding pressures without utilizing an internal mandrel, and the provision for intermittent periods during which the composite structure would be cured. Thus, the applied composite structure and metal liner would serve to support the pressures from subsequent windings.

### SECTION III

#### ANALYTICAL METHODS (PHASE I)

The primary objective of this task was to review existing thick-wall theory used for the analysis of homogeneous pressure vessels, and to develop a new method for the analysis of filament-wound (anisotropic) pressure vessels formed by a general surface of revolution. The analysis was then to be used for the evaluation of various methods to obtain a high-performance structure.

##### 1. ANALYSIS

Existing thick-wall theory was investigated for the possibility of revisions which would account for a general surface of revolution with pre-tensioned-fiber composite walls and variable radii of curvature. Several Lamé-type solutions, which had been adapted for the analysis of isotropic spheres and cylinders, were available for consideration. A more general method formulated by Love (Reference 6), which expresses the stress components in terms of a single function that satisfies a fourth-order partial-differential equation, was also available for analysis of an isotropic solid of revolution. Adaptation of these analyses to orthotropic structures with variable properties through the wall appeared to be inadvisable, however, because digital computers could be used to solve the problem efficiently with the aid of a finite-difference technique. In addition, the establishment of a finite-difference analysis required considerably less time.

For the finite-difference technique, the structure may be divided into a series of thin-wall pressure vessels. It should be noted that the analysis and equations for each vessel must include factors that are not considered in standard thin-wall theory. Such factors include the different radii of curvature of each layer, the different sizes of each layer within an element of the shell, and the change in layer thickness caused by radial stress (pressure) and strains in the surface direction (Poisson's-ratio effect).

Equations were developed for the analysis of thick-wall heads by finite elements. These equations and their development are covered in Appendix I. The analysis provides for the variation in fiber properties from layer to layer, as well as a means of defining winding tensions for optimum pressure-vessel performance. The equations were arranged for ease of programing on a high-speed digital computer.

##### 2. COMPUTER PROGRAM

A computer program was developed to perform calculations for the design and structural analysis of thick-wall, filament-wound pressure vessels using the equations shown in Appendix I. The logic was based on an existing computer program ("Analysis of Filament-Reinforced Metal-Shell Pressure Vessels," Reference 5), which was written to cover the relatively low-pressure (thin-wall) range of pressure vessels with two load-carrying layers.

The thick-wall program was written in Fortran IV for the IBM 7094-II Computer and was designed to accept as many as seven variations in material

for both hoop and longitudinal layers of composite. These layers may be assigned individual filament properties (fiber modulus and Poisson's ratio), thicknesses, resin contents, and design stresses or winding tensions. Briefly, the program uses strain compatibility equations to solve for the total composite thickness and winding or design fiber stress distribution at the equator of the head. The neutral position of the head contour is then defined by solution of a differential equation that describes both the balance of force field in the head and the path of the filaments on the surface. Rating properties (internal volume, weight of vessel, performance factor, etc.) are also computed for the entire vessel.

The number of layers required to establish the realistic pressure vessel performance was investigated using the computer program and (a) one, three, five, and seven layers of material, (b) a design stress of 330 ksi in all fibers, and (c) a filament winding stress of 9.5 ksi (4 lb tension<sup>(1)</sup>) for the inside layer of fibers. The results of this investigation are shown in Figures 1 and 2. As indicated in Figure 1, approximately identical weights were predicted for the five- and seven-layer composite system. The single-layer and three-layer systems predicted weights lower than the other layered systems, primarily because of inaccurate assumptions of strains in the outer layer of the composite and, therefore, falsely provided a higher performance structure. Figure 2 indicates the expected nonuniform wall stress distribution as the number of elements is increased from a single shell model (one layer corresponds to a thin-wall model) to a multishell model. It should be noted in the figure that the seven-element system predicts a maximum wall stress which is six times the expected wall stress as calculated from thin-wall theory. Based on these data, it is recommended that investigations of thick-wall composite pressure vessels assume at least five layers of material in order to determine actual performance, winding tensions, or design stresses.

### 3. PARAMETRIC STUDY

A study of the vessel performance and fiber stress distributions for conditions of winding, zero pressure, and design pressure was made in order to provide an analysis of the influence of design and material parameter variations on the performance of the vessel. Parameters considered in this study were shape (spheroidal or integral cylindrical and end-dome vessels), winding tensions, fiber design stress levels, fiber modulus, and design pressure. For all cases, the weight of the composite shell and 0.006-in.-thick stainless-steel liner was used as a measure of structural performance - a lower weight indicating higher performance. All vessels assumed a seven-layer composite.

The data defining the variation of fiber stress at various points on the heads of thick-wall pressure vessels are presented in Figure 3. Values shown are for the middle layer of material. Stresses in other layers are approximately the same as those shown. Figure 3 shows that oblate spheroids have a maximum fiber stress at the equator, with variations across the wall as described in a subsequent paragraph. For pressure vessels with cylindrical sections, maximum stress - which occurs at some finite distance from the equator - is slightly greater (1.2% for a vessel with an  $L/D = 2$ ) than the

<sup>(1)</sup>Per 20-End here and in the ensuing discussion.

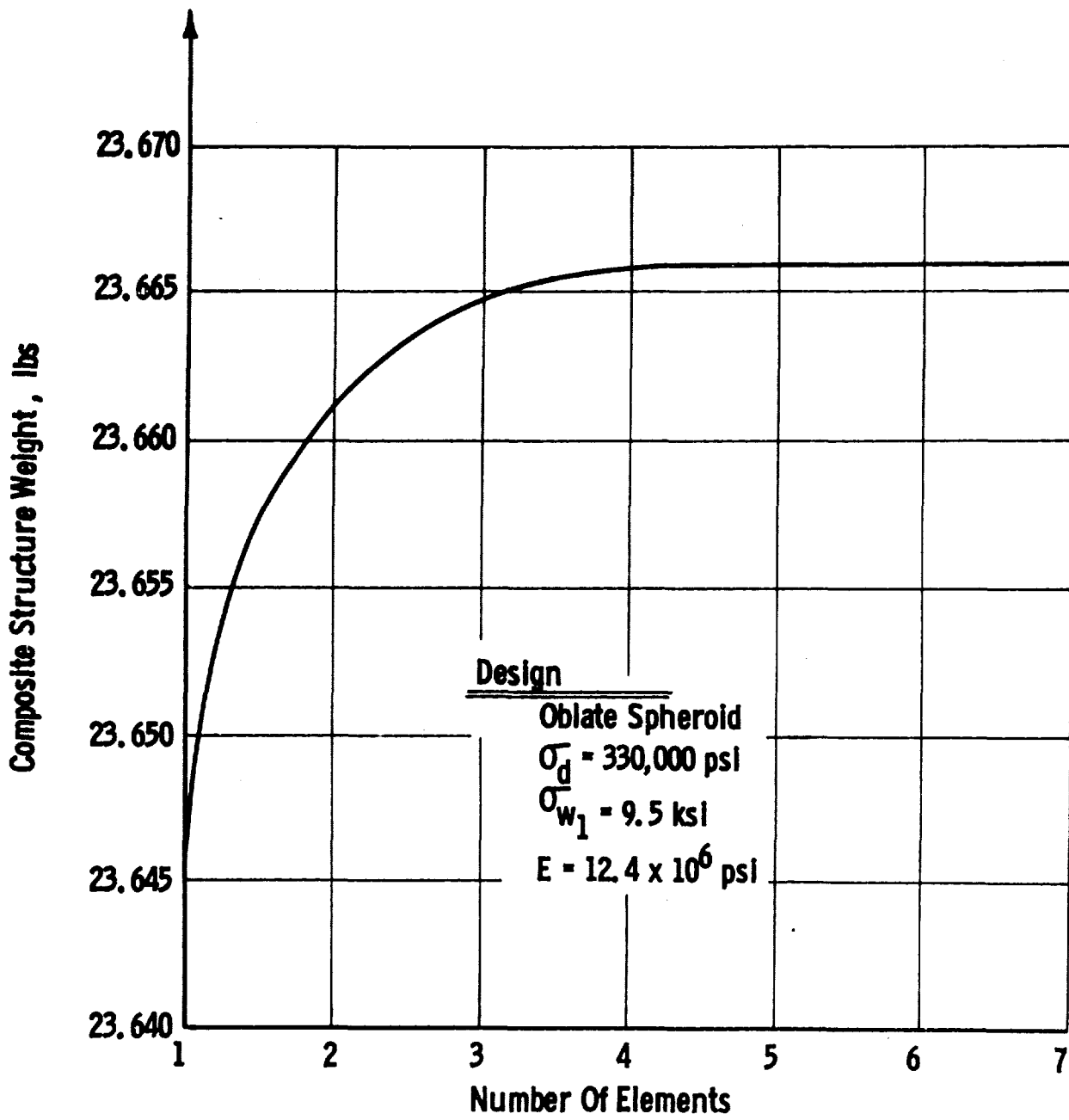


Figure 1. Effect of Number of Elements on Weight of Structure

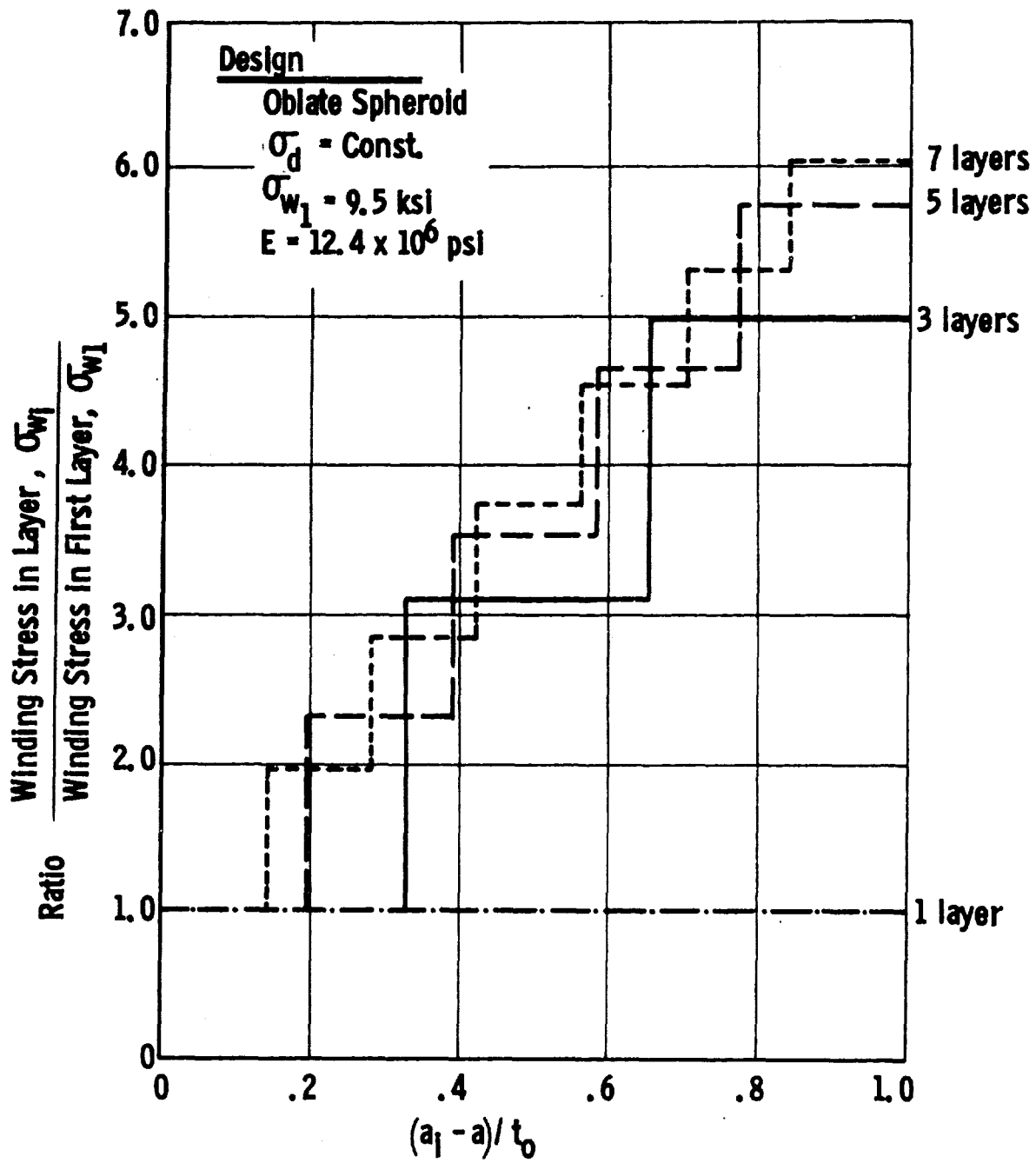


Figure 2. Effect of Number of Elements on Winding Stress Distribution

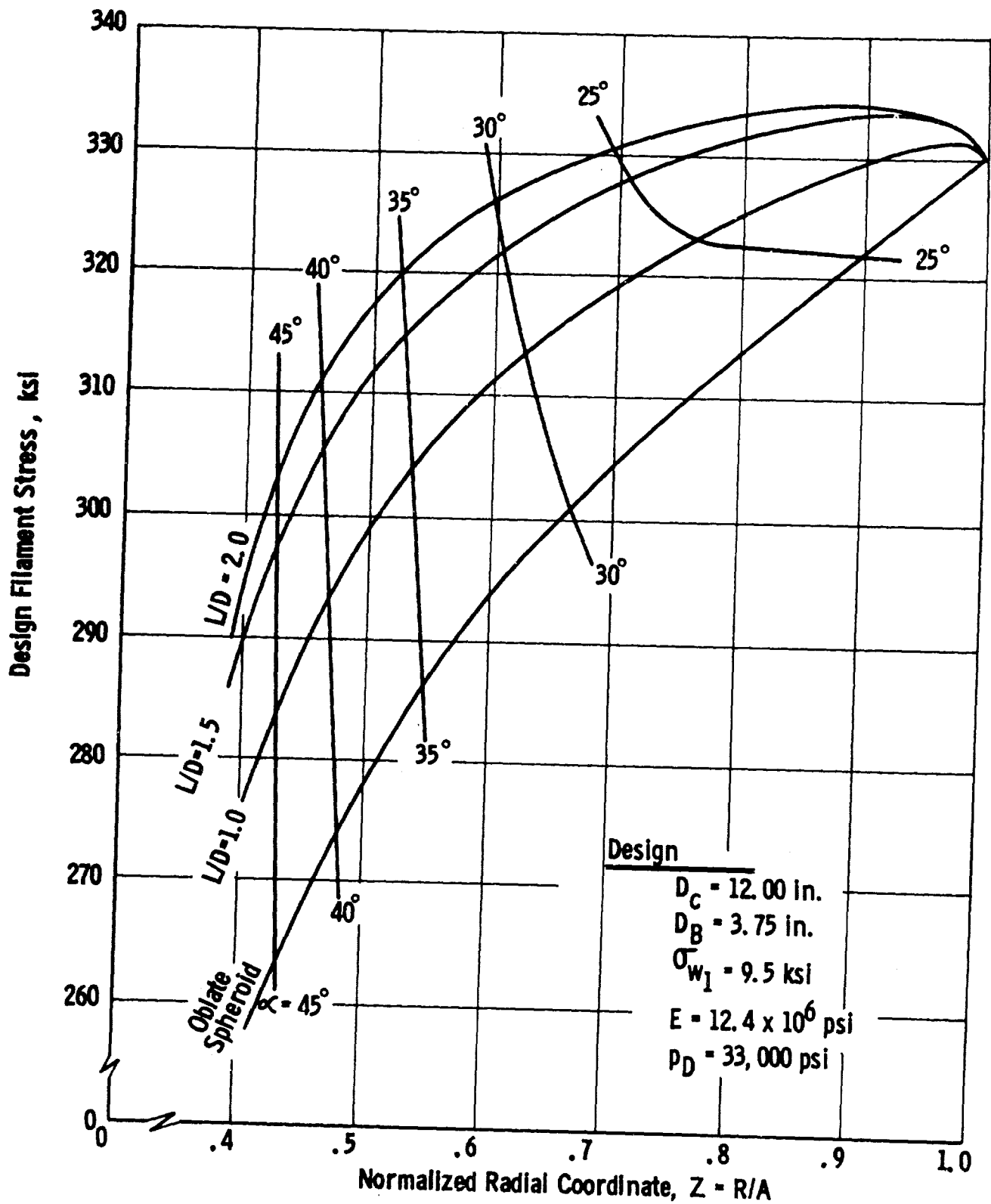


Figure 3. Variation of Filament Stress Over Contour

stress at the equator. This location of maximum stress has been verified by tests of thin-wall pressure vessels with cylindrical sections, since failure in the heads rarely occurs at the equator. Fiber stresses in the center of the heads would be less than the fiber stress at the equator for all designs.

The change in the performance of the ultra-high pressure vessel of spheroidal configuration is shown in Figure 4 as a function of the variation in winding tension. Three winding tensions (0, 4, and 8 lb, corresponding to filament winding stresses of 0, 9.5, and 19 ksi) were assumed for the first layer of the seven layer systems. In order to isolate the effect of the change in winding tension, fiber moduli and design fiber stresses were held constant for all layers. It should be noted that little difference exists between vessels with initial layer winding stress variation for the range considered. In actual practice, the minimum winding stress used for high-performance structures employing preimpregnated fibers would be 4 lb because of requirements for the removal of catenaries and the desire to collimate fibers. Maximum winding tensions are a function of equipment and the level of tension at which fiber damage starts. This maximum tension is approximately 20 lb for 20-end prepreg roving, when equipment of the type employed by Aerojet is used. (Subsequent modification to equipment has increased the tension to 40 lb per 20 end roving range - see Section V,2,c.) Based on these limits, the maximum performance of a design where only tensions of the layer were varied would be limited to an initial tension of 4 lb, and a tension increase of 2.67 lb per layer  $[(20-4)/6]$  is shown in Figure 4.

The variations in filament stresses across the wall of the composite for the equator of a spheroid are shown in Figure 5. The computer program provides for either the employment of assumed winding stresses or design filament stresses in layers other than the first layer. Figure 5 provides a comparison between the case of a constant winding tension or a constant design stress for all layers. For both cases, the winding and design stresses of the first layer were assumed to be 9.5 ksi and 330 ksi, respectively. Figure 5 indicates that for the condition of equal winding stresses in all layers, the maximum fiber stress achieved at design pressure will be less than 330 ksi for layers other than the first or inside layer. When constant design fiber stresses are required in order that the maximum performance of the vessel can be achieved, winding stresses would have to vary from 9.5 ksi on the inside layer to a maximum of 60 ksi in the outer layer.

Stress distributions in the walls of ultra-high pressure vessels made from homogeneous materials vary in a hyperbolic manner across the wall. The filament-wound spheroidal pressure vessel, with its primarily meridional orientation of fibers, has a t/R ratio of approximately 0.09. This ratio of t/R places the design for the filament-wound spheroid under consideration in the program at a value very close to the condition where thin-wall theory would be applicable. For this reason, and because the computer program has been set up to optimize the design and thus control the stress distribution, the expected hyperbolic shape of the stresses across the wall were not noted for this design. Computer runs made at higher pressures indicated that a nonlinear stress distribution was more evident at high t/R ratios.

The performance of a pressure vessel with constant fiber moduli and equal winding stresses in all layers is shown in Figure 6 as a function of design

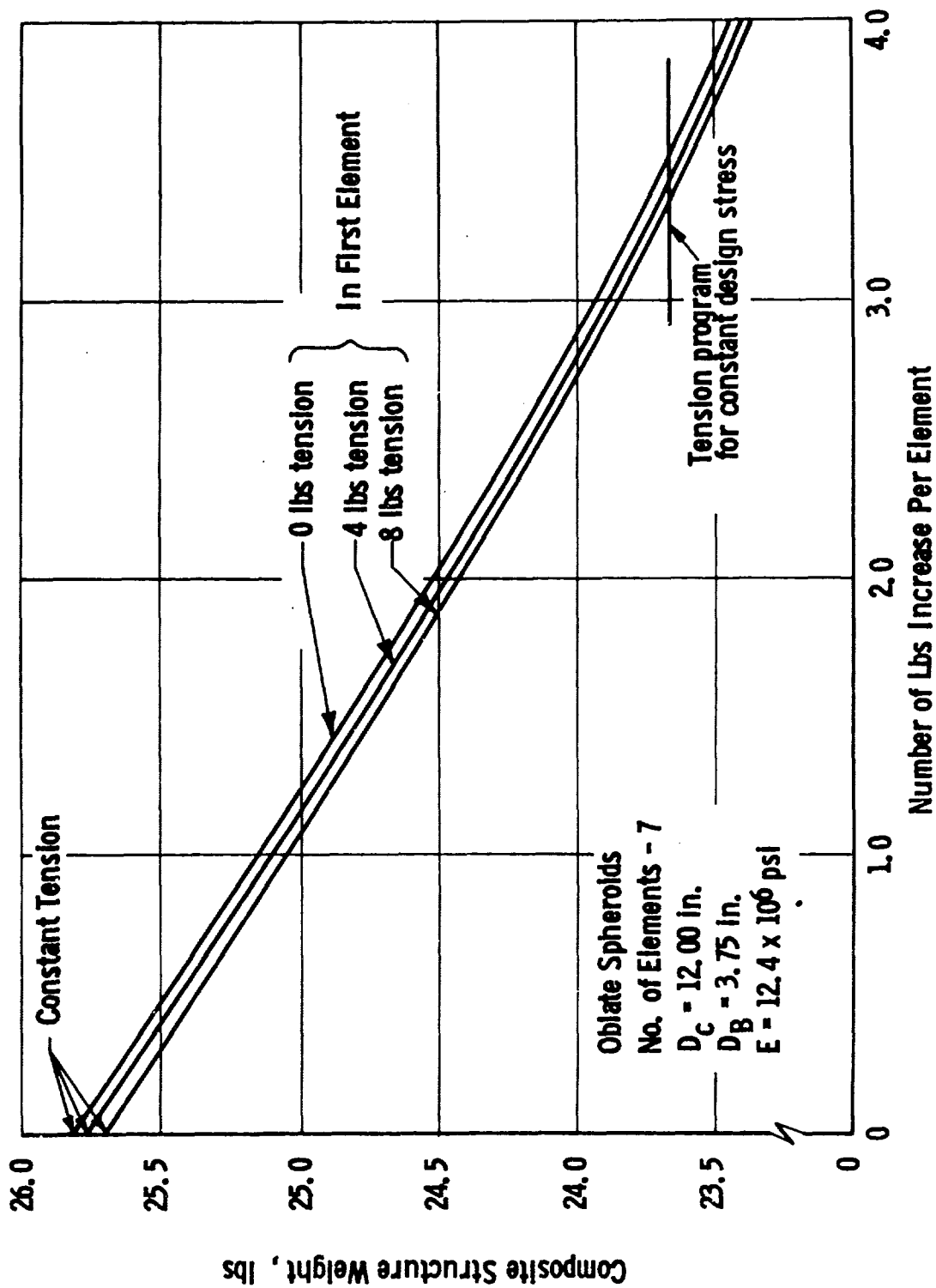


Figure 4. Effect of Wrap Tension Program on Weight of Structure

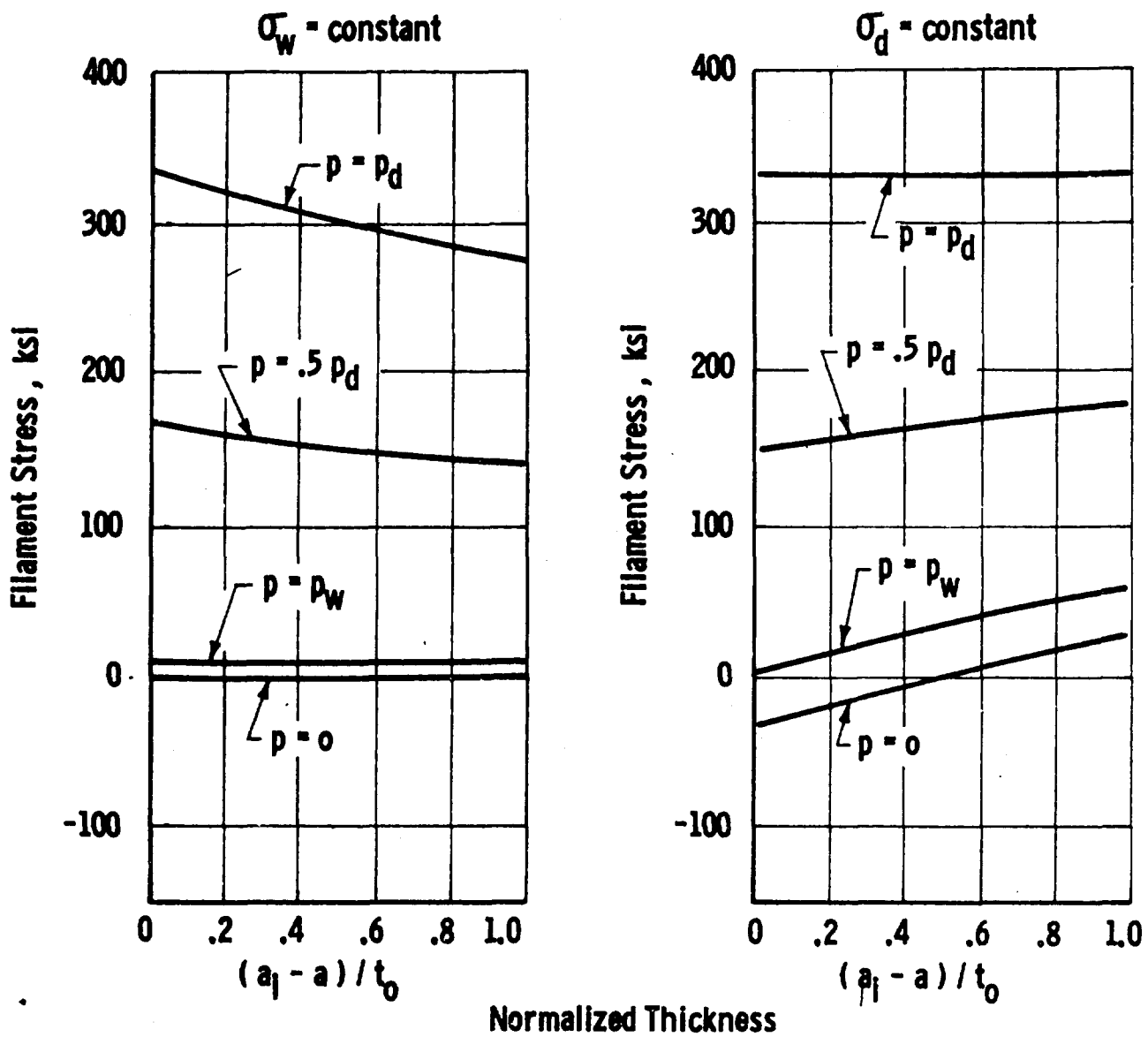


Figure 5. Wall Stresses in Oblate Spheroid at Equator

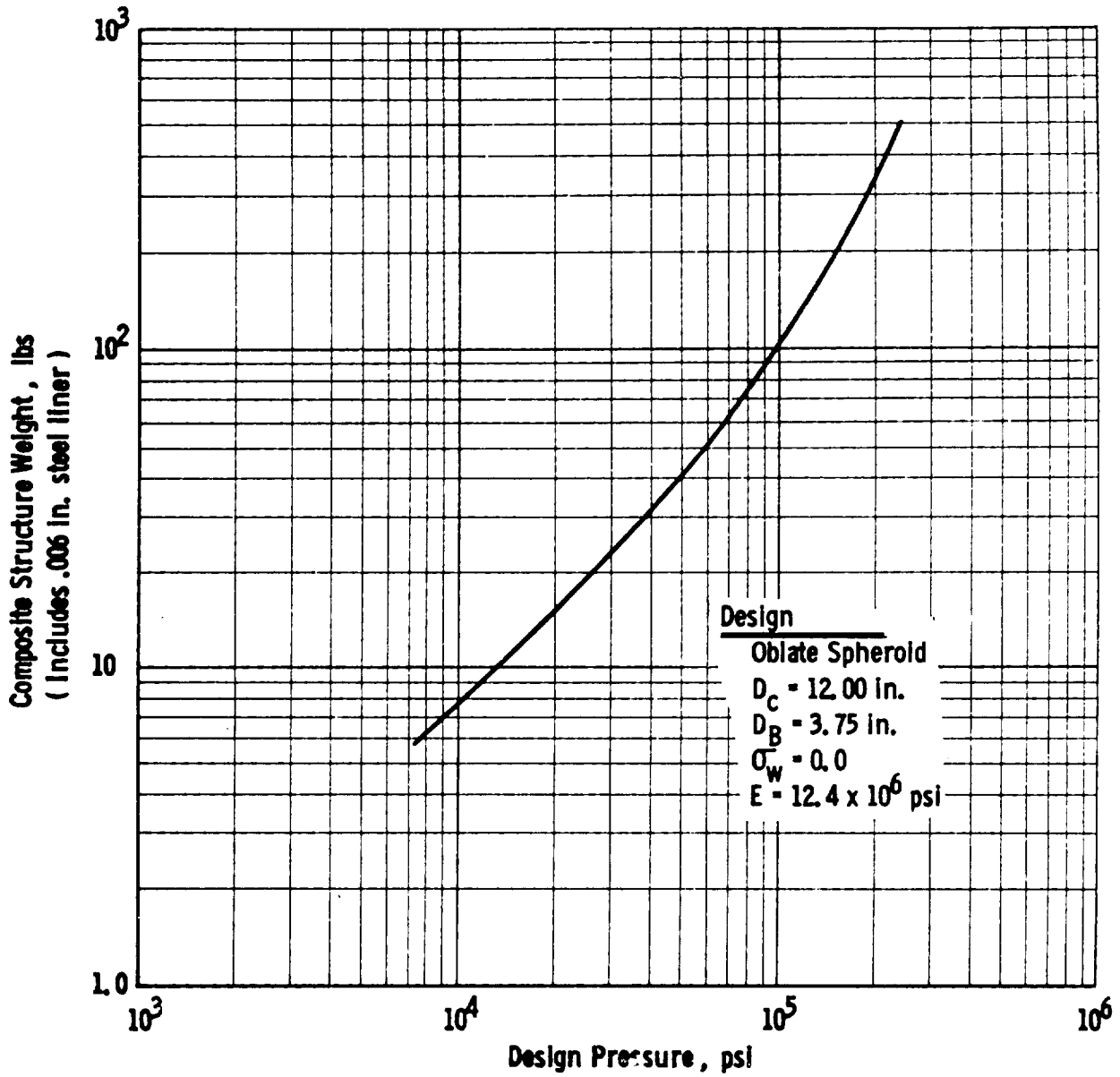


Figure 6. Effect of Design Pressure on Weight of Structure

pressure. As shown in the figure, pressure vessel weight will be increased by a rate in excess of the ratio of design pressures, thus appearing to show that higher performances will be achieved with lower pressures. As an example, three vessels at 10,000 psi have a composite structure weight approximately equal to, or slightly less than, one equivalent volume vessel at 30,000 psi. However, increased weight would result from the added manifolding and valving required. In addition, statistical reliability of the three vessel system would decrease.

The variation in filament stresses across the wall of the pressure vessel for the position where the wrap angle equals  $45^\circ$  is smaller than the variation at the equator, as noted in a comparison of the data presented in Figures 5 and 7. The most important features of Figure 7 are that the design stresses for both the constant winding tension and the constant design fiber stress are considerably below those values shown for the equator of the spheroid. In addition, the stresses in the fibers of the constant design stress condition are not constant across the wall at the point of  $45^\circ$  wrap angle. Finally, a comparison of the data presented in Figures 5 and 7 indicates that the fiber stresses in the inside layers are diminishing at a slightly greater rate than those for the outer fibers as the center of the head is approached and the wrap angle increases.

An evaluation of the effect of modulus change is presented in Figure 8. An oblate spheroid was used for this study with the following conditions assumed: a winding tension on the inside fibers of 9.5 ksi, a design fiber stress of 330 ksi for the inside fibers, and a seven-layer composite structure. A review of the data presented in Figure 5 indicates that the design stress across the wall of the shell varies approximately as a straight line. Therefore, it was assumed for this study that the change in modulus from one layer of composite to the next is a direct function of the position in the wall thickness. When layers of equal thickness are considered, the increase in modulus from layer to layer may thus be assumed to be constant. For the data of Figure 8, the modulus of the fibers in the inner material was assumed to correspond to the modulus of S-901 glass fibers ( $12.4 \times 10^6$  psi). The calculated weight of the pressure vessel with a constant modulus for all layers across the wall was 25.7 lb, and the fiber stress in the outer layer of composite was 280 ksi. Weight reductions can be achieved by the gradual increase of fiber moduli across the wall and the subsequent increase in filament design stress. Maximum performance for a combination of materials with equal design stresses of 330 ksi for all layers would be achieved when the modulus in each layer was approximately 3% greater than the modulus of the previous layer. (Note: a seven-layer system was used for this evaluation.) It is important to note that the computer program is not limited to layers of equal thickness or layers of uniform modulus increase. The preceding parametric investigation was limited to layers of equal thickness to eliminate one of many variables, and also limited to layers of uniform modulus increase for clarity in the presentation of data. Layers of any thickness with different moduli in each layer may be used as computer input. Higher performances can be achieved only if fiber strength increases as well as fiber moduli.

Figure 9 provides data for the selection of the optimum design for an oblate spheroid with a constant design fiber stress of 330 ksi and a winding

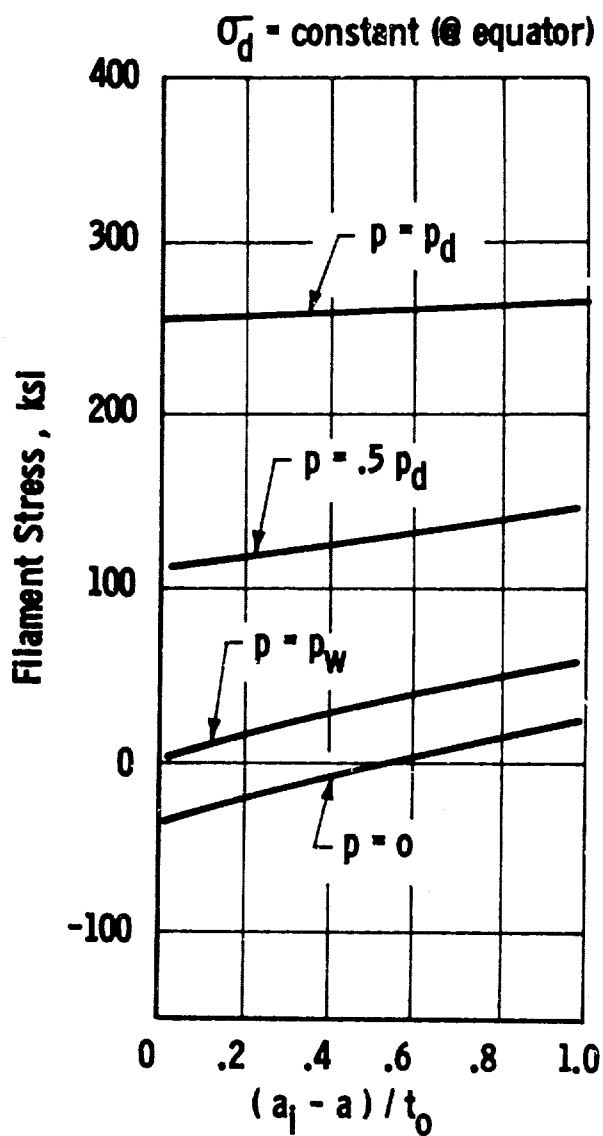
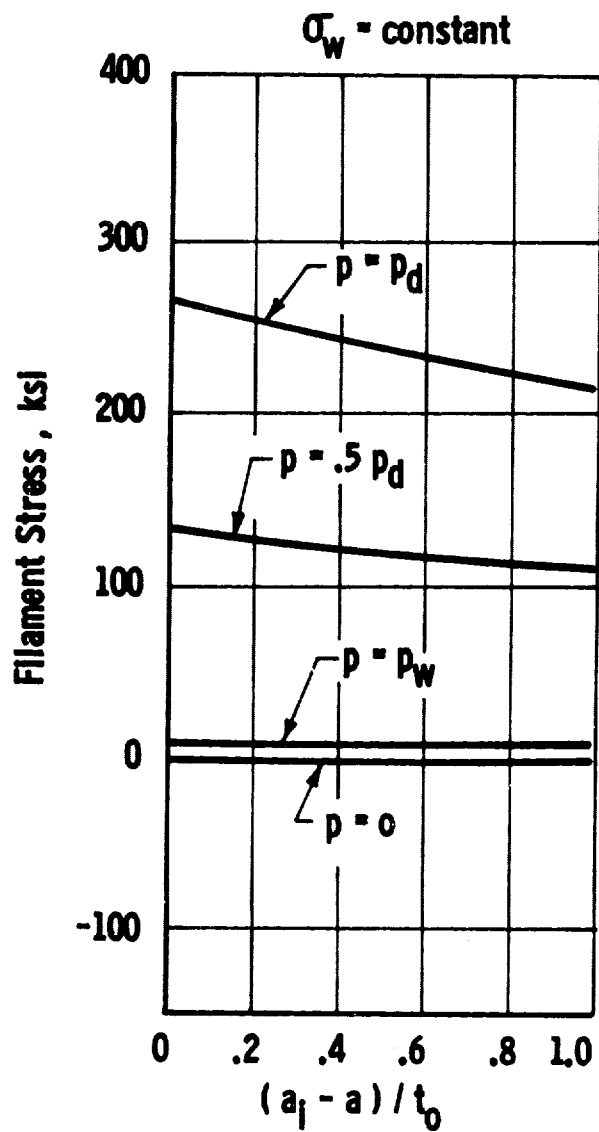


Figure 7. Wall Stress in Oblate Spheroid at  $R/A = 0.43$ , Wrap Angle  $(\alpha) = 45^\circ$

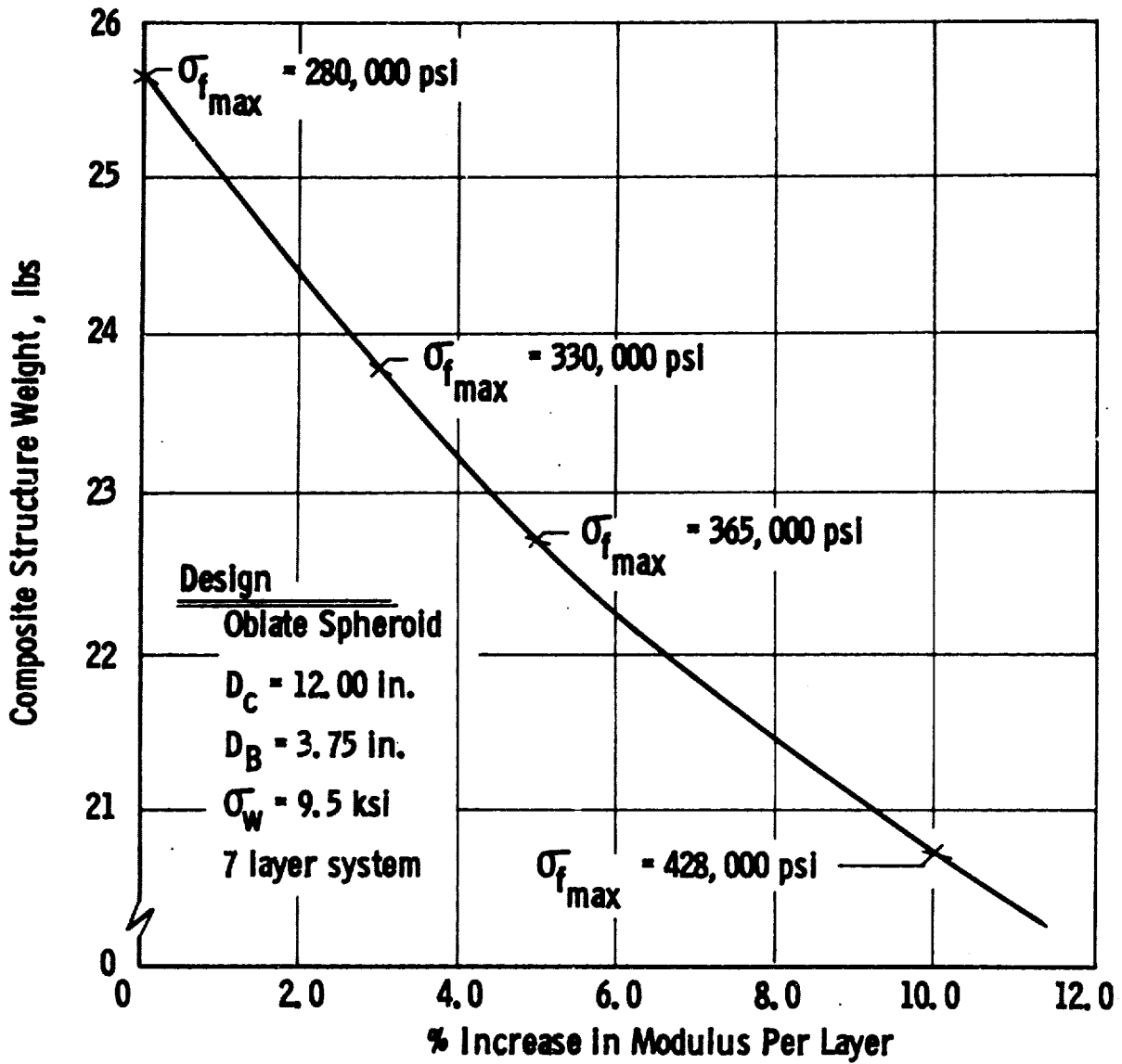


Figure 8. Effect of Variation in Modulus on Weight of Structure

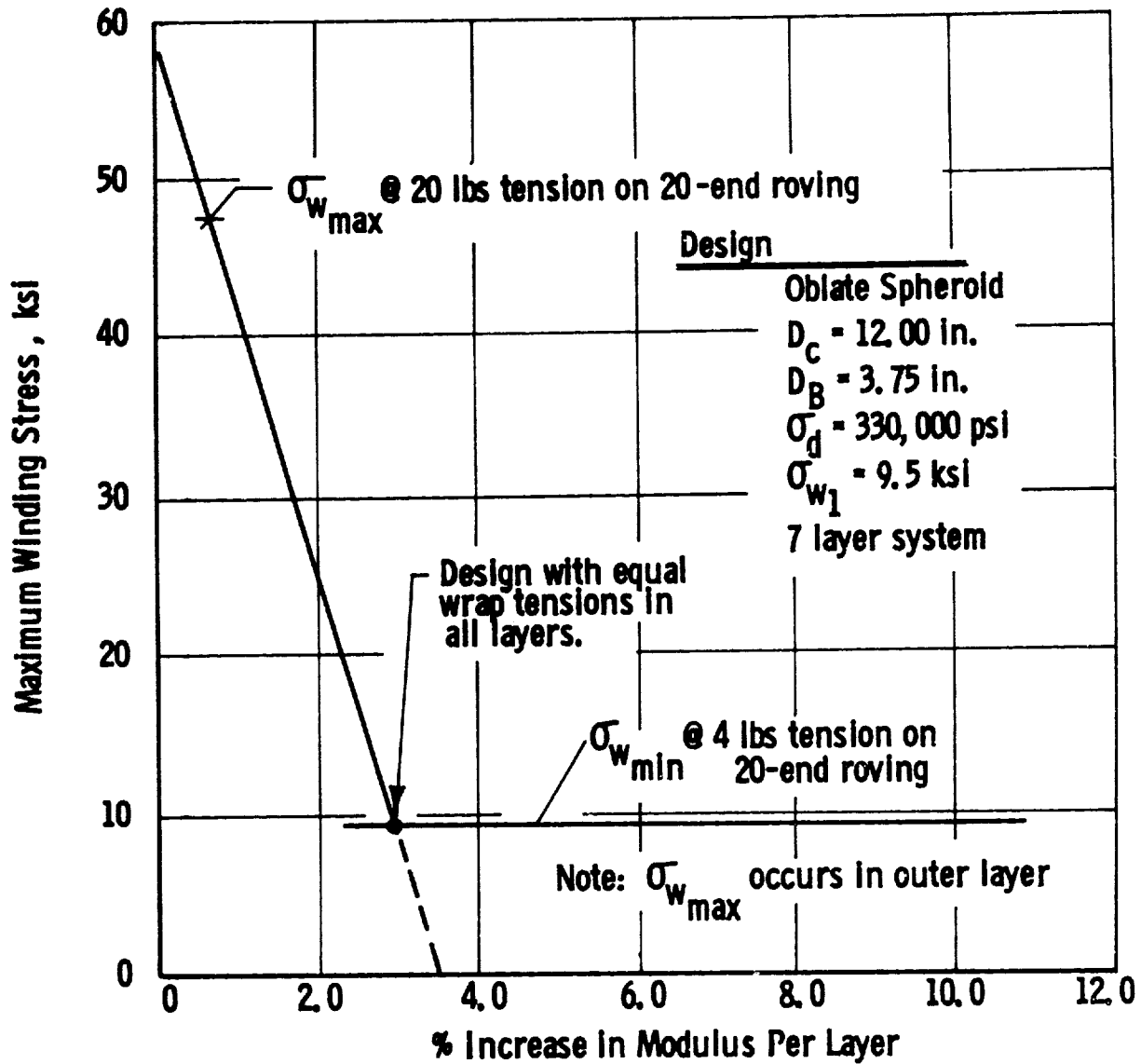


Figure 9. Combination of Tension Programs and Modulus Variations to Achieve a Constant Design Stress in All Layers of Composite

stress of 9.5 ksi on the inside fibers. The seven-layer system shown in Figure 8 indicates that a constant winding stress of 9.5 ksi can be used for the graduated increase in modulus of 3% per layer. For this system the maximum winding stress in the outer layer would be approximately 59 ksi, if a constant fiber modulus were used for all composite layers. Figure 9 indicates that since the maximum winding stress that can be used with current Aerojet equipment would be approximately 48 ksi, maximum efficiency cannot be achieved with a constant fiber modulus within the range of practical winding tensions (9.5 to 48 ksi).

The design parameters for the cylindrical section of a pressure vessel were also analyzed in this study. Predicted winding tensions for the hoop composite were a continuation of the tension program developed for the longitudinal layers, if a constant fiber modulus were used for all layers. Since the winding tensions in the longitudinal layers of material were greater than the allowable value, maximum winding tensions for the hoop composite would be even further removed from the practical range. Thus, the employment of materials with greatly increased fiber moduli is mandatory for the hoop composite of vessels in the pressure range under study.

## SECTION IV

### PRESSURE-VESSEL DESIGN (PHASE II)

#### 1. CRITERIA

A preliminary design for the thick-wall pressure vessel was initiated during the Phase I analytical study. This preliminary design provided the required lead-time for the fabrication of metal liners and tooling, and was useful also in the consideration of materials, fabrication processes, tooling, and comparative costs. Finalization of the design - including defining dimensional coordinates of the pressure vessel head and other vessel characteristics - was accomplished with the aid of the Phase I-developed computer program that analyzed and designed the vessels. This design is presented in Figure 10. Input variables were based on design criteria presented in Table I.

The pressure vessel has an inside diameter of approximately 12.0 in., and a volume of about 500 cu in. It was designed for a working pressure of 15.00 ksi and an expected single-cycle burst pressure of 33.00 ksi. The vessel design was analyzed to determine the stresses in the glass filaments within the wall and at various points along the heads at the design operating pressure. The safety factor based on comparison of the single-cycle-design-allowable ultimate filament strength of 330.00 ksi with the filament stress produced at the design operating pressure, was 2.2. For an allowable filament stress of 330.00 ksi, the longitudinal filament-wound composite thickness was calculated to be 0.56 in. at the equator of the heads. Design calculations are presented in Appendix II.

#### 2. CONFIGURATION

An oblate spheroid was selected for the vessel configuration on the basis of the Phase I analysis and previous evaluations. Theoretically, all filament-wound pressure vessel shapes have the same performance efficiency. Previous studies (Reference 7) have shown that a sphere, which represents the optimum configuration for homogeneous metal pressure vessels, is theoretically no more efficient for filament-wound structures than is a vessel of any other shape. Test results indicate that the nonuniformities and stress concentrations caused by the filament cross-overs of the multiple wrap patterns required to react the 1-to-1 biaxial force field relegate the filament-wound sphere to an efficiency below that of oblate spheroids and cylindrical pressure vessels. Studies indicate that the oblate spheroid is the most efficient filament-wound pressure vessel structure, followed by cylindrical and toroidal vessels. For this reason, an oblate spheroid was selected as the filament-wound design configuration for the pressure vessel.

#### 3. MATERIALS

Table II summarizes the properties of several candidate materials that were considered for the metal liner of the filament-wound pressure vessel. A 0.006-in.-thick, Type 347 stainless-steel material was selected because of the successful forming and seam-welding fabrication technology previously demonstrated by Aerojet (References 1, 2, and 3). The liner design utilizing



TABLE I  
 DESIGN CRITERIA FOR  
 12-IN.-DIAMETER, THICK-WALL, FILAMENT-WOUND, HIGH-PRESSURE VESSEL

Inside diameter, in.	11.940
Length, in.	6.594
Polar-boss diameter, in.	2.75
Metal-liner thickness, in.	0.006
Longitudinal-filament-wound-composite thickness, in.	0.560
Design operating pressure, ksi	15
Design burst pressure, ksi	33

<u>Properties</u>	<u>Type 347 Stainless Steel, Annealed</u>	<u>Glass-Filament-Wound Composite</u>
Density, lb/cu in.	0.286	0.075
Coefficient of thermal expansion, in./in.	$6.760 \times 10^{-6}$	$2.010 \times 10^{-6}$
Tensile-yield strength, ksi	120	---
Derivative of yield strength with respect to temperature, psi/°F	-116.0	---
Elastic modulus, $10^6$ psi	27.0	12.4
Derivative of elastic modulus with respect to temperature, psi/°F	-8030	-2410
Plastic modulus, $10^6$ psi	0.8	---
Derivative of plastic modulus with respect to temperature, psi/°F	-0.1	---
Poisson's ratio	0.295	---
Derivative of Poisson's ratio with respect to temperature, 1/°F	0.0	---
Volume fraction of filament in composite	---	0.673
Design-allowable filament stress, ksi	---	330

TABLE II

## CANDIDATE LINER MATERIALS

Type of Material	Direction*	Tensile Strength ksi		Elongation, %	Density lb/cu in.	Strength Ratio		Remarks
		Yield	Ultimate			Notched/	Unnotched	
Ti-6Al-4V alpha-beta	L	105-140	130-160	11-16	0.160	1.08/1.28	} Expensive to form and weld	
	T	125-140	140-160	8-16	---	1.10/1.25		
Ti-5Al-2.5Sn alpha	L	115-140	125-140	12-17	0.161	1.01/1.30		
	T	115-140	125-140	14-17	---	1.15/1.35		
Titanium-Base Alloys								
Aluminum Alloys								
1100-0	-	5	15	15	0.098	0.75/0.99	---	
2219-T87	L	50-58	65-75	8-14	0.102	0.73/0.98	---	
	T	53-58	62-72	8-12	---	---	---	
Steel								
4340 annealed	-	80	120	18	0.283	---	---	
4340 heat-treated	-	225	269	12	---	---	---	
4130 annealed	-	60	80-90	30	0.283	---	---	
4130 heat-treated	-	195	225	11	---	---	---	
Stainless Steel								
301 annealed	L	38	85	65	0.290	---	---	
301 extra full hard	L	185	20	8	---	---	---	
347 annealed	-	45	90	50	0.290	1.14	Readily welded to 17-4	
15-5 heat-treated (H-900)	-	185	200	14	0.282	---	Heat treatment at relatively low temperature	
17-4 heat-treated (N-900)	-	185	200	14	0.282	---	---	
17-7 annealed	T	40	130	35	0.282	---	---	
17-7 heat-treated (TE-1050)	T	185	200	9	0.276	---	---	

\* L = longitudinal, T = transverse.

this material is shown in Figure 11. Adhesive bonding was also considered as an alternate approach in joining the liner components. Although this method is probably less expensive than welding, it was rejected because of (a) the difficulties in producing reliable joints where the bond thickness must be accurately controlled, (b) the successful results previously achieved by the roll-resistance seam-welding technique, and (c) the fact that the program was not directed toward metal-liner fabrication processes which required further development on bonded joints to ensure integrity.

Boss, head, and hydrotest-closure designs based on the Appendix II analysis, are presented in Figures 12 through 15. Heat-treatable stainless steel (Type 17-4PH, Condition A, heat-treated in accordance with MIL-H-6875 to Condition H) was used for the bosses in order to reduce section sizes to a reasonable thickness.

Only the forward boss had an opening; the aft boss was permanently closed to eliminate an additional leakage source during hydrostatic testing. This boss had an inside axially located threaded spud for winding-shaft attachment. The size of the diameter opening in the forward boss (1.75 in.) was established by the size of the seam welding backup roller fixture which could be removed from the vessel interior after welding. An internal buttress thread was first considered for attachment of the hydrotest plug and as a means of installing the mandrel shaft for the filament-winding operation. The design was subsequently revised to a plug which was joined to the boss by electron-beam welding because of the excessive cost required for machining the thread and the positive sealing method resulting from welding. The forward boss had six No. 8-32 equally spaced threaded holes for mandrel shaft attachment. The forward boss was designed with a straight, stepped, aperture bore for simplicity and low cost.

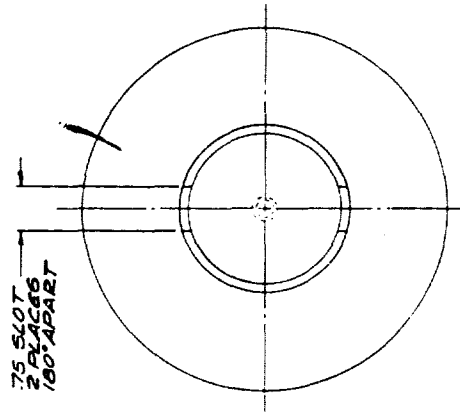
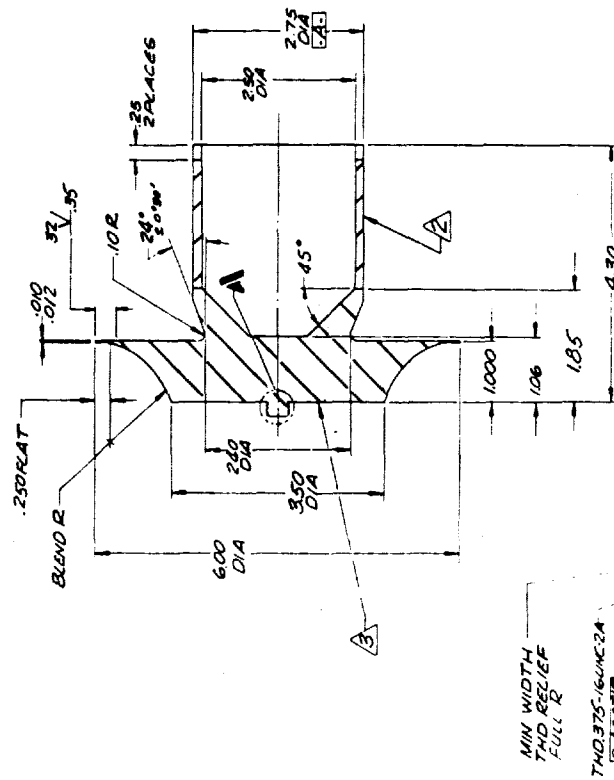
The physical properties of a number of materials that could be filament-wound to form layers of the composite shell were reviewed and summarized in Table III. Filaments examined for the program were considered on the basis of the tensile modulus, winding-tension limits, strength, and cost. The program did not consider the more expensive and experimental advanced fibers, but the data covered in Table III did cover the complete spectrum of available properties.

Table IV summarizes the characteristics of candidate resin systems. A rigid resin with high compressive strength was expected to be required for the inner layers. Otherwise, the high bearing stresses induced by the small fiber diameter and high force on the layer might cause the fibers to cut themselves. The outer layers were expected to employ a tough resin with high elongation to minimize crazing (and thus avoid moisture penetration) of the surface at operating pressures, and increase the service life. A protective coating was applied to the outside surface of the vessels to ensure maximum service life; it was not expected that complete prevention of crazing could be attained. The coating was designed to offer moisture and abrasion resistance for the vessel.





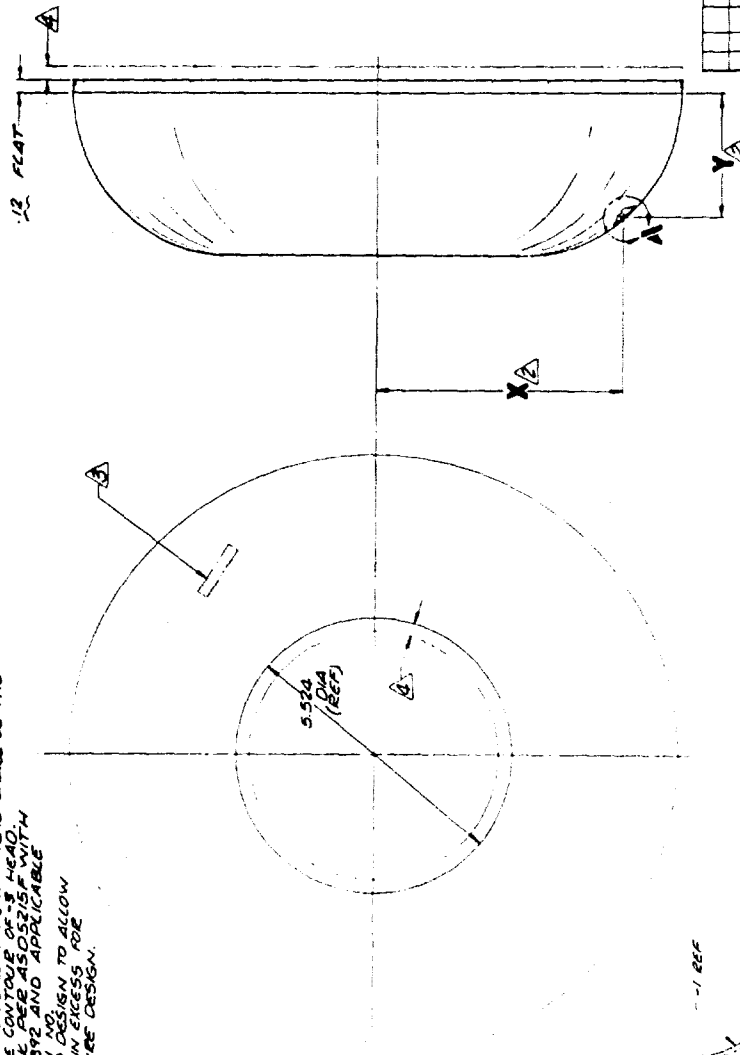
- NOTES: 1. REMOVE ALL BURRS AND SHARP EDGES  
 2. NOTED SECTION MAY BE FABRICATED AS A SEPARATE PART & WELDED  
 3. MARK PER ASD5215F WITH 126890-1.  
 4. ALL MACHINED SURFACES TO BE 125 UNLESS OTHERWISE NOTED.  
 5. HEAT TREAT PER MIL-H-6075 TO COND H-900.



REV	SYN	CODE	IDENT	DESCRIPTION	DATE	BY	CHKD	APP'D	DESCRIPTION	DATE	BY	CHKD	APP'D	DESCRIPTION	DATE	BY	CHKD	APP'D	DESCRIPTION	
1																				
MATERIAL: 17-4 PH C885 SPECIFICATION: AMS-55689 MANUFACTURER: AEROJET-GENERAL CORPORATION PART OR DESCRIPTION: AFT BOSS FOR WELDED LINER DRAWING NO: 126890-1 SCALE: D 70143 RELEASE DATE: 2-27-64										FINISH: 125 TOLERANCES: 125 DIMENSIONS: 125 SURFACES: 125 UNLESS OTHERWISE SPECIFIED DIMENSIONS ARE IN INCHES DECIMALS ARE IN THOUSANDS ANGLES ARE IN DEGREES UNLESS OTHERWISE NOTED DO NOT SCALE DIMENSIONS TREATMENT: 125										

Figure 13. Aft Boss for Welded Liner.

NOTES: 1. MAKE ALL DIMS AND DIMENSIONS IN INCHES.  
 2. COORDINATES DENOTE INSIDE CONTOUR OF -1 HEAD.  
 3. THE OUTSIDE CONTOUR OF -1 HEAD SHALL BE THE INSIDE CONTOUR OF -3 HEAD.  
 4. HEADS ARE TO BE DESIGN WITH 1/8" RADIUS AND APPLICABLE DASHING.  
 5. MAKE DESIGN TO ALLOW 25 MIN EXCESS FOR FUTURE DESIGN.



CONTOUR	
X <sub>E</sub>	Y
5.966	0.000
5.967	0.385
5.972	0.517
5.989	0.689
5.045	0.860
5.765	1.032
5.721	1.203
5.648	1.373
5.552	1.543
5.448	1.712
5.329	1.880
5.194	2.047
5.042	2.212
4.868	2.375
4.671	2.535
4.446	2.690
4.185	2.839
3.878	2.977
3.509	3.096
3.046	3.172
2.762	3.172



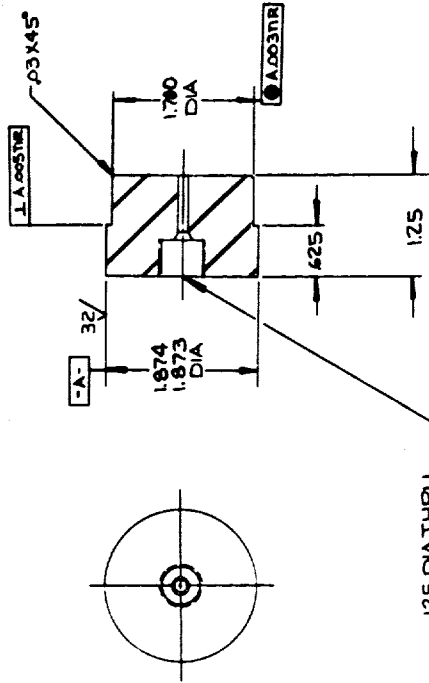
310  
 # 1054  
 F-14

REV	DATE	BY	CHKD	APP
1				
2				
3				
4				
5				
6				
7				
8				
9				
10				
11				
12				
13				
14				
15				
16				
17				
18				
19				
20				
21				
22				
23				
24				
25				
26				
27				
28				
29				
30				
31				
32				
33				
34				
35				
36				
37				
38				
39				
40				
41				
42				
43				
44				
45				
46				
47				
48				
49				
50				
51				
52				
53				
54				
55				
56				
57				
58				
59				
60				
61				
62				
63				
64				
65				
66				
67				
68				
69				
70				
71				
72				
73				
74				
75				
76				
77				
78				
79				
80				
81				
82				
83				
84				
85				
86				
87				
88				
89				
90				
91				
92				
93				
94				
95				
96				
97				
98				
99				
100				

Figure 14. Forward and Aft Heads for Welded Liner

NOTES:

1. REMOVE ALL BURRS AND SHARP EDGES.
2. MARK PER ASD5215D WITH 1268922-1.
3. ALL MACHINED SURFACES TO BE 125 UNLESS OTHERWISE SPECIFIED
4. HEAT TREAT PER MIL-H-6875 TO COND H-900.



.125 DIA THRU  
C BORE .5065 / .5106 DIA  
X .44 DEEP  
C SK 60° X .188 DIA  
.562-18 UNF-38 X MAX DEPTH

QTY REQD	SYM	CODE IDENT	PART OR IDENTIFYING NO.	NOMENCLATURE OR DESCRIPTION	MATERIAL	SPECIFICATION	UNIT WT.	ZONE NO.	ITEM NO.
			-1		2.00 DIA, 17-4 PH SST				
<p>UNLESS OTHERWISE SPECIFIED DIMENSIONS ARE IN INCHES TOLERANCES ON DECIMALS ±.005 ±.010 DO NOT SCALE DRAWING</p> <p>TREATMENT: <b>A</b></p> <p>SYMBOL TO ACTUAL CALG WT</p> <p>DRAWING LEVEL: <b>O</b></p> <p>ON THRU PART NOT FINAL USED ON EFFECTIVE SERIAL NO. APPLICATION DRAWING LEVEL</p>									
<p>LIST OF MATERIALS</p> <p><b>AEROJET-GENERAL CORPORATION</b> AZUSA, CALIFORNIA</p> <p>CONTRACT NO. <b>10-2-66</b> PART NO. <b>18-2-54</b> REV. <b>10-1-66</b> BY <b>W. J. Campbell</b> DATE <b>10-28-66</b></p> <p>DESIGN ACTIVITY AND DRAWING BY <b>10-1-66</b> OUTNUMBER <b>1268922</b></p> <p>SCALE: <b>C</b> 70143 DWG NO. <b>1268922</b> RELEASE DATE: <b>10-23-66</b> SHEET</p>									

Figure 15. Hydrotest Closure for Thick-Wall, Filament-Wound, High-Pressure Container

TABLE III  
MATERIALS AVAILABLE FOR FILAMENT WINDING

Filaments	Room-Temp Values			Remarks
	Tensile Modulus 10 <sup>6</sup> psi	Ultimate Tensile Strength ksi	Density lb/cu in.	
Steel, 4-Mil Rocket Wire				
Standard Type 302	29	325	0.283	---
Standard music wire	30	439	---	---
N-S carbon steel	29.3	575	---	---
N-S 355 stainless	---	500	---	---
N-S T302	---	400	---	---
"Elgiloy"				
Single 2-mil wire	---	173	---	---
"Rene 41"				
Single 6-mil wire	32	300	---	---
"Chromel R"				
Single 2-mil wire	---	134	---	---
Glass Monofilaments				
ECG 140/HTS	10.5	500	0.092	Commercial production
S-901	12.4	650	0.088	Commercial production
4H-1	13.9	700	0.091	Experimental
Hi-Stren 198	13.0	780	0.090	Pilot-plant production
970-S-36	15	800	0.091	Experimental
Other				
Titanium-clad beryllium	45	150	---	---
Boron, 4 mil	60	300-450	0.090	Production for laboratory research
Graphite, "Thornel 25"	25	200	0.054	Pilot-plant production
Graphite, "Thornel 50"	50	300-400	0.054	Laboratory production
Carbon	6	180	---	Pilot-plant production
Silicon carbide	70	300-400	0.115	---

TABLE IV  
CANDIDATE RESIN SYSTEMS\*

	Elonga- tion, %	Strength, ksi		Modulus, ksi		Notch Toughness psi in.
		Tension (Ulti- mate)	Compres- sion	Ten- sion	Compres- sion	
DER 332/HHPA/BDMA (100/84/0.5 pbw)	3.4	12.1	17.8	450	480	454
"Epon 828"/"Epon 1031"/ MNA/BDMA (58-68R system = 50/50/90/0.5 pbw)	3.0	11.8	21.0	480	600	377
DER 332/"Epi-Cure 855" (20%)						
(100/90 pbw)	20-25	3.5	---	170	---	---
(100/100 pbw)	50-60	2.2	---	87	---	---

\* DER 332 = proprietary epoxy resin; HHPA = hexahydrophthalic anhydride; BDMA = benzyl dimethylamine.

"Epon 828; and "Epon 1031" = proprietary epoxy resins; MNA = methyl nadic anhydride.

"Epi-Cure 855" = proprietary epoxy resin. Ratios shown parenthetically give parts by weight (pbw).

Twenty-end, S-901 glass roving, impregnated with the 58-68R<sup>(2)</sup> epoxy resin system was selected for the first half of the filament-wound layers. The S-901 glass filaments were selected for the reinforcement because the material was the highest strength glass filament commercially available. The filament, preimpregnated with a 58-68R resin system was also available in uniform high quality. This well characterized material had proved acceptable on numerous Air Force, Navy, and NASA programs. With the prepreg material there was less tendency of the resin to flow; therefore, there was a protective layer around the filaments to prevent the fibers from cutting each other as a result of high compressive loads. The 58-68R resin system possessed the high compressive strength required for the inner layers of the vessel - a necessary property in view of the high radial compressive stresses produced by the design burst pressure of 33.00 ksi. The high-compressive-strength resin would prevent the fibers from cutting themselves despite the high bearing stresses induced by the small fiber diameter and the high radial force on the inner layers.

The Phase I analytical studies showed that one filament material could be used with a proper tension program during winding. The studies also indicated that maximum performance in the outer layers of the structure, where radial compressive stresses were lower, could be achieved through the use of a tough, flexible resin. Therefore, it was initially planned to wind the outer half of the composite vessel with 20-end, S-901 glass roving in-process impregnated with the epoxy resin "Epon 828"/"Epi-Cure 855." This resin system, in a 100/60 pbw ratio, was extremely tough and had a 10.5% elongation.

<sup>(2)</sup>58-68R = "Epon 828"/"Epon 1031"/MNA/BDMA (50/50/90/0.5 parts by weight).

## SECTION V

### PRESSURE-VESSEL FABRICATION AND TESTING (PHASE III)

The performance of the glass-filament-wound, thick-wall, high-pressure gas-storage containers was evaluated in Phase III. A total of 16 vessels were fabricated and tested in lots of 9, 3, and 4 units each. Processing problems encountered early in the phase contributed to the initial low burst pressures, and resulted in variations in processing techniques and materials of construction. Material parameters and fabrication techniques were modified extensively during fabrication of the first nine units (TW-1 through TW-9) in order to resolve the problems encountered. Basic changes in the next three vessels (TW-10 through TW-12) resulted in utilizing higher winding tensions and a wider band width. The final iterative design was reflected in the last four units (TW-13 through TW-16). All phases of pressure-vessel fabrication are discussed below, together with the test results. Specific problem areas in fabrication and test are reviewed in detail.

#### 1. METAL LINER

The same liner configuration was used throughout the program because of the long lead period required for liner fabrication and delivery, and because of cost considerations. Liners were fabricated from 0.006-in.-thick Type 347 stainless-steel foil using fabrication techniques which included pressure-forming of the head sections, machining of the axial bosses, and roll-resistance seam welding of the components. The head sections of the liner were fabricated by a hydroforming process in which the metal-foil was cut to the required size, placed between thin mild-steel plates, and positioned on the work table. A pressure dome was lowered onto the steel plates, and hydraulic pressure was applied.

A male punch moved upward, forcing the steel plates against a rubber diaphragm backed by hydraulic fluid under controlled high pressure. As the punch moved upward, proper control of the pressure in the dome (or forming cavity) caused the diaphragm to form the metal to the exact configuration of the punch. The punch was then lowered, the dome was lifted, and the part was removed. Negligible part thin-out occurred, because this was a forming rather than a drawing operation. After each hydroforming operation, the mild-steel plates were discarded. Each formed metal-foil head section was stress-relieved and trimmed to the required dimensions. A center opening was cut to accommodate the boss. Typical formed head sections are presented in Figure 16.

The axial bosses were machined from stainless-steel bar stock (Type 17-4PH). The forward and aft bosses are shown in Figures 17 and 18, respectively. Particular care was taken to maintain the flange thickness at the edge at 0.010 to 0.012 in.

Resistance-roll-seam welding was used to join each boss fitting to the center opening of the head and to join the head sections to each other. A typical section of the boss was fabricated and heat treated, and rings to simulate the liner were stamped of 0.006-in.-thick Type 347 stainless steel. These specimens, shown in Figure 19, were then resistance-seam welded to



Figure 16. Head Sections of Liner



Figure 17. Forward Boss



Figure 18. Aft Boss



Figure 19. Seam-Welded Specimens

establish the required welding machine parameters prior to welding the actual liner components. Sections of the welds were subsequently X-rayed and found to have full penetration and to be continuous.

Liner components are fixed in position by spot welding prior to the roll-resistance-seam welding. The bosses were then welded to the head sections as shown in Figure 20. As noted in Figure 21, forward and aft head sections were joined with the aid of a special collapsible electrode roller assembly which was inserted and removed after welding through the forward boss opening. The weld thus produced consisted of a series of overlapping spot welds made progressively along a lapped joint with the roller-type electrodes.

The completed liner assembly is presented in Figure 22. Particular attention was given to handling and shipping the thin-wall liner assemblies. Special crates shown in Figure 23 were designed and fabricated to facilitate shipping and prevent possible damage to the thin-wall liners.

Each welded metal liner was subjected to a total of three separate leakage tests before filament winding was initiated. First, the welder made a dye-penetrant test by applying a liquid penetrant on each welded joint and viewing for imperfections and discontinuities. In the second test, the welded areas were examined after application of a soap solution over and around each joint and internal pressurization of the tanks. A final, more sensitive, mass spectrometer test was performed by placing the liner assembly in an enclosed aluminum tank and creating a vacuum inside and outside the liner. Helium gas was used to pressurize the liner to 5 psig while the area between the liner and aluminum tank was monitored for traces of helium leakage. All metal-foil liners successfully passed the tests.

Typical sections of the Type 17-4PH stainless-steel forward boss and hydrotest closure (Figure 24) were fabricated and electron-beam welded to establish welding machine parameters. This work was done on samples rather than on finished parts. A section (Figure 25) was cut across the welded area, polished, etched, and inspected. Visual inspection of the section and examination of subsequent X-rays, indicated that no problems in the weld were to be expected. A section identical to the one above was fabricated and electron-beam welded using the established parameters (Figure 26). X-rays were taken to ensure integrity of the weld. This simulated boss-and-closure assembly was then hydrostatically tested to verify adequacy of the weld and the threaded center hydrotest fitting. Leakage was not encountered, and the specimen sustained an ultimate internal pressure of 35.00 ksi. Figure 27 shows the hydrotested specimen.

## 2. FILAMENT WINDING

Fabrication procedures were defined for the vessels constructed on the program. These procedures, presented in Appendix III, reflect the finalized approach adopted after the initial processing problems had been corrected. The detailed discussions below present fabrication approaches, problems, corrective actions, and other specific data considered significant with regard to the filament winding of the vessels during Phase III.

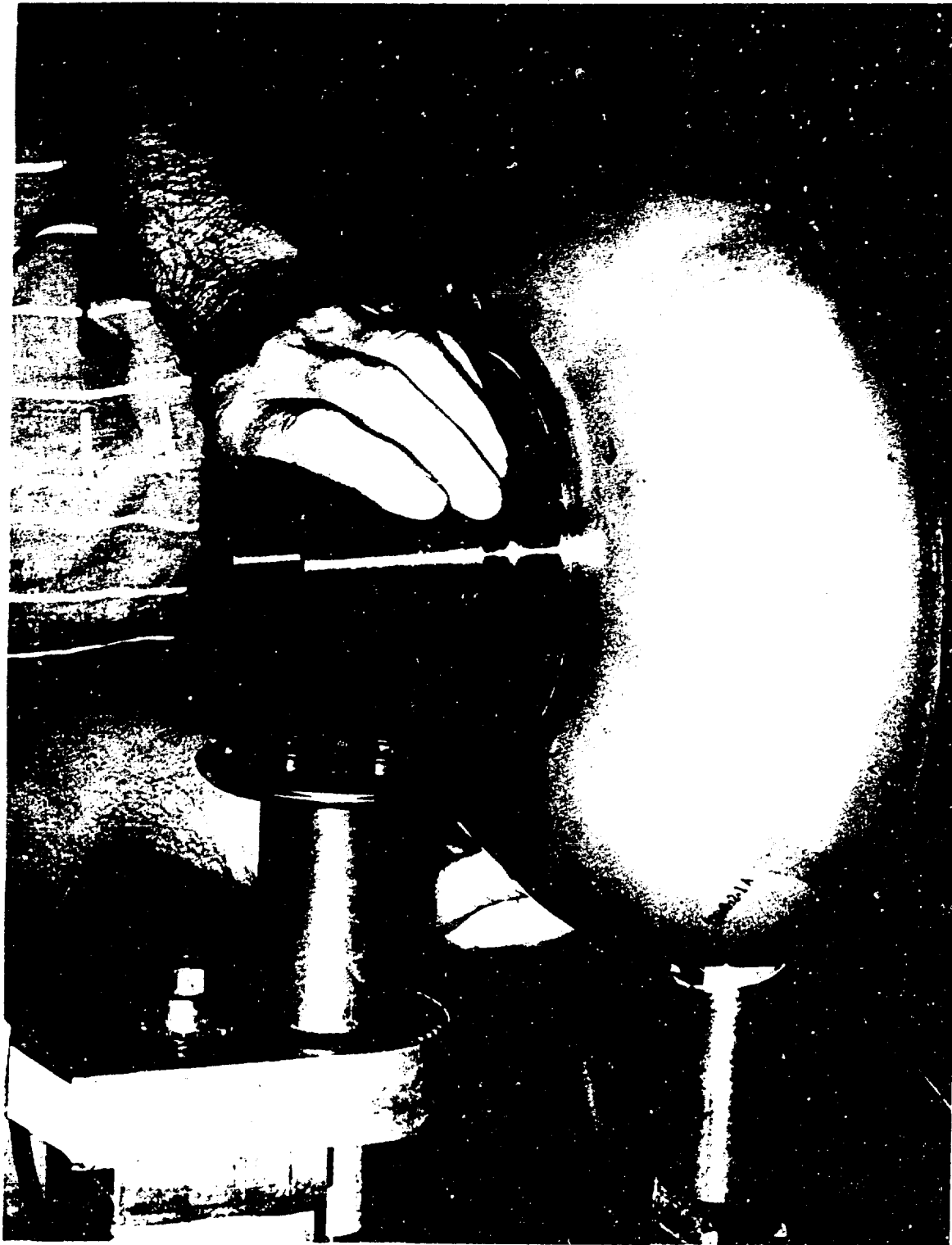


Figure 20. Boss-to-Head Weld



Figure 21. Head Section Weld

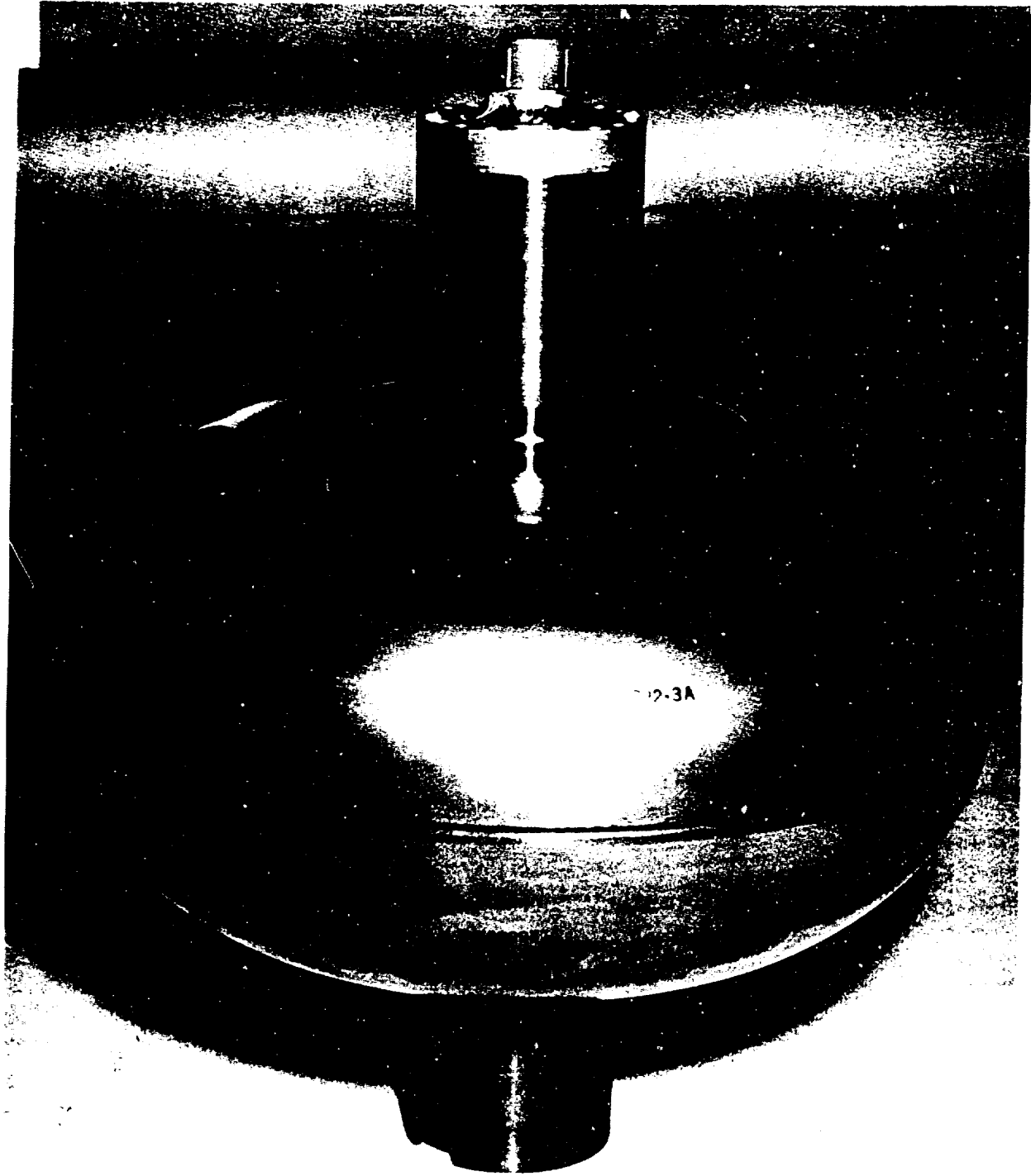


Figure 22. Completed Liner

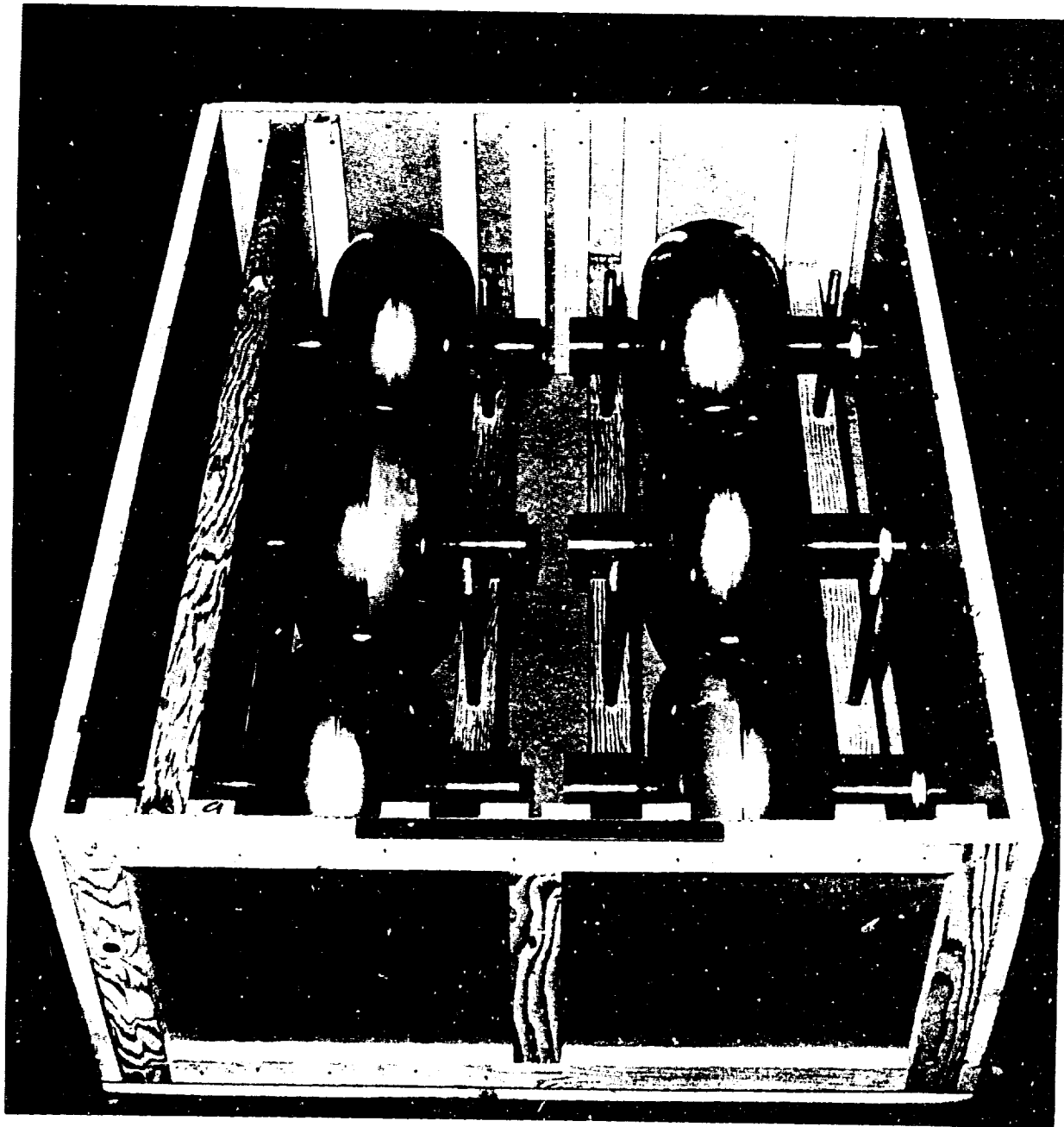


Figure 23. Completed Liners in Shipping Crate

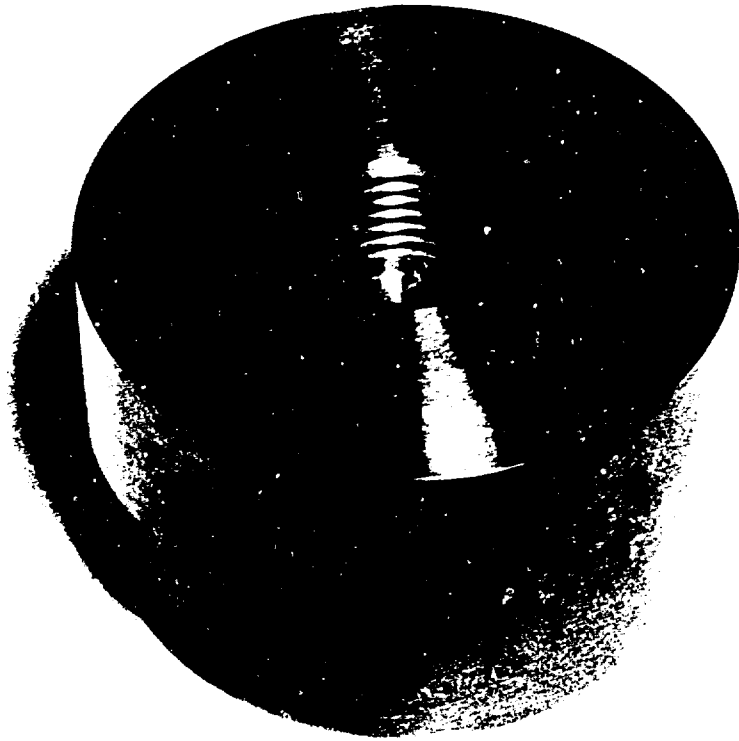


Figure 24. Hydrotest Closure

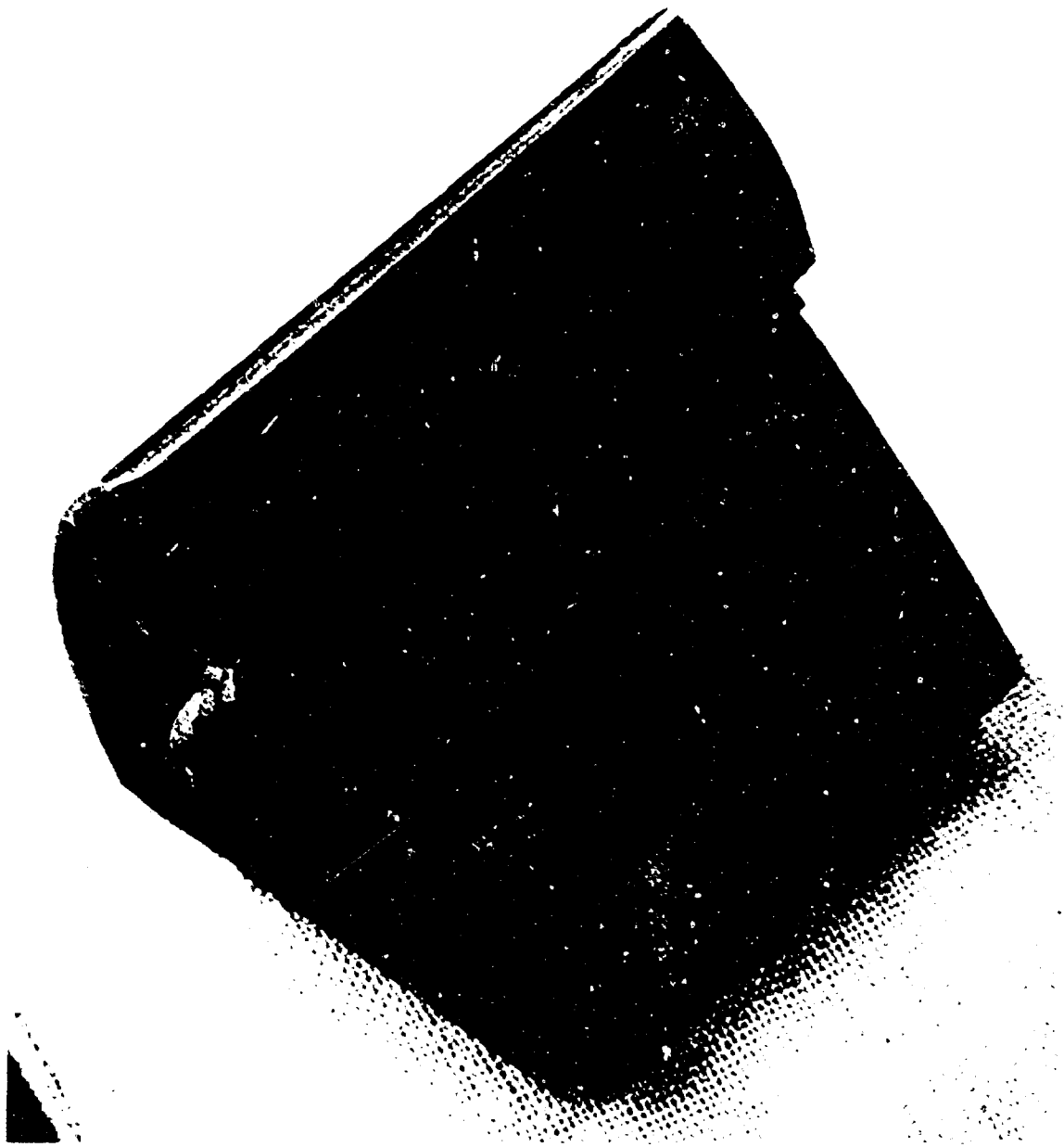


Figure 25. Electron-Beam Weld Section



Figure 26. Electron-Beam Closure Weld



a. Fabrication Over Wood Mandrel

In order to establish winding parameters, evaluate tooling fixtures, and resolve unanticipated winding questions, a wood mandrel (Figure 28) was fabricated with an outside configuration identical to that of the metal liner. Preparations were then made for trial winding runs. The standard winding shaft (Figure 29) to be used in overwrapping on the actual liners was inserted into the wood mandrel, assembled on the filament-winding machine, and tightened in place.

The mandrel was then overwound with 17 double layers (revolutions) of S-901 glass/58-68R epoxy resin prepreg roving (as shown in Figure 30), vacuum-bagged, and cured in accordance with the fabrication instructions. After cure (2 hours at 150°F, 2 hours at 250°F, and 4 hours at 325°F) and removal of the vacuum bag, the unit was wet-wound with 18 double layers of S-901 glass roving in-process-impregnated with a high-elongation resin system ("Epon 828"/"Epi-Cure 855") in a ratio of 100:60 parts by weight. The unit was again vacuum-bagged, and cured for 16 hours at room temperature and 2 hours at 212°F, as determined by an imbedded thermocouple in the composite. The completed unit was then halved for visual inspection of the plies. The appearance of the cross section was excellent, as can be verified from Figure 31. A slight resin-rich area can be seen between the two wraps, below the knuckle near the bosses. This was caused by compaction of the prepreg layers and slight bridging of the first wet-wound layers. No problems were anticipated in connection with this resin-rich area; however, had such problems arisen, glass-reinforcement doilies or an epoxy filler material could have been used to fill the resin-rich area.

Slight slippage of the wet-wound roving was experienced during the winding of the final layers on the wood mandrel. A modification of the winding head was expected to eliminate this slippage. A more thorough wiping action was utilized to remove excess resin from the tape, and thereby reduce resin carryover to subsequent layers which contributed to the slippage. The sectioned overwrapped wood mandrel, with an overlay to show the liner-to-overwrap relationship, is shown in Figure 32.

Four strain-gage instrumentation pins were located within the composite during winding to evaluate the effect of winding over these pins. Winding and vacuum-bagging over the pins was somewhat difficult; two pins were broken during processing. Preparations were made to wind the actual vessels at a slower rate whenever the pins were overwound.

b. Vessels TW-1 Through TW-9

After successfully passing the helium spectrographic leak test, the first metal liner assembly (TW-1) was coated on the inside with the plaster mandrel, and cured. Fatigue-type strain gages were then applied to the surface of the cleaned liner, followed by application of an 0.002-in. nylon scrim cloth impregnated with the 7343/7139 resin system. The unit was then overwrapped as shown in Figure 33, and processed in accordance with the detailed fabrication instructions (i.e., 17 layers of prepreg, vacuum-bag, cure; then 18 layers of wet winding, vacuum-bag, cure, and application of the moisture-resistant coating). A winding tension program established in accordance with the analytical

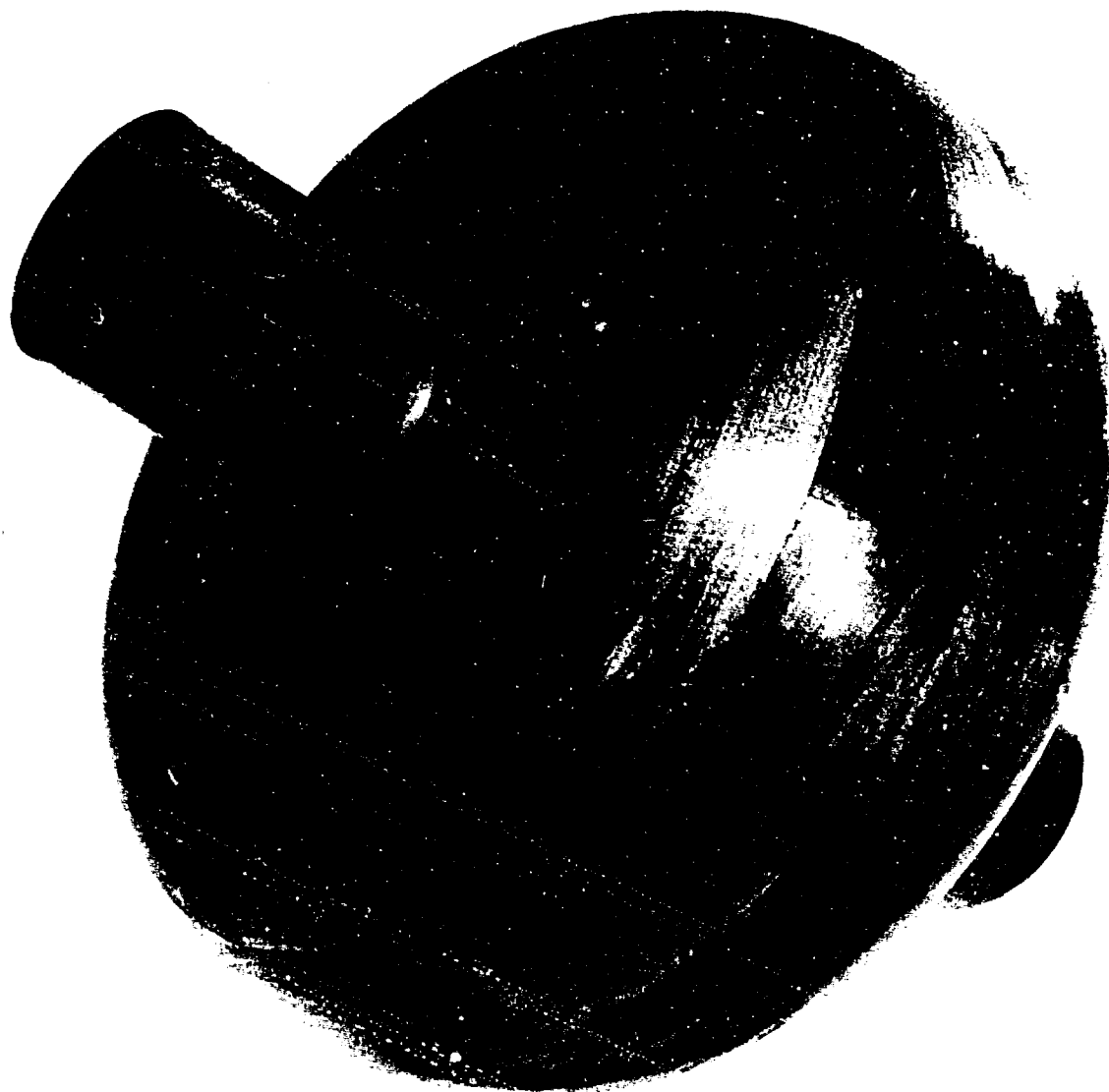


Figure 28. Wood Mandrel





Figure 30. Wood Mandrel Being Wrapped

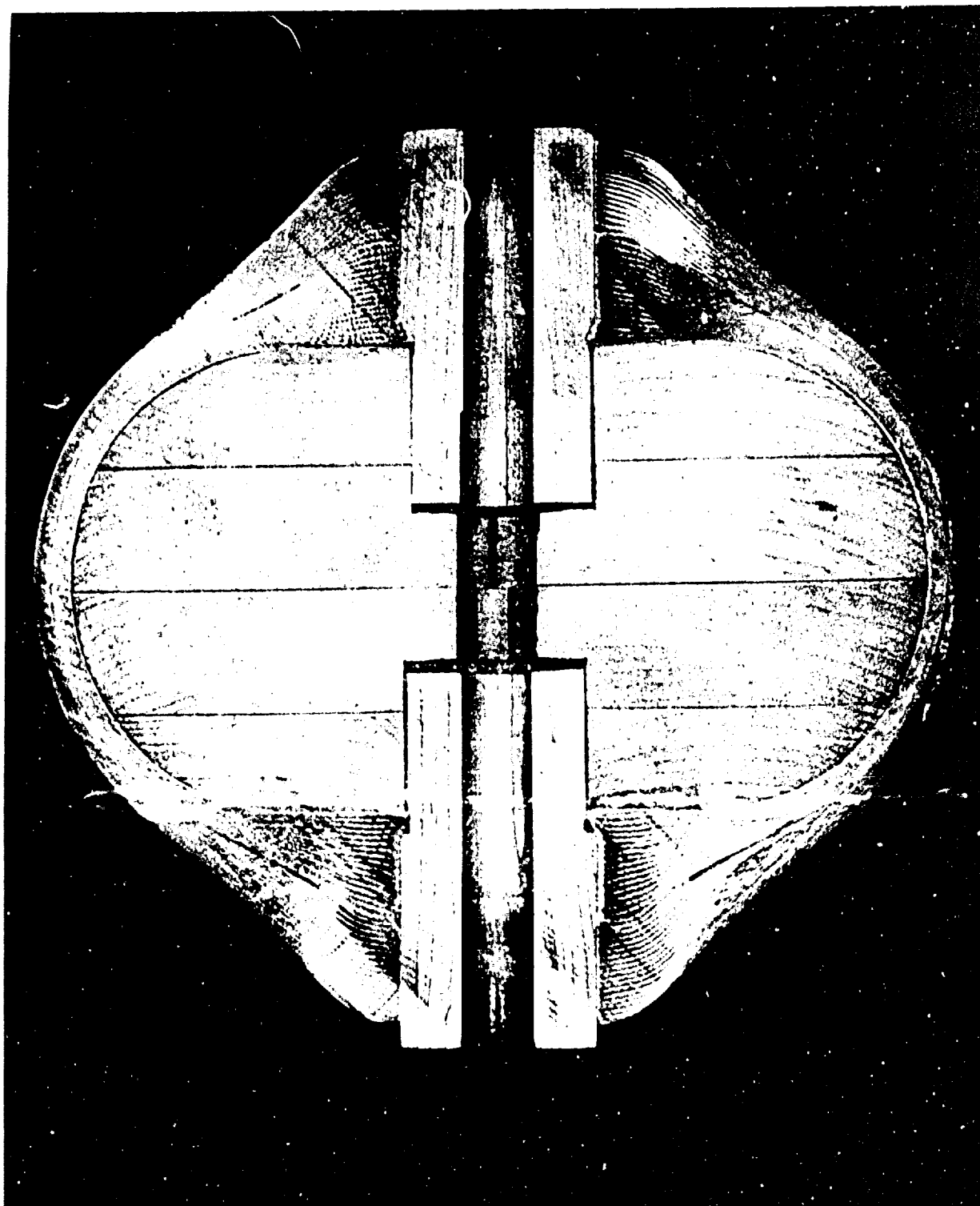


Figure 31. Sectioned Overwrapped Wood Mandrel

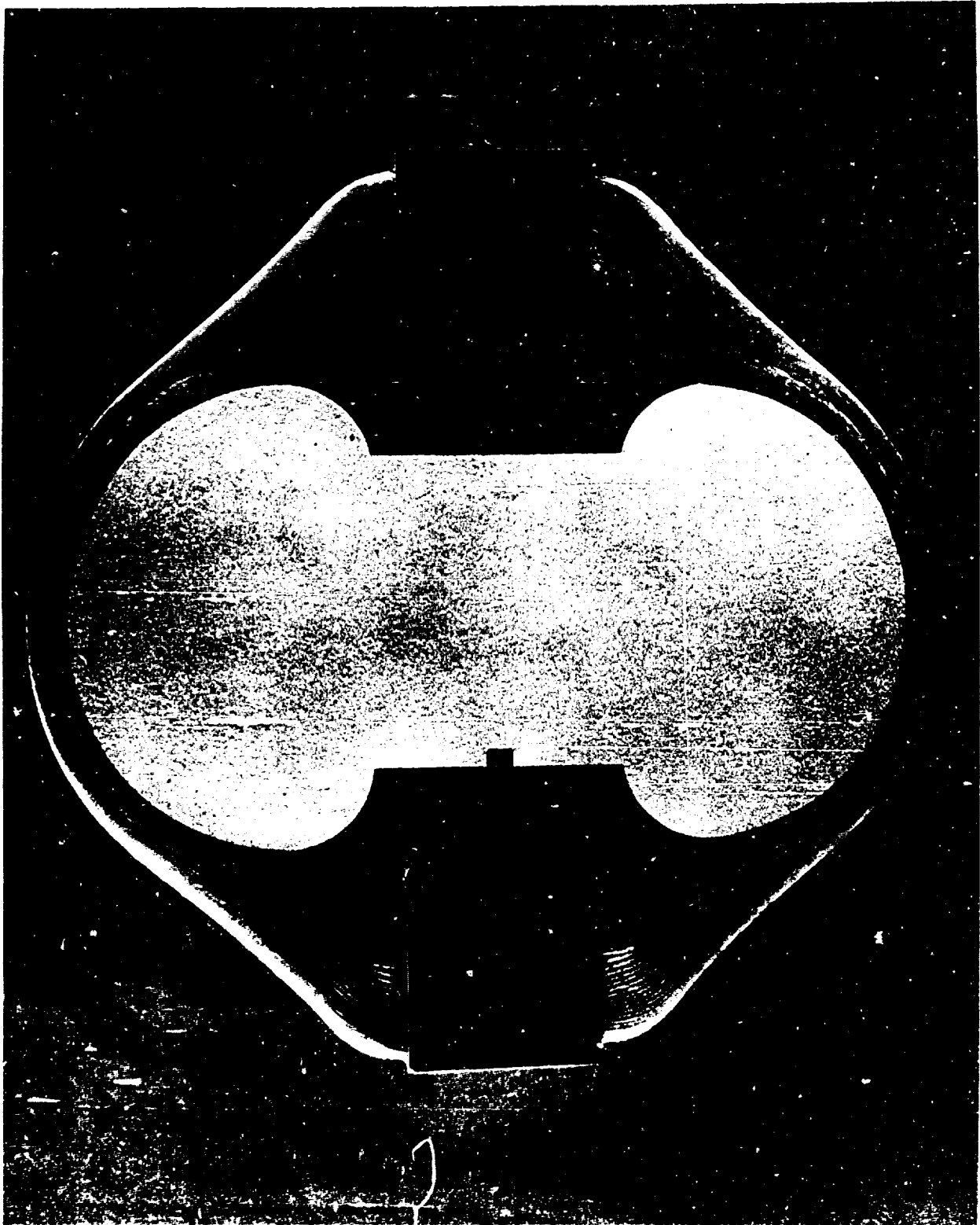


Figure 32. Sectioned Overwrapped Wood Mandrel with Overlay



Figure 33. Winding of Container TW-1

studies of Phase I was used throughout winding. The appearance of this unit after final wind was excellent; no slippage was experienced during wrapping (see Figure 34). Difficulties were again experienced during winding over the strain-gage instrumentation pins (five pins were lost). Subsequent instrumented units employed fine wire leads to run from the strain gage along the composite to the boss. After the plaster mandrel of TW-1 was washed out with a warm 15% acetic acid solution, the forward boss closure was welded in place with an electron-beam welder.

During inspection of the interior of the TW-1 vessel - after plaster mandrel washout and prior to closure installation and welding - slight compressive buckling of the metal liner was noted. This buckling was believed to have been caused by partial failure of the plaster mandrel due to the imposed winding pressure, or inadequate bond between the liner and the overwrapped composite layers, or both.

Calculations showed that, with an increasing tension program (from 4 to 20 lb/20-end roving), the total pressure imposed on the mandrel at the completion of winding is approximately 3.00 ksi. A rigid, strong mandrel is therefore needed to support the high compressive load. In view of the support given the liner by the mandrel shaft, and the fact that the filament-wound composite was step-cured at the midpoint of winding, the plaster (if uniformly cast and properly cured) should have had sufficient strength to support the winding load. It was suspected that the small forward boss opening made it difficult to accomplish water vapor removal during plaster curing. Thus, the desired maximum strength achieved in the plaster by drying at elevated temperatures was not attained.

Changes in casting and curing techniques were investigated. The next three liners were cast full with plaster (except for a 1-in. tapered opening for the mandrel shaft). The plaster in the first of these units was cured at 175°F, using a gradually decreasing vacuum on the exposed interior plaster surface to remove the water vapor from the curing plaster. Shrinkage of the plaster surface away from the liner was noted after 54 hours. The second liner was oven-cured using 1-1/2 in. of vacuum, and the third liner was oven-cured with the addition of circulating warm air on the exposed interior plaster surface. Shrinkage of the plaster away from the liner occurred on both units. (Shrinkage was noted by observing that the metal liner was "springy" - not tight on the plaster.)

A fourth liner was cast with green plaster and then overwound with eight layers of roving without curing the plaster. This unit, TW-2, which was wound entirely using glass roving preimpregnated with the 58-68R epoxy resin system, was step-cured after the 8th, 16th, 24th, and 32nd layers had been wound. With this approach it was believed that the successive cured laminate shells would act as successive mandrels to help support the increasing winding load and inhibit liner buckling. Examination of the vessel interior after the plaster washout operation revealed that this method had significantly reduced buckling. However, slight wrinkling adjacent to the boss welds was still observed.

It was noted after the pressure test that the wrinkles adjacent to the welds had been bent and crimped. The liner was cracked at some of the

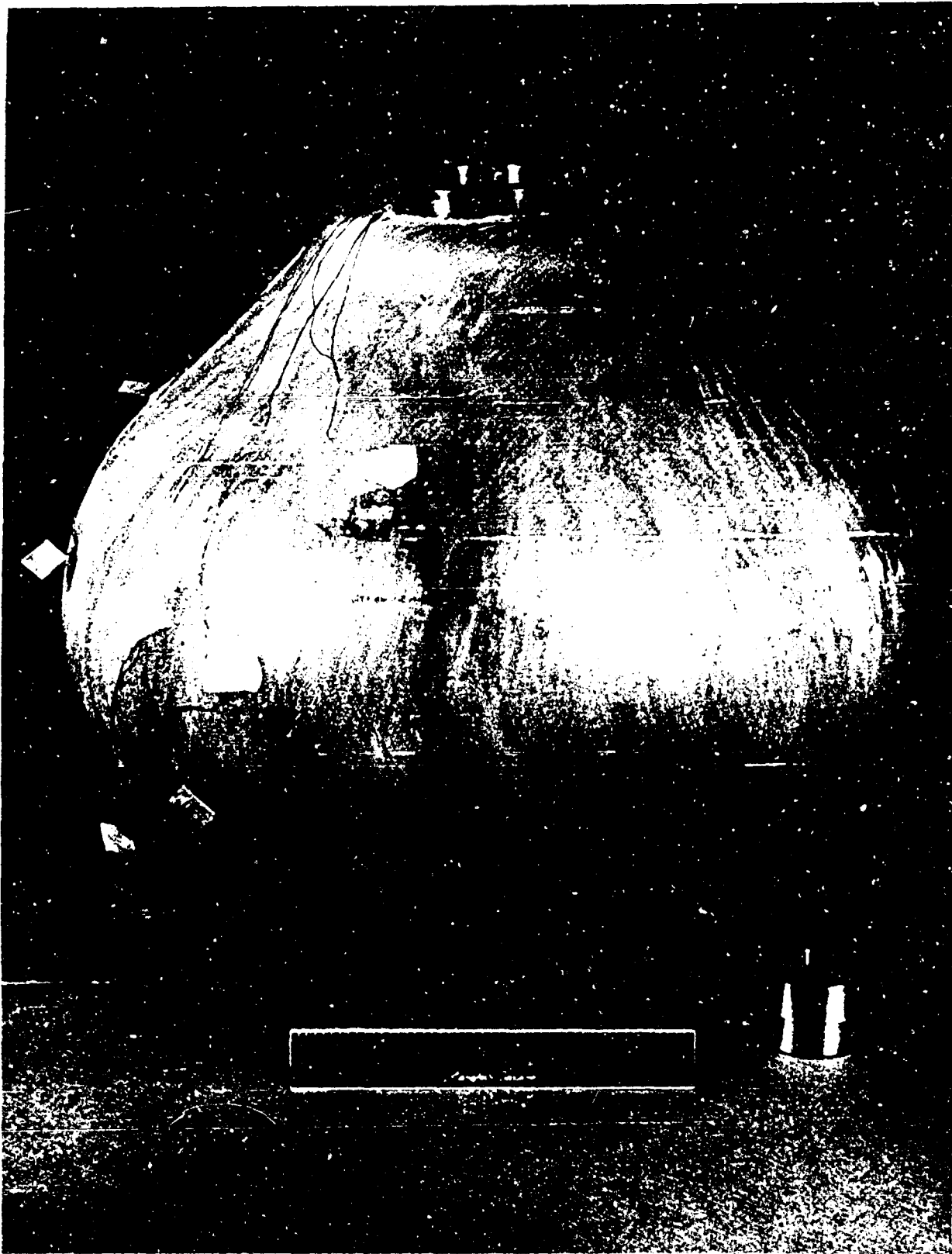


Figure 34. Container TW-1 Before Closure Welding

crimp points. These cracks were obvious leak paths. It was apparent that the liner must be tight against an incompressible mandrel during winding in order to eliminate wrinkling and subsequent liner leakage. Conclusions from the investigation were that there was no apparent improvement for this particular design resulting from either the use of internal pressure during casting and cure, or the use of a gradually decreasing vacuum on the exposed internal plaster during elevated-temperature cure to remove water vapor from the curing plaster.

(1) Mandrel Support for Liner

An Aerojet-sponsored program was initiated on the development of an improved mandrel for support of the metal liners during winding in an attempt to resolve the problem of liner wrinkling due to inadequate mandrel support. Basic requirements for the mandrel material were (a) dimensional stability (i.e., no shrinkage on curing), (b) a coefficient of thermal expansion approximately that of the metal liner, (c) castability, (d) ease of removal, and (e) sufficient compressive strength and modulus.

Aerojet's approach in past programs for providing mandrel support to thin metal liners has been to cast a shell of soluble mandrel material inside the liner, cure the mandrel, overwind and cure the pressure vessel, and then wash out the mandrel. This approach has been successfully utilized by Aerojet in various programs and more recently in work with thin-metal-foil-lined vessels (References 8 and 9). It was initially planned in this program to introduce the soluble Kerr DMM plaster in liquid form through the forward boss opening and rotate the liner under slight internal pressure until a uniform hardened coating was formed. Additional plaster was to be cast in subsequent operations until the desired thickness was obtained. The liner and plaster were then to be oven dried for a minimum of 24 hours at 200°F to evaporate sufficient water and produce a rigid support structure for filament-winding.

(a) Plaster Mandrel

Laboratory tests were run to ascertain if the basic Kerr-DMM material was satisfactory. The material was found to have the correct chemical constitution and properties. Other brands of washout plaster were also investigated. Although set expansion was claimed for several plasters (including the Kerr-DMM plaster), cast samples showed less than adequate dimensional stability for use with the metal liners. Furthermore, it was found that when plaster samples were subjected to a simulated filament-wound composite resin matrix cure at 300°F, the condition became even worse. For example, cylinders of Kerr-DMM plaster measured 3.823-in. in diameter and 4.923-in. long before cure, and 3.816-in. in diameter and 4.920-in. long after 300°F cure cycles. Ultracal 30 plaster measured 3.828-in. in diameter and 4.962-in. long initially and 3.822-in. in diameter and 4.969-in. long after 300°F cure.

(b) Tin-Bismuth-Alloy Mandrel

Investigations were made of casting techniques required for the use of a tin-bismuth alloy (with melting point of 281°F) as a

liner support. This material, which expands +0.92% on freezing, was cast into a 0.006-in.-thick, 12-in.-dia. stainless-steel liner as the liner was being rotated. After the casting was completed, and the unit cooled down, inspection revealed that the mandrel was tight against the liner. However, because of the high density of the alloy, it was very difficult to cast into the thin liners.

(c) Pressure Mandrel

A pressure mandrel system has been developed and successfully used by Aerojet. This approach was used during the fabrication of Containers TW-3 and -4, and -6. At the completion of winding and during the cure of TW-3 and -4, 1500 psig (about 5% of the ultimate pressure) was maintained to support the liner. Even at this extreme mandrel pressure, no processing problems were encountered. After resin cure and removal of the hydraulic fluid, the interior of the liners of TW-3 and TW-4 (wound with a programmed tension of 3 to 12 lb/20-end) were inspected. Small ripples were noted in the metal liner at the roving crossover points. Only four double layers of roving at a 4 lb/20-end constant tension were wet-wound on Container TW-6. After cure, inspection of the chamber interior again indicated the presence of ripples in the metal liner at the roving crossover points.

This slight rippling is attributed primarily to the shape of the liner - a shape substantially different from the neutral axis configuration of the complete wound tank. The design head shapes for the liner and completed container are based on the thickness of the overwrap, which varies from about 0.5 in. at the equator to almost 3.0 in. adjacent to the bosses. When the liner is pressurized alone, however, or with less than the full thickness of overwrap, the shape is not the ideal design configuration to carry the pressure load and is therefore susceptible to distortion and subsequent wrinkling of the thin liner.

(d) Sand-Acrylic Mandrel

The most promising results have been obtained using a castable sand-acrylic mandrel material which dissolves in water. Compressive strength of the material is high, and dimensional stability is excellent. This material was used for mandrel support of the 12-in. dia by 0.006-in.-thick liners of Container TW-5, -7, -8, and -9 during overwrapping with 70 layers of glass roving under tensions ranging from 4 lb/20-end to 12 lb/20-end. Inspection of the tank interior after mandrel removal showed a good, solid mandrel support had been provided to the liner.

(2) Liner-to-Composite Adhesive Bond

Unlike the metal liner, which has both elastic and plastic components in its stress-strain curves, glass filaments are elastic throughout the entire stress-strain range. When a metal-lined, glass-filament-wound vessel is loaded to its operating strain of about 2%, the liner strains elastically to its yield point (about 1/4 to 1/2% strain), and then plastically (about 1-1/2 to 1-3/4%) to the operating strain level. On depressurization, the metal liner springs back along its offset strain-stress curve, recovering about 1/4 to 1/2% strain elastically. It is then pushed plastically into high

compression where it remains so long as the liner does not buckle from the compressive stress. For thin, smooth, metal liners with high diameter-to-thickness ratios, an adhesive bond between the metal liner and filament-wound-composite tank wall is required to prevent the liner from buckling under compressive stress. More detailed discussions on the subject of metal-lined, filament-wound pressure vessels are presented in References 4 and 5.

The bond must be capable of straining with the filament-wound composite to operating strain levels without having adhesive failure with either surface, or having cohesive failure within itself. This bond integrity must be maintained during repeated applications of the strain cycle during pressure cycling of the vessel. Should the bond fail, local buckling followed by fatigue failure of the liner and leakage would occur. Thus, adhesive bond integrity is one of the keys to success for thin metal-lined filament-wound tanks which must sustain fatigue cycling.

In order to remove contaminants and provide the cleanest possible metal surface for bonding to the composite shell, the outside of the TW-1 and TW-2 metal liners were cleaned and etched in accordance with Aerojet Standard AGC-STD-1221 (Method of Hot Nitric Acid Pickling). The process involved preliminary cleaning in a strong alkaline solution at 180°F, followed by a 30-min dry at 200°F in a pickling solution of 63.0 ±6.0% nitric acid and 0.4 ±0.001% hydrofluoric acid. The liners were then allowed to dry, after which they were enclosed in plastic bags until they were prepared for application of the adhesive bond.

To ensure adequate bonding of the filament-wound composite to the liner, a 0.002-mil nylon scrim cloth (impregnated with a mixed solution of 100 parts by weight of 7343 resin and 11 parts by weight of 7139 curing agent) was applied to the cleaned liner surface. The curing agent was first heated to 250°F to facilitate mixing with the resin, and the mixture was thinned with methyl ethyl ketone (MEK) to brushing consistency. The adhesive-scrim cloth layer was air-cured for 5 hours at room temperature to provide a tacky, non-flowing surface for the glass roving.

During inspection of sectioned containers TW-1 and -2 it was observed that there was inadequate bond, as indicated by wrinkles adjacent to the liner-boss welds, and by lack of peel strength between the liner and the first layers of filaments.

An immediate investigation was conducted with Aerojet funds to improve the adhesive bond between the liner and the filament overwrap. This involved the fabrication and testing of 96 T-peel and lap-shear coupons employing different cleaning methods and eight resin systems. Based on these results, shown in Table V, a strong, workable cleaning method and adhesive system was selected. This adhesive exhibited good peel strength and a lap shear strength almost six times that of previously used adhesives. This final selected process and materials involved cleaning of the liners with the Ex-B727-6 paste cleaner, and application of FM-123-3 film adhesive and 828/MNA/BDMA/COS filler.

TABLE V  
MECHANICAL PROPERTIES OF ADHESIVES (METAL-TO-METAL BONDS)

Specimen	Cleaning with Paste-Type Acid		Alkaline Cleaner	
	T-Peel lb/in. width	Lap Shear psi	T-Peel lb/in. width	Lap Shear psi
"Epon 871"/828/AEP with nylon scrim	3.1	663	4.0	2438
7343/7139 with nylon scrim	18.0	372	13.0	275
FM-123-2 (film adhesive)	11.5	3335	15.0	4163
FM-123-2 with BR-38 one side	11.0	2201	11.5	1517
FM-123-2 with "Epon 828"/MNA/ BDMA one side	15.0	3715	13.0	3220
BR-38 (liquid adhesive) with nylon scrim	3.0	743	2.5	989
BR-38 with "Epon 828"/MNA/ BDMA (no scrim)	3.4	2549	2.7	2786
"Epon 828"/MNA/BDMA with nylon scrim	3.8	2549	3.5	2858

\*AEP = aminoethylpiperazine.

### (3) Additional Design and Processing Considerations

Further investigations were made to supplement the studies conducted earlier to resolve problems in liner buckling due to inadequate mandrel support and/or insufficient bond strength between the liner and composite. As a result of the later work, modifications in design and processing were incorporated to correct premature failures and to increase the burst pressure and fatigue characteristics of the vessels. These technical problem areas investigated included: (a) minimizing filament bridging and excessive buildup, and improving strain compatibility between the bosses and the surrounding filaments by utilizing a wider band tape width, (b) reducing high radial strains in the filaments around the bosses and approaching uniform stress distributions in composite by increasing the winding tensions, (c) optimizing the head contour and further reducing radial strains by utilizing glass reinforcement dollies, and (d) examining the seam welds for the presence of flaws or potential leak paths.

The roving tape width, the planar winding pattern, and the nearly constant winding angle being used to fabricate the filament-wound structure of the vessel resulted in a roving buildup adjacent to the boss that was approximately six times the thickness at the equator. With the winding pattern used for the first nine vessels, some bridging of the fibers occurred in the area between the 6 in. and the 9 in. diameter of the vessel on top of the metal liner boss-to-membrane transition (see Figure 35). Since the outer layers bridge more than do the inner layers, the inner layers strain more when the vessel is pressurized, and fail before the outer layers carry their design load. The metal-liner-to-boss weld is also subjected to higher strain, and therefore is more susceptible to failure than any other area of the liner since the boss-to-head weld is within this 6- to 9-in.-dia bridging area. It was expected that the bridging, and therefore the high strain on inner layers of winding, would be reduced by winding with a wider roving band, or by changing the winding angle during fabrication to minimize bridging, or both.

Parametric computer runs have been made to evaluate this approach to improving the vessel design. The results are presented graphically in Figures 36 through 39. These curves show the variation of the wall thickness and the composite buildup at the bosses for various winding angles, tape widths, and boss diameters. Data on the curves indicate that the composite buildup at the boss can be reduced from the present 3 in. to approximately 2.16 in. by increasing the tape width from 0.56 to 0.88 in. (This width was selected by multiplying the 0.080 in. width of the roving by 11 - the number of tension devices available for the Aerojet sphere winding machine.) While this reduced buildup at the bosses will in turn reduce bridging, the net effectiveness can be determined only by actually winding and testing vessels. It should be noted that winding with a band width of 0.88 in. instead of 0.56 in. results in a change in the vessel shape, and the length of the neutral axis of the vessel decreases from 8.7 to 8.3 in. Thus, winding with a wide tape on existing liners would be expected to result in slightly lower test values than winding on the theoretically ideal contour liners designed for the wider band width.

Further interpretation of these curves shows that the use of a 0.56-in.-wide tape band, and a change in the winding angle of alternate

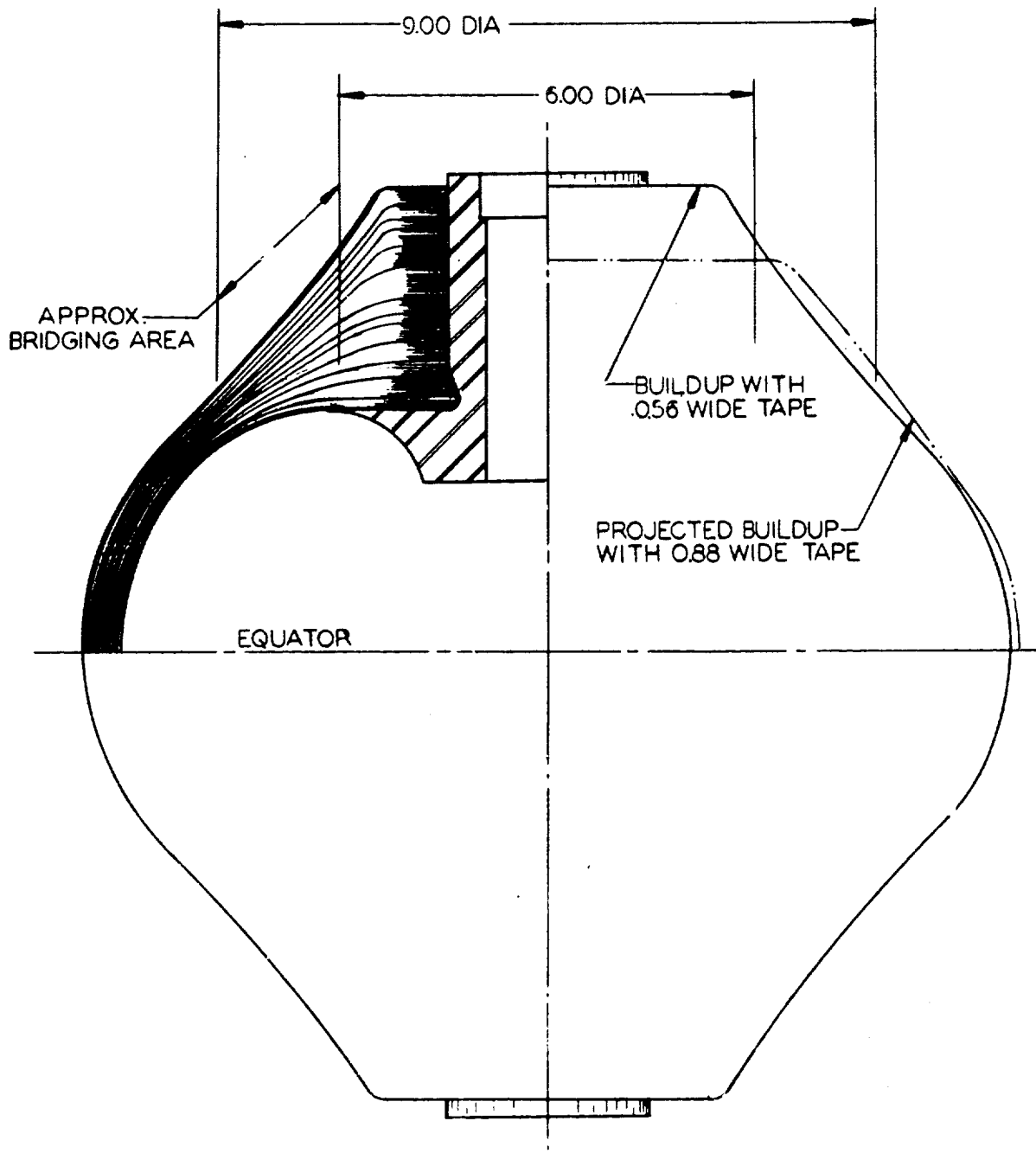


Figure 35. Roving Buildup

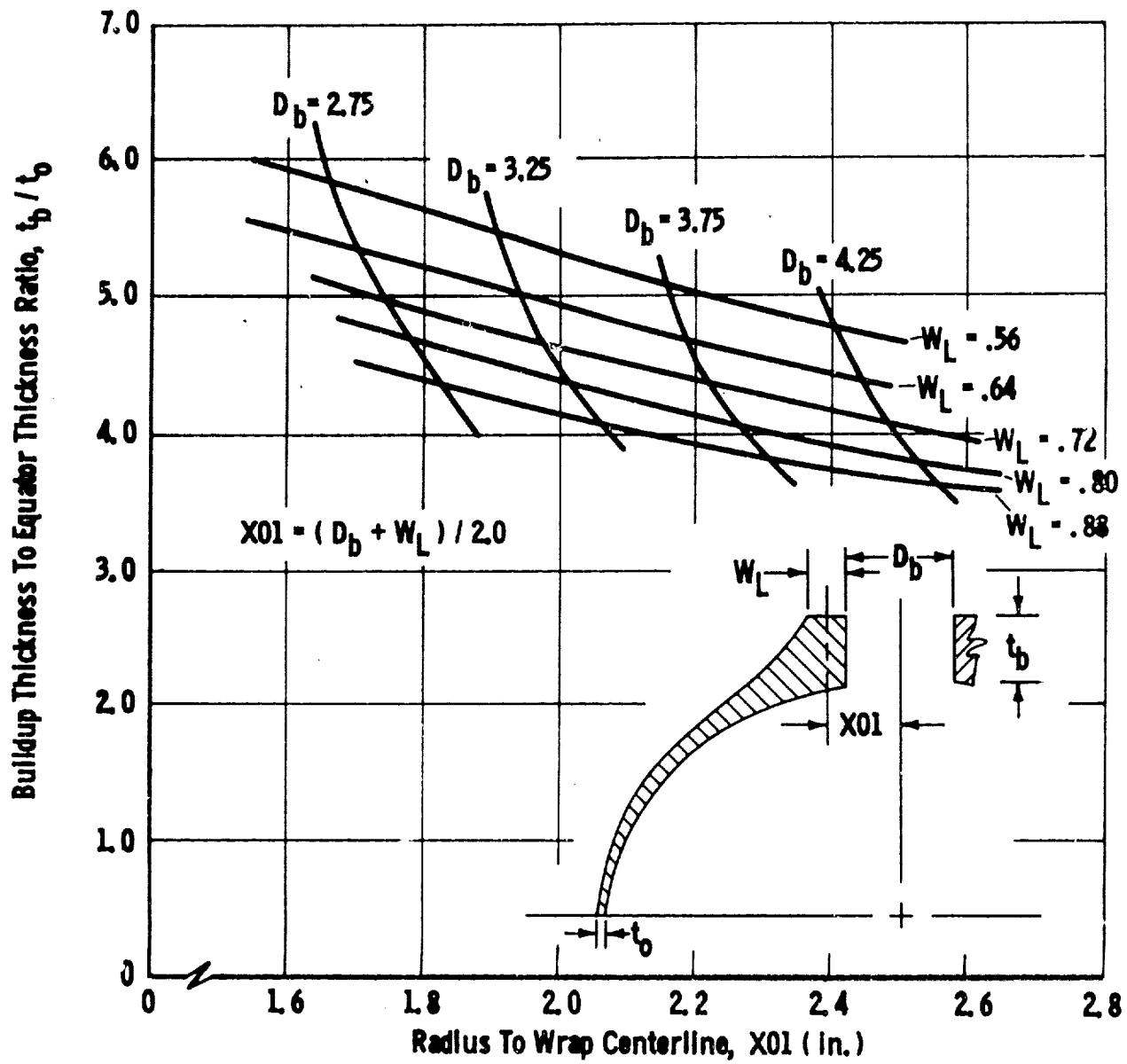


Figure 36. Roving Buildup For Various Tape Widths and Boss Sizes

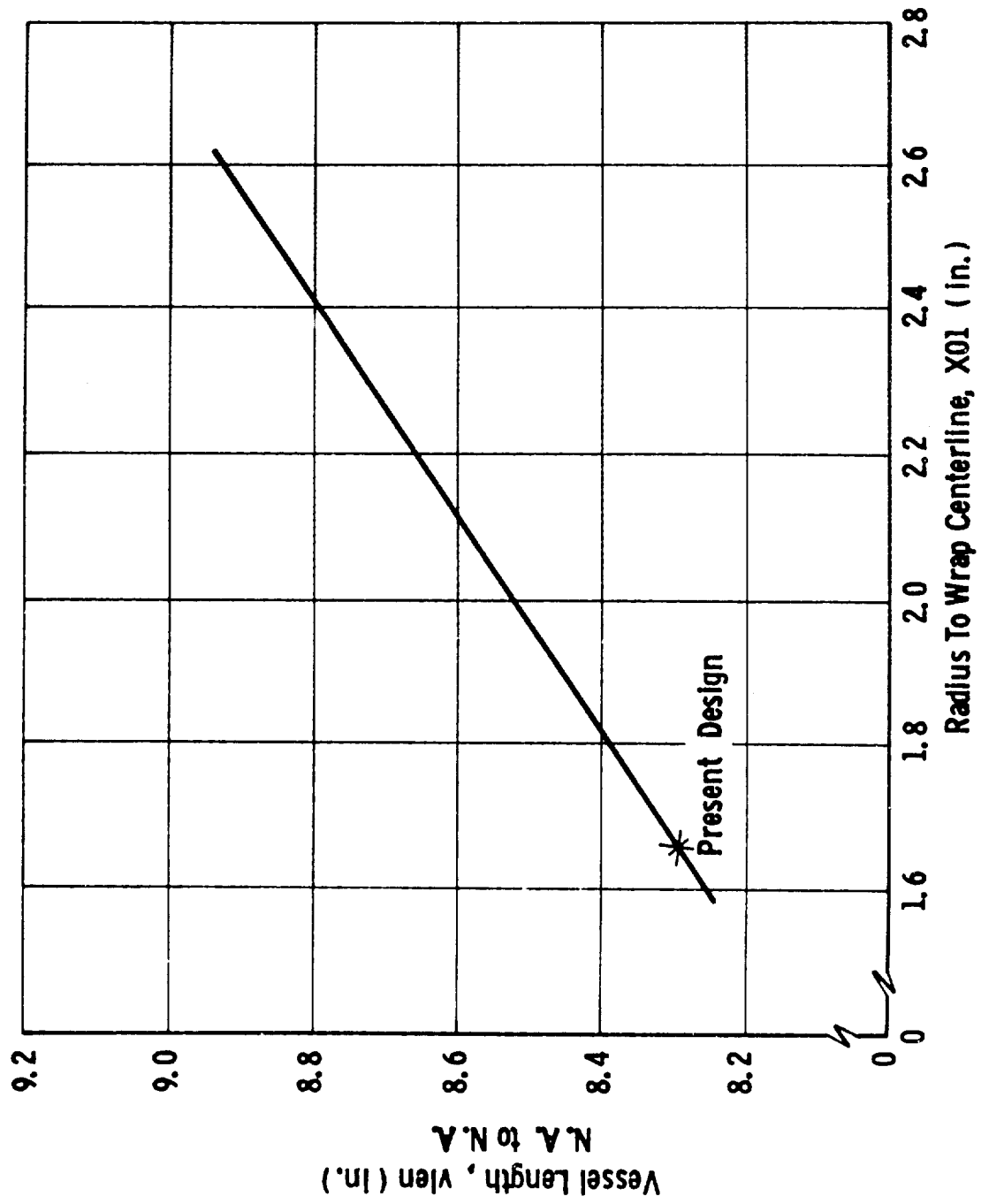


Figure 37. Vessel Length For Various Tape Widths and Boss Sizes

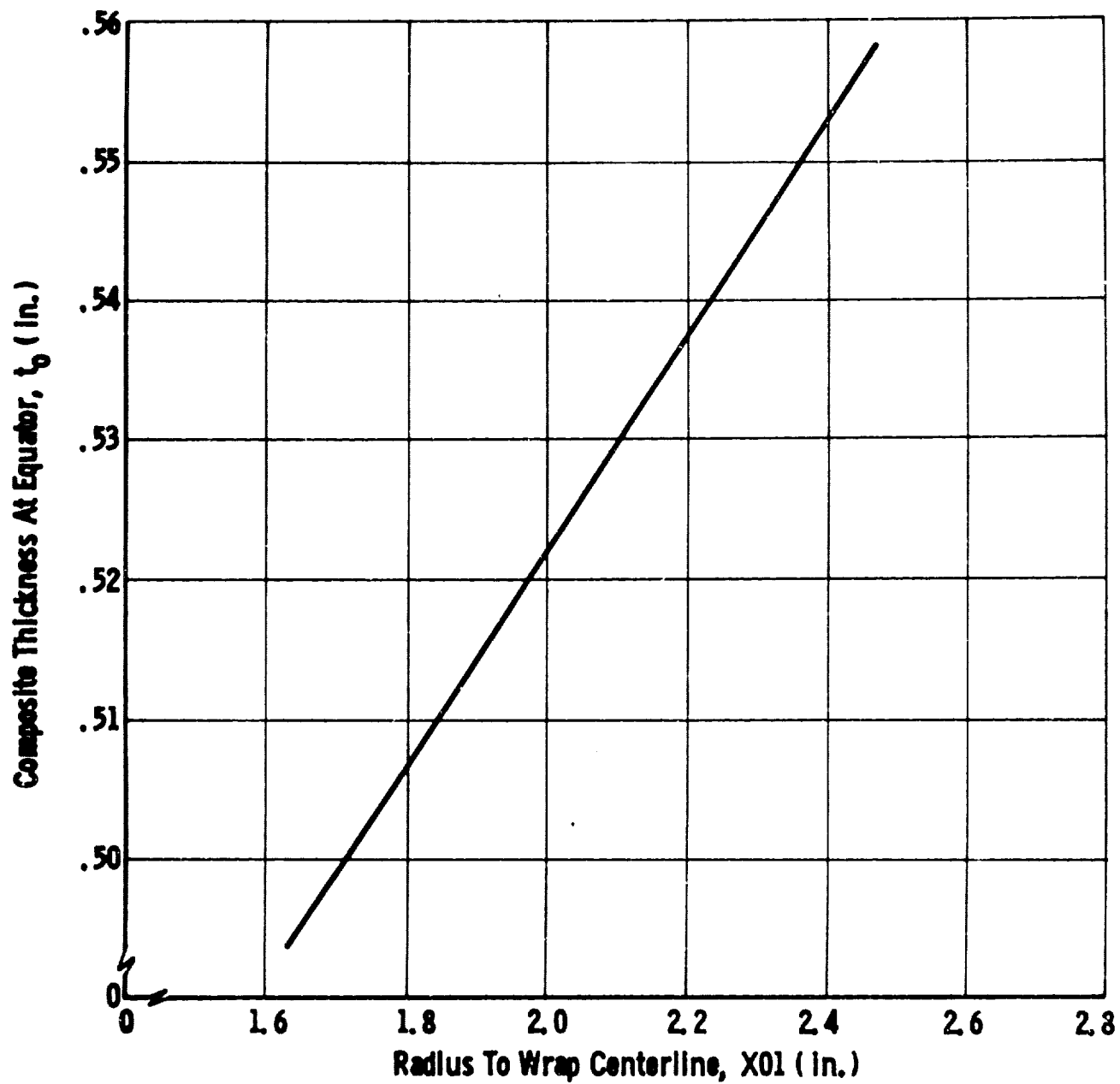


Figure 38. Thickness at Equator for Various Tape Widths and Boss Sizes

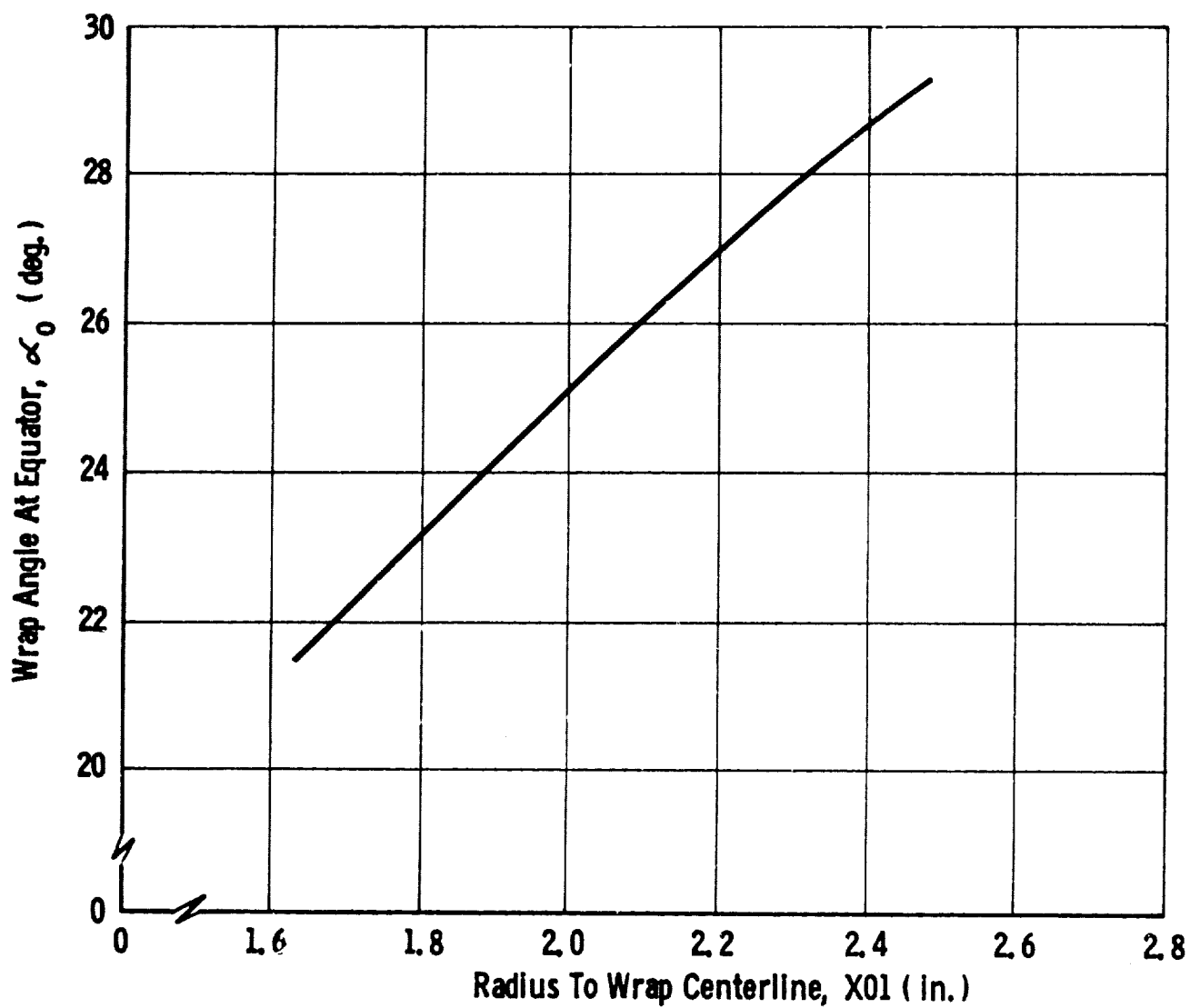


Figure 39. Wrap Angle for Various Tape Widths and Boss Sizes

layers so that the even layers would be wound adjacent to the boss and odd layers wound approximately 0.8 in. away from the boss, would reduce the buildup from 3 to 2.75 in. While bridging would be reduced, changing the angle in this instance would not be nearly so effective as increasing the band width.

Increasing the band width to 0.88 in., and changing the angle to wind alternate layers 0.5 in. away from the boss, would not bring any further significant reduction in buildup height. However, such measures might result in further reduction in bridging, and for this reason were worth investigating.

Another very important consideration involves rigidity of the boss compared with extensibility of the filament-wound composite on top of the boss. In the shell away from the boss, both the metal liner and the filament-wound composite, strain uniformly. However, as the transition from the metal liner to the metal boss is made, the filaments remain essentially isotensoid (with their high strains) while the rigidity of the thick boss does not permit it to strain with the filaments. This leads to a mismatch of strains and relative movement between the metal boss and overwrapped composite. Localized strain magnification will occur in the transition area between the metal liner and the metal boss in order to maintain overall strain compatibility between the filaments and metal structure.

It has been found from the analysis of a number of test results that this strain magnification occurs at a length 15 and 20 times the thickness of the metal liner. Based on this length and a typical boss, specific strain regions may be defined, and a theoretical strain curve drawn as shown in Figure 40.

Calculation of a value for strain magnification is based on matching filament and metal-shell extensions,  $\delta_f$  and  $\delta_m$ , respectively, which requires that

$$\delta_m = \delta_f$$

where the filament extension is

$$\delta_f = \epsilon_f L = \epsilon_f \left( \frac{D_w}{2} + 20 t_L \right)$$

and the metal shell extension is

$$\delta_m = \int_0^{R=L} \epsilon_m dR$$

where  $\epsilon_m$  is some function of the radial distance (R) as shown in Figure 40.

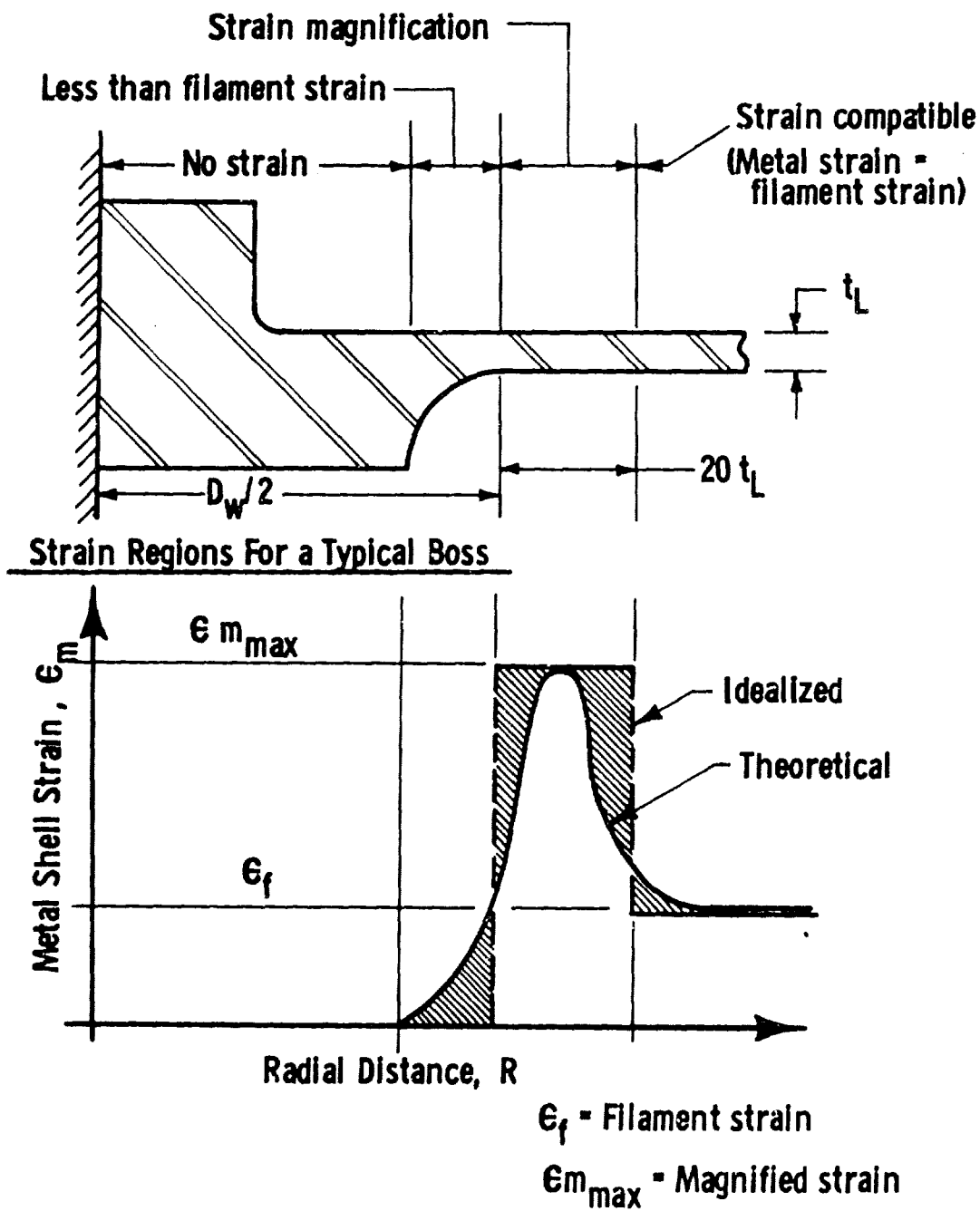


Figure 40. Strain Distribution in Metal Structure

Assuming the strain magnification is constant and limited to the region of length  $20 t_L$ , then metal-shell extension is

$$\delta_m = \epsilon_{m \max} (20 t_L)$$

By combining equations, the strain magnification is found to be

$$\frac{\epsilon_{m \max}}{\epsilon_f} = 1 + \frac{D_w}{40 t_L}$$

Subject to the present design criteria,

$$t_L = 0.006 \text{ in.}$$

and

$$D_w = 6.00 \text{ in.}$$

The strain magnification is

$$\frac{\epsilon_{m \max}}{\epsilon_f} = 26$$

Data have been accumulated from the testing of thin-walled, filament-wound pressure vessels and analyzed using the above procedures. The pressure vessels all contained 0.006-in.-thick, Type 304 stainless-steel liners joined to the bosses at a diameter ( $D_w$ ) of 2.90 in. Data indicates that a very few of the vessels may have leaked prematurely at filament strain levels of 3 to 4%. The calculated value of strain magnification for this design was 13, and the corresponding localized strain in the metal when leakage occurred was 40 to 50%. Using the lower strain level (40%) as a failure threshold for Type 304 stainless steel, leakage of the present thick-wall pressure vessel could occur at a filament strain level of 1.5% (15.00 ksi). From tests on TW-1 through TW-9, leakage occurred at a median value of 11.00 ksi.

For maximum compatibility with the high glass-filament-wound composite strains in the end domes, the metal boss should have low rigidity and should be as small as possible (i.e., the metal liner should have the minimum possible dimensions which do not plastically deform to the same strains as the isotenoid filaments of the vessel end domes). In practice, this is accomplished by reducing the body of the boss to the smallest practical dimensions in width and thickness. By keeping the width dimension small, the magnitude of mismatch between deflections of the filament-wound composite on top of the boss and on the boss can be reduced, and the strain absorbed by the liner

membrane at the edge of the boss flange can be minimized. By keeping the thickness small, the boss flange can be blended into the liner membrane over a short distance to reduce the effective width dimension of the boss.

Excessive radial strain of the composite laminate adjacent to the boss in relation to the radial strain of the metal boss was suggested as a possible cause of leakage. Block specimens (approximately 0.50 by 0.25 by 0.25-in.) were cut from various sections in the laminate of Container TW-4. The compressive modulus in the radial (thickness) direction of these specimens was determined. Results of the tests were as follows:

Radial compressive modulus (at equator)	1.4 x 10 <sup>6</sup> psi
Radial compressive modulus (at midpoint)	0.5 x 10 <sup>6</sup> psi
Radial compressive modulus (near boss)	0.4 x 10 <sup>6</sup> psi

These low moduli values, combined with the differential strains between the boss and adjacent composite structure, indicated that the composite was being radially compacted (compressed) during pressurization. As a result, the inner filaments were being stressed much higher than anticipated while the outer fibers were not being stressed to levels required for optimum conditions. These high radial strains were the principal cause for premature liner failure. In order to improve the conditions encountered, winding tensions in the glass fibers were incrementally increased during the winding operation beginning with Container TW-10. The glass layers had been applied at varying tensions from 4 to 12 lb/20-end. Tensioning devices previously used in the 260-in.-dia filament winding case program were obtained, installed, and adapted to increase winding tension from 4 lb/20-end in the inner fibers to 40 lb/20-end in the outer fibers.

Computer output data, taking into account the wider glass-tape width and reduced filament buildup, indicated that the optimum contour of the pressure vessel had now increased outwardly approximately 0.08 in. in the area adjacent to the axial bosses. Layers of unidirectional glass tape were made up into reinforcement doilies and placed between the first and second, and the second and third revolutions of filament windings in order to compensate for the difference in contour dimension.

It was believed that leakage could have occurred for other reasons in the seam weld, which joins the head to the boss. The seam welding was actually a continuous series of small overlapping spot welds. Reliability was generally high, and random examination of the welds, by cross-sectioning and microphotographic examination (Figures 41 through 46), showed that the weld penetration was adequate in the samples inspected. Nevertheless, the nominal variation in the 60 in. of seam weld in each liner, under strain, could have resulted in a leak path. Also, the strength and elongation of the seam welds was less than that of the metals being joined.

#### c. Vessels TW-10 Through TW-12

Three major processing steps were implemented in the fabrication of the second-iteration vessels (TW-10 through TW-12) in order to obtain improvements in the container structure. These steps included (1) applying the glass filaments at increased winding tensions to minimize high radial

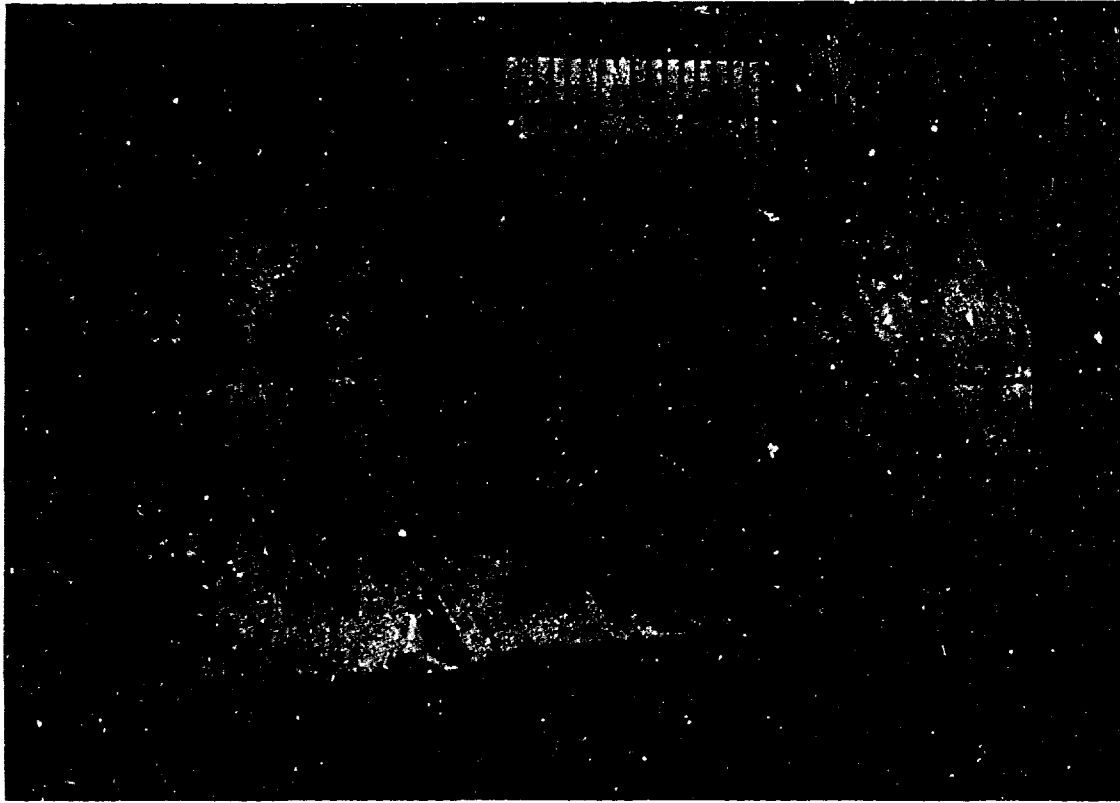


Figure 41. Liner Section at Equator

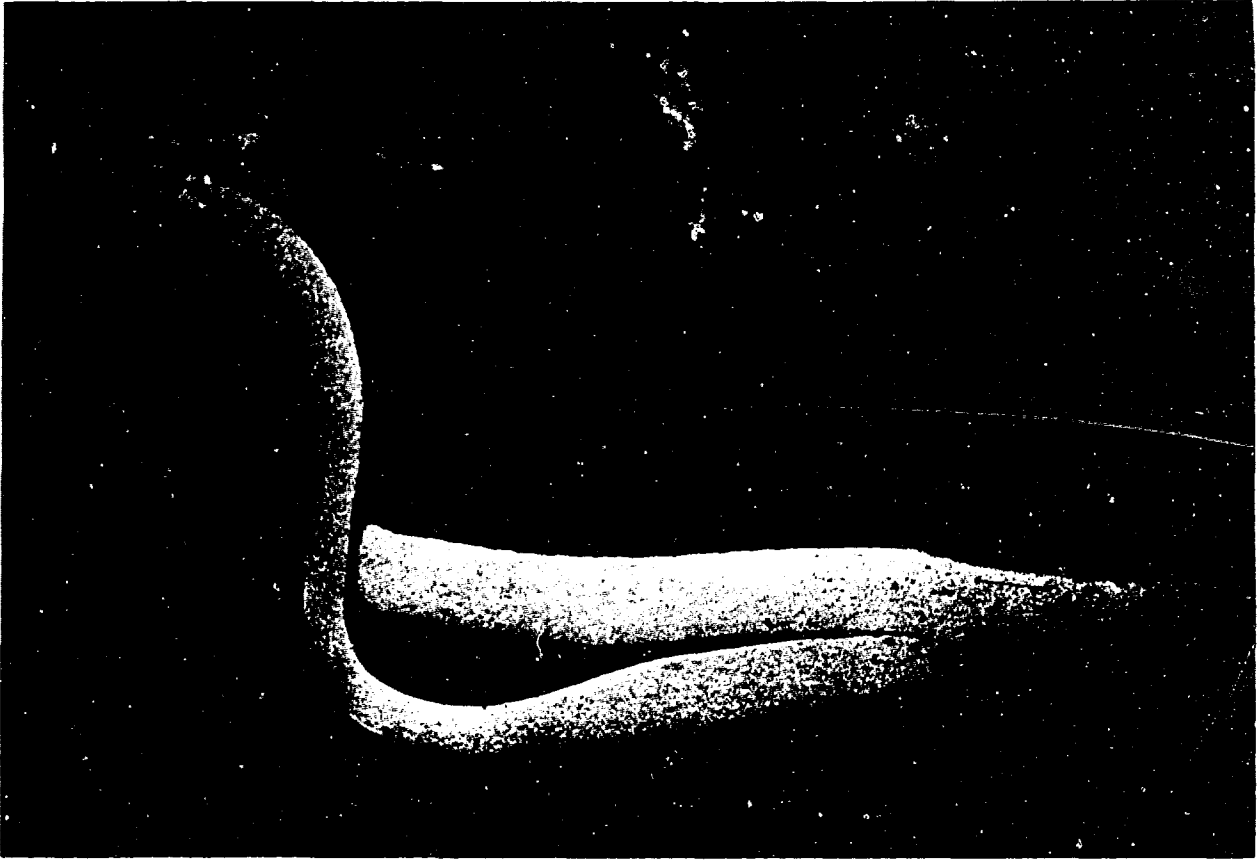


Figure 42. Seam-Weld Cross Section at Equator (40X)

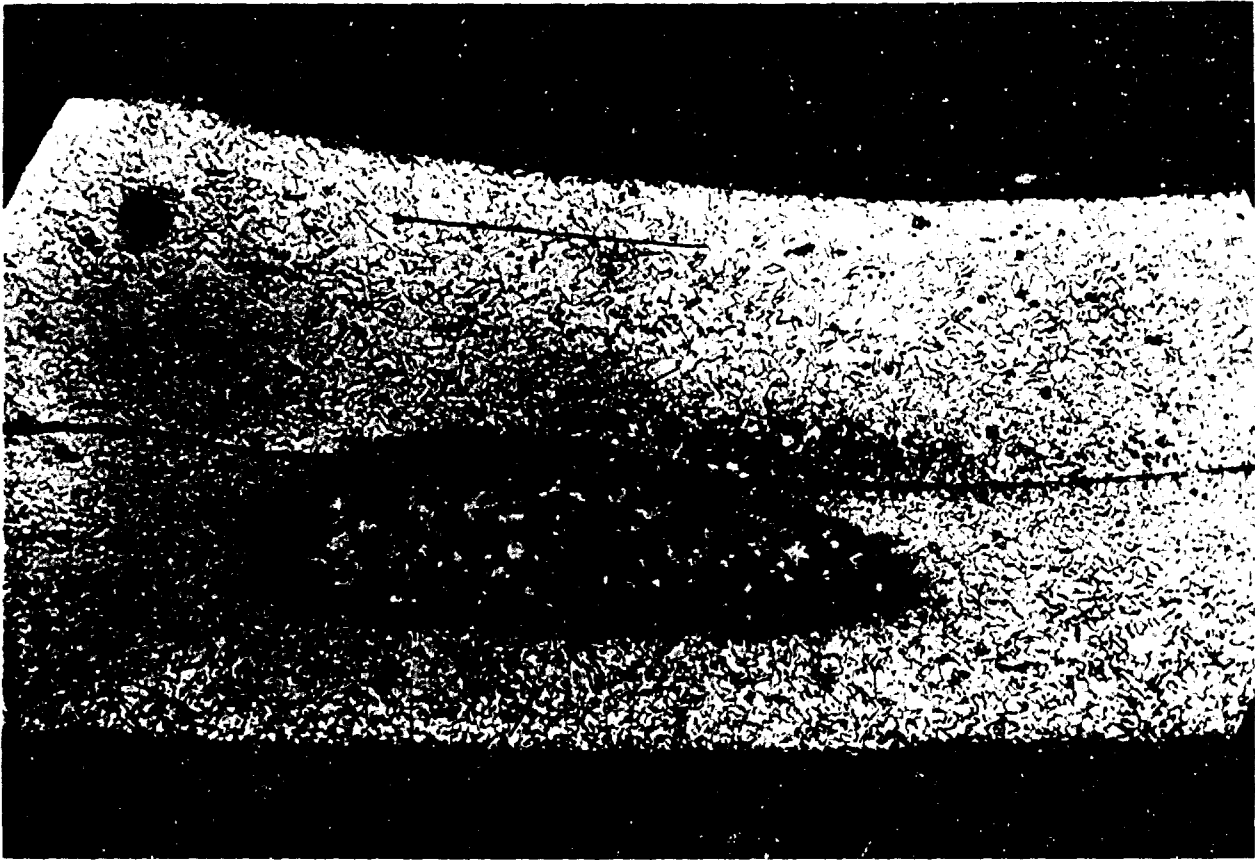


Figure 43. Weld Nugget No. 1 at Equator (150X)



Figure 44. Grain Boundary of Weld Nugget No. 1 at Equator (500X)



Figure 45. Weld Nugget No. 2 at Equator (150X)



Figure 46. Weld Nugget No. 3 at Equator (150X)

deflections noted in the metal boss in relation to the radial strain in the composite laminate, (2) increasing the payoff tape width to eleven strands from the seven-strand system previously used in order to reduce filament bridging and excessive filament buildup adjacent to the axial bosses, and (3) utilizing glass-reinforcement-tape doilies between the first three revolutions in order to compensate for the difference in contour dimensions resulting from the use of wider tape band and thus obtaining an optimum contour in the composite shell.

Modifications were made in equipment and fixtures in order to incorporate these improvements. The tensioning devices formerly used in the 260-in.-dia filament-winding case program were obtained, and some of these devices were adapted to work in conjunction with the available sphere-winding machine. An eleven-strand payoff roller system was installed on the winding machine, replacing the seven-strand system used in fabricating the previous containers.

Containers TW-10 through TW-12 were filament-wound after the improvements were incorporated. Glass filaments, preimpregnated with the Shell 58-68R resin system, were used throughout the winding. This material was available, and its use simplified the winding of the composite structure. As previously outlined in Section IV,3, this particular resin system was initially selected for use in the inner layers where a more rigid resin system possessing high compressive strength was required. Although a tougher resin system with higher elongation characteristics was desirable for the outer layers because of possible crazing and subsequent degradation from moisture penetration, the prepreg material was considered quite adequate, particularly since an elastomeric moisture barrier was applied on the outer composite surface. Because of the higher resin content in the prepreg material and its lesser tendency to flow during cure, high filament buildup was still noted in the areas adjacent to the metal bosses. Some weight redundancy is therefore noted in Containers TW-10 through TW-12 because of the higher resin content. In addition, a redundant revolution was applied in winding the initial filaments after the first 17 revolutions had been vacuum-bagged and oven-cured. This revolution was applied at lower winding tension (8 lb per end) in order to obtain a tacky surface and thus prevent filament slippage for subsequent windings at higher tensions (20 lb to 40 lb per end).

d. Vessels TW-13 Through TW-16

Test results in Containers TW-10 through TW-12 were significantly higher (two vessels burst at pressures more than 20% greater than had previously been attained, and one of these vessels was cycled twice between zero and 40% above the operating pressure prior to the burst). It therefore appeared that the processing improvements incorporated in the fabrication of these vessels had contributed to the burst pressure increase. Since these pressures were still only 72% of the design values, further processing modifications were incorporated in the fabrication of TW-13 through TW-16. These included increasing the winding tensions on the remaining vessels still higher to a maximum of 45 lb per 20-end for the last four revolutions, and a redesign in the final payoff roller by machining in grooves to keep the filaments separated and permit them to be applied as a more uniform band. The latter modification was incorporated when it was noted that the filaments being

applied at the higher winding tensions had a tendency to migrate over each other causing slight gaps in the tape band width. The filaments in revolutions 18 through 20 (after curing the composite in revolutions 1 through 17) were also applied at a band width (approximately 1 in.) away from the axial bosses in order to reduce filament buildup around the bosses. With the exception of TW-16, the vessels were wound in a similar manner.

A 1-in.-dia depressed area formed midway between the boss and equator after six revolutions of glass roving had been filament-wound over the liner of TW-16. It appeared that the sand-acrylic mandrel supporting the liner had collapsed locally in this area from the compressive pressures generated by the winding tension. This collapse may have been caused by insufficient cure of the sand-acrylic mandrel material. As more roving was applied and the winding tension increased, the depressed area enlarged until it was approximately 2-in.-wide by 8-in.-long at the end of the 12th revolution. The winding was terminated at this time and a decision was made to internally pressurize the vessel to 600 psig with nitrogen gas and attempt to cure the applied glass layers prior to winding additional layers. Under pressurization the collapsed area in the vessel was brought to a condition that appeared to approximate the desired contour. The composite structure was cured under pressure and the cured layers, in addition to the sand mandrel, served to support the subsequent glass windings applied at increased tensions. In contrast to the other vessels in this group, the composite structure was oven-cured without vacuum-bagging because of the potential hazard involved in applying the bleeder cloth and the PVA (poly-vinyl alcohol) bag over the pressurized vessel.

While mounting the winding shaft to TW-16 in order to complete the windings, it was noted that the boss-to-boss length had increased sufficiently to prevent attachment of the shaft to the stud on the back side of the aft boss. The shaft was assembled with larger bolts to the forward boss. This caused a slight amount of wobble in the applied layers around the aft boss which became excessive at the end of the 33 revolutions. At this time it was noted that the weld in the shaft had developed cracks and that the shaft was bending excessively because of the high winding tensions in the glass roving. The winding was therefore terminated at this point.

### 3. TEST RESULTS

Definitive test procedures were adopted in order to obtain the maximum amount of information for use in evaluating the thick-wall, filament-wound, high-pressure containers. This test plan is described in detail in Appendix IV. Tests were performed on a total of 16 pressure vessels in three separate lots of 9, 3, and 4 vessels each. Vessel variations in materials and processes for the containers were described in Section V,2,b and V,2,c, and summarized in Table VI.

Each tested unit was prechecked by filling with hydraulic oil and pressurizing to 1000 psig prior to conducting the actual test. Pressures were applied at the rate of 10,000 psig per minute in accordance with the applicable procedures. This pressurization rate induces a strain rate in the containers of approximately 1%/min, which is standard Aerojet practice. This strain rate was formerly selected for testing filament-wound pressure vessels

TABLE VI

FABRICATION SUMMARY, 12-IN.-DIAMETER, THICK-WALL, FILAMENT-WOUND, HIGH-PRESSURE VESSEL

Serial No.	Type of Mandrel	Liner Cleaner	Liner-to-Composite Bond		Winding Data*				Tension lb
			Nylon Scrim mills	Adhesive (ptw)**	Reinforcement		Matrix Material	Vacuum Cure	
					Double Layers	Form			
TW-1	Cured plaster	Nitric acid pickle	2	7343/7139 (70/30)	1-17 18-35	PP WW	Yes Yes	58-68R 828/855	4-11 13-20
TW-2	Raw plaster	Nitric acid pickle	2	7343/7139 (100/11)	1-8 9-16 17-26 27-33	PP PP PP PP	No No Yes Yes	58-68R 58-68R 58-68R 58-68R	4-7 8-11 11-16 16-20
TW-3	Pres-surized	Ex-B727-6	3	871/828/AEP (60/40/15.5)	1-5 6-23 24-35	PP PP PP	No No No	58-68R 58-68R 58-68R	3-4.5 4.5-10.5 11-15
TW-4	Pres-surized	Ex-B727-6	3	871/828/AEP	1-5 6-35	WW PP	No No	828/855 58-68R	3-4.5 4.5-15
TW-5	Sand	Ex-B727-6	3	871/828/AEP	1-5 6-35	WW PP	No No	58-68R 58-68R	4-5 4.5-12.7
TW-6	Pres-surized	Ex-B727-6	3	871/828/AEP	1-4	WW	No	58-68R	4
TW-7	Sand	Ex-B727-6	3	871/828/AEP 828/MMA/BDMA/COS	1-17 18-35	WW PP	Yes Yes	58-68R 58-68R	4-8 8-12
TW-8	Sand	Ex-B727-6	None	FM 123-2 828/MMA/BDMA/COS	1-17 18-34	WW PP	Yes No	58-68R 58-68R	4 4

\* PP = prepreg; WW = wet-wound; 58-68R system = "Epon 828"/"Epon 1031"/MMA/BDMA (50/50/90/0.5 ptw); throughout table, tension per 20-end roving.

\*\* COS = "Cab-O-Sil;" AEP = aminoethylpiperazine.

TABLE VI (cont.)

Serial No.	Liner-to-Composite Bond				Winding Data				
	Type of Mandrel	Liner Cleaner	Nylon Scrim mils	Adhesive (pbw)	Reinforcement		Vacuum Cure	Mat'l	Tension lb
					Double Layers	Form			
TW-9	Sand	Ex-B726-6	None	FM 123-2 828/MNA/EDMA/COS	1-17 18-34	WW	No	53-68R 56-68R	4 4
TW-10	Sand	Ex-B727-6	None	FM 123-2 828/MNA/EDMA/COS	1-13 14-26 27-36	PP	Yes	58-68R 58-68R 58-68R	4-24 26-37 37-40
TW-11	Sand	Ex-B727-6	None	FM 123-2 828/MNA/EDMA/COS	1-17 18-36	PP	Yes	58-68R 58-68R	4-29 29-40
TW-12	Sand	Ex-B727-6	None	FM 123-2 828/MNA/EDMA/COS	1-17 18-36	PP	Yes	58-68R 58-68R	4-29 29-40
TW-13	Sand	Ex-B727-6	None	FM 123-2 828/MNA/EDMA/COS	1-17 18-36	PP	Yes	58-68R 58-68R	4-24 26-42
TW-14	Sand	Ex-B727-6	None	FM 123-2 828/MNA/EDMA/COS	1-17 18-36	PP	Yes	58-68R 58-68R	4-24 26-42
TW-15	Sand	Ex-B727-6	None	FM 123-2 828/MNA/EDMA/COS	1-17 18-36	PP	Yes	58-68R 58-68R	4-24 26-42
TW-16	Sand	Ex-B727-6	None	FM 123-2 828/MNA/EDMA/COS	1-12 13-33	PP	Yes	58-68R 58-68R	4-14 16-40

and rocket-motor cases in order to produce a failure approximating that occurring in a steady-state condition, and to minimize the amount of scatter caused by the time-rate sensitivity of the materials being used. Test results and pertinent data on each vessel are summarized in Table VII.

a. TW-1

This vessel was hydrostatically tested by pressurizing with oil from 0 to 11,100 psig at which pressure a sharp cracking noise (presumably resin crazing) was heard. The pressure was inadvertently (manually) released to 8,200 psig and immediately increased to a maximum of 14,100 psig, at which time the unit leaked approximately 1 gallon per min. After the pressure was reduced to zero psig, the vessel was examined, but the leak area could not be identified. An attempt was made to establish the leak location by viewing the vessel without the protective blast shield during a repressurization cycle. At 13,700 psig, an oil spray was observed to penetrate through the vessel structure, preventing further pressurization. Divergence of the oil spray obscured identification of the leak area.

The container after hydrotest is shown in Figure 47. Figure 48 shows the container after sectioning. It appeared from examination of the sectioned parts that the leakage occurred in the crimped liner area adjacent to the boss-to-liner welds.

Strain-pressure curves for the vessel are presented in Figures 49 and 50 for the two cycles. Location of the strain gages is shown in Figure 51. Results of the curves in Figures 49 and 50 indicate, essentially, that strain at the boss-to-liner weld joint is approximately twice the strain at the equator.

b. TW-2

This vessel was hydrotested by pressurizing with hydraulic oil at a rate of approximately 10,000 psig per min. Leakage occurred at a maximum pressure of 9,980 psig. An attempt was again made to observe the vessel under pressurization in order to identify the leak area. Divergence of the oil spray after penetrating through the vessel at the leak area prevented identification. Examination and X-rays of the sectioned container also did not indicate the exact point of leakage. Buckling of the TW-2 liner occurred, but was less severe than in TW-1 indicating that (1) a poor adhesive bond between the liner and composite structure still existed, and (2) compressive loads after depressurization were less than in TW-1, as anticipated, since a lower maximum pressure was attained.

c. TW-3

Inspection of the interior of Container TW-3, fabricated using the pressure mandrel, indicated that some wrinkling and slight buckling of the liner had occurred. The vessel was tested to 10,400 psig at which pressure excessive leakage was encountered.

An attempt was made to determine the exact point of failure of the liner. The hydrotest oil was first drained out, the opening in the

TABLE VII

TEST SUMMARY, 12-IN.-DIAMETER, THICK-WALL,  
FILAMENT-WOUND, HIGH-PRESSURE VESSEL

Serial No.	Outside Diameter, in.		Vessel Weight lb*	Remarks
	Liner	Composite		
TW-1	11.975	13.030	38.3	Proofed to 14.08 ksi (1st cycle) Leaked at 13.66 ksi (2nd cycle)
TW-2	11.964	12.984	37.9	Leaked at 9.975 ksi (1st cycle)
TW-3	11.968	13.066	39.5	Interior coated with "Fliobond"/MEK (20/80) Leaked at 10.35 ksi (1st cycle)
TW-4	11.980	13.095	40.0	Leaked at 10.82 ksi (1st cycle) Interior coated with 828/LP-3/DMP- 30 (100/100/10) Leaked at 7.980 ksi (2nd cycle) Failed at 14.06 ksi (3rd cycle)
TW-5	11.973	13.173	40.1	Leaked at 4.775 ksi (1st cycle) Leaked at 5.040 ksi (2nd cycle) Rubber bladder installed Leaked at 3.150 ksi (3rd cycle)
TW-6	11.970	---	---	Vessel not completed
TW-7	11.970	---	---	Interior coated with 828/LP-3/DMP- 30 (100/100/10) Failed at 19.64 ksi (1st cycle)
TW-8	11.984	13.060	41.4	Interior coated with 828/LP-3/DMP- 30 (100/100/10) Leaked at 12.92 ksi (1st cycle) Leaked at 12.92 ksi (2nd cycle) Leaked at 12.75 ksi (3rd cycle) Failed at 9.180 ksi (4th cycle)
TW-9	11.976	13.110	41.0	Interior coated with 828/LP-3/DMP- 30 (100/100/10) Leaked at 9.030 ksi (1st cycle) Rubber bladder installed Leaked at 8.673 ksi (2nd cycle)
TW-10	11.973	13.377	46.0	Leaked at 16.70 ksi (1st cycle)
TW-11	11.973	13.155	45.6	Filament failure at 23.70 ksi (1st cycle)

\*Throughout table, includes weight of metal liner and bosses (approximately 14.2 lb).

TABLE VII (cont.)

Serial No.	Outside Diameter, in.		Vessel Weight lb	Remarks
	Liner	Composite		
TW-12	11.973	13.275	44.9	Pressurized to 21.30 ksi (1st cycle) Pressurized to 20.70 ksi (2nd cycle) Filament failure at 23.80 ksi (3rd cycle)
TW-13	11.973	13.255	44.1	Subjected to cycling tests from 0 to 15.00 ksi Leaked during 13th cycle
TW-14	11.973	13.095	44.4	Leaked at 21.80 ksi (1st cycle)
TW-15	11.973	13.093	44.1	Subjected to cycling tests from 0 to 15.00 ksi Leaked during 7th cycle
TW-16	11.973	13.073	39.6	Leaked at 15.30 ksi (1st cycle)

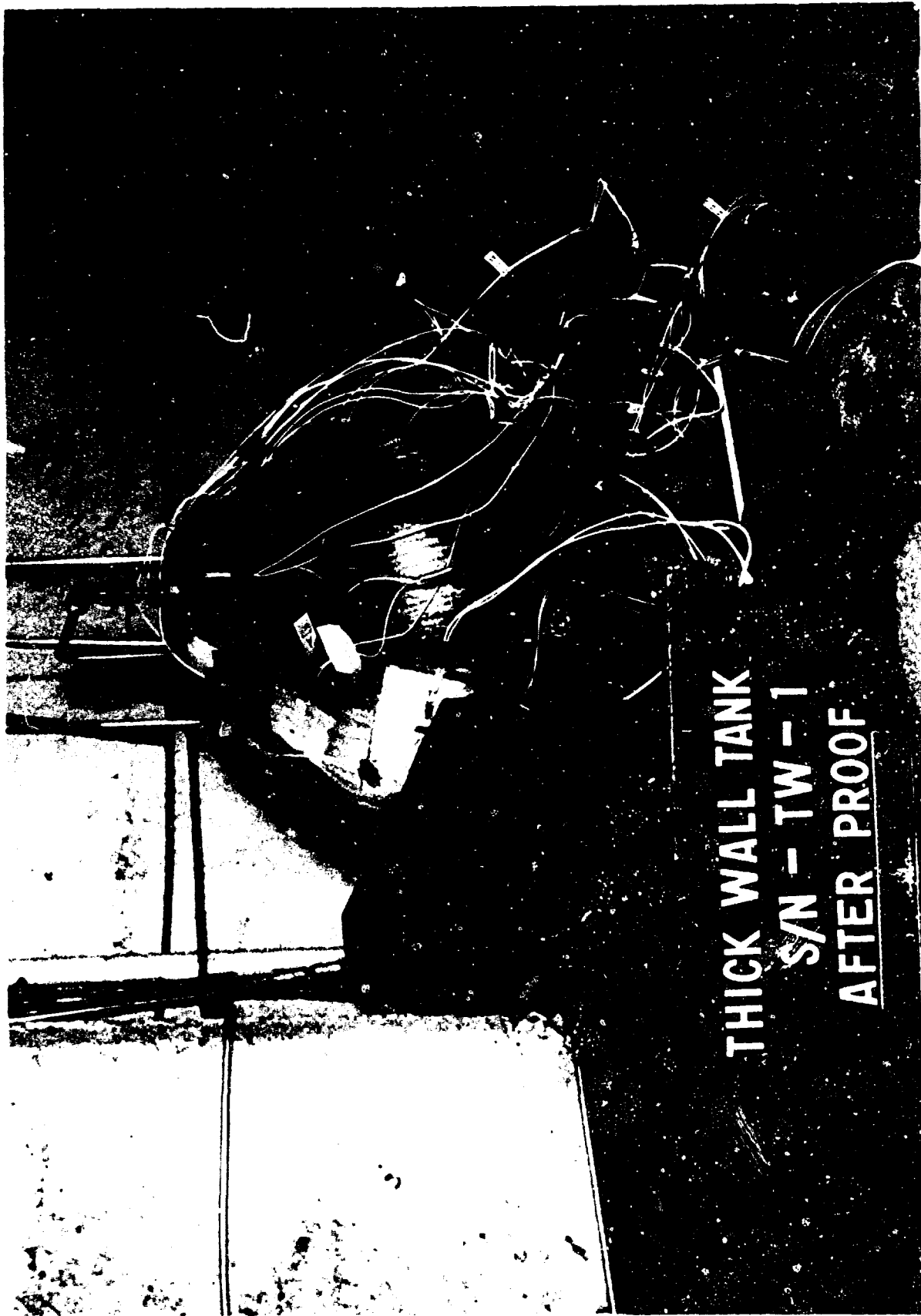


Figure 47. Container TW-1 After Hydrotest

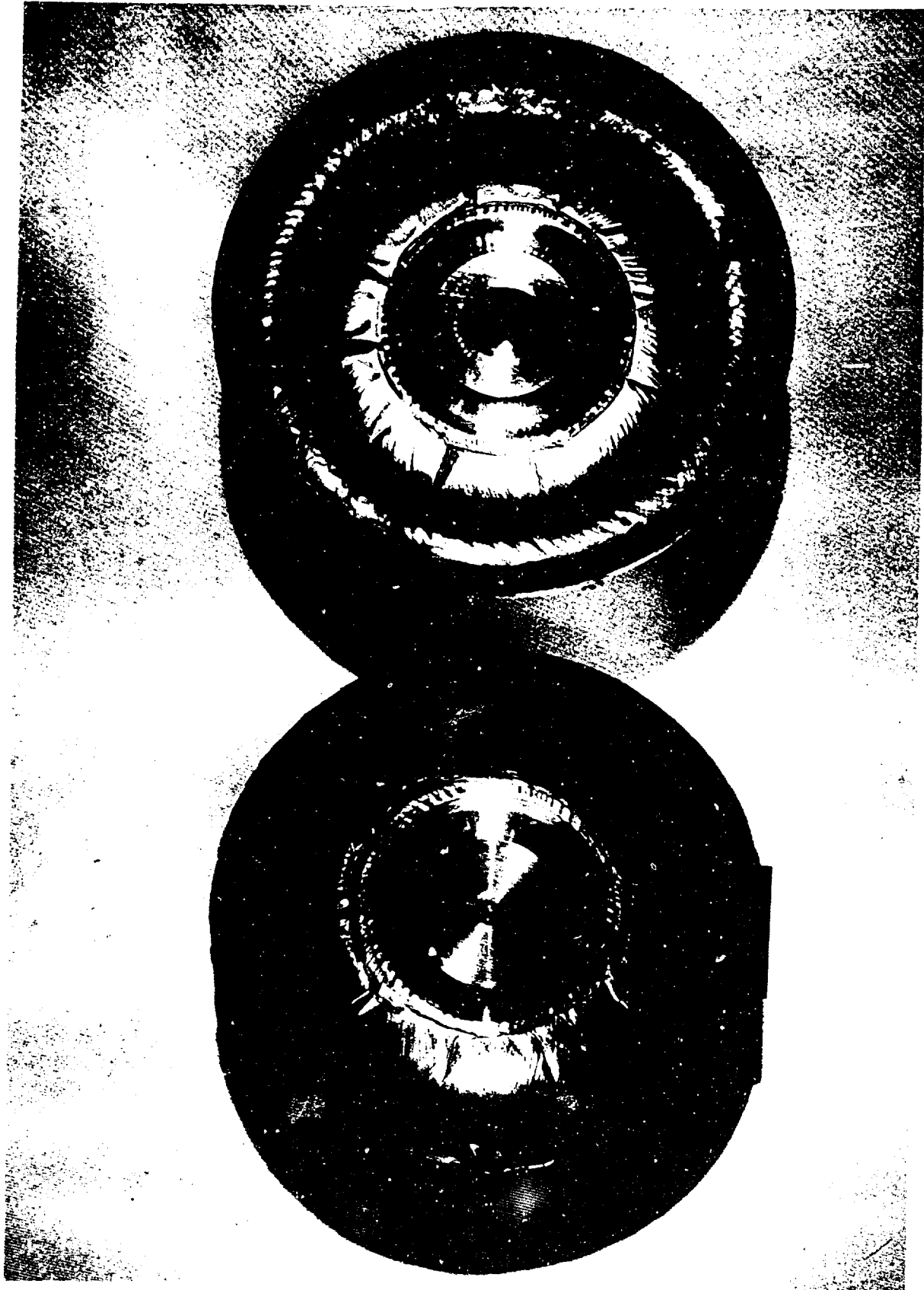
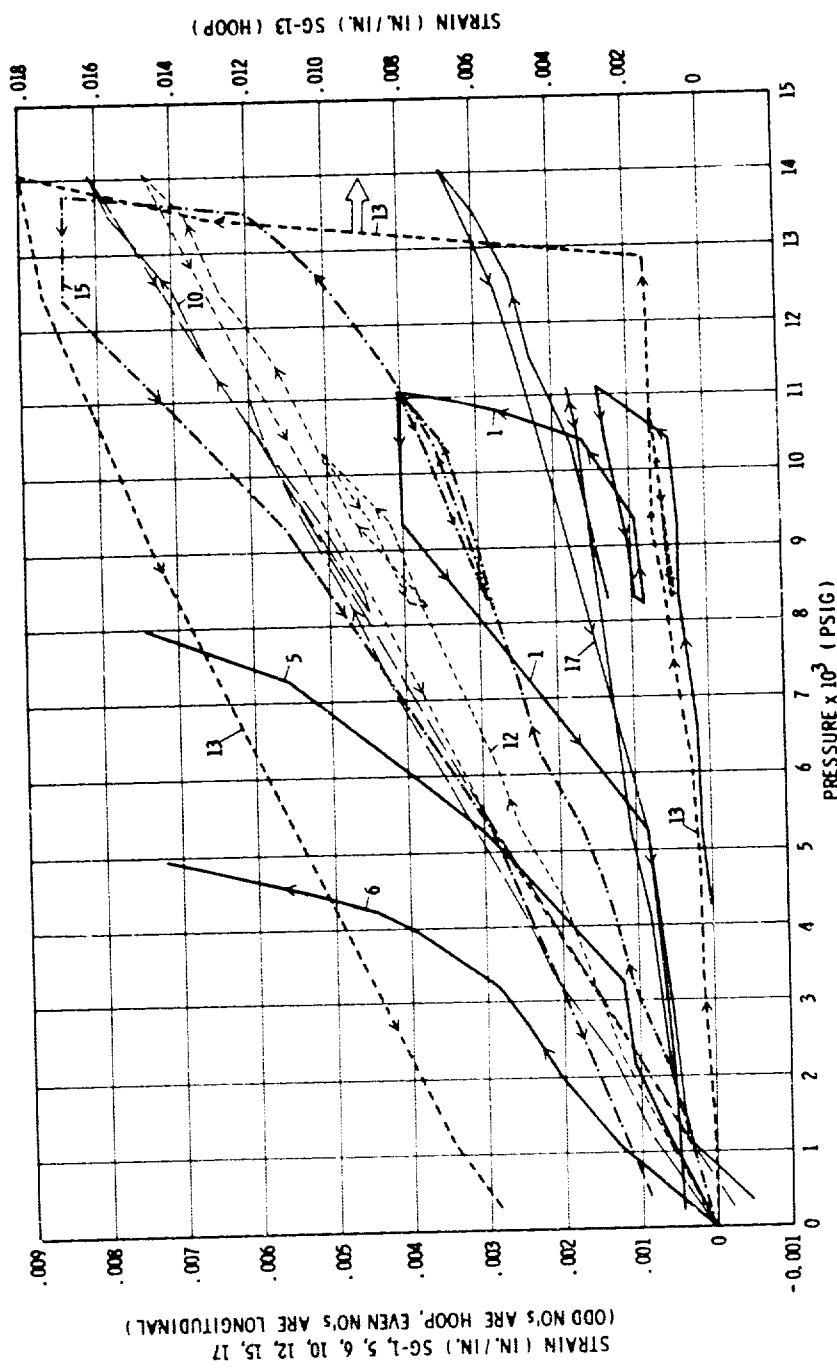
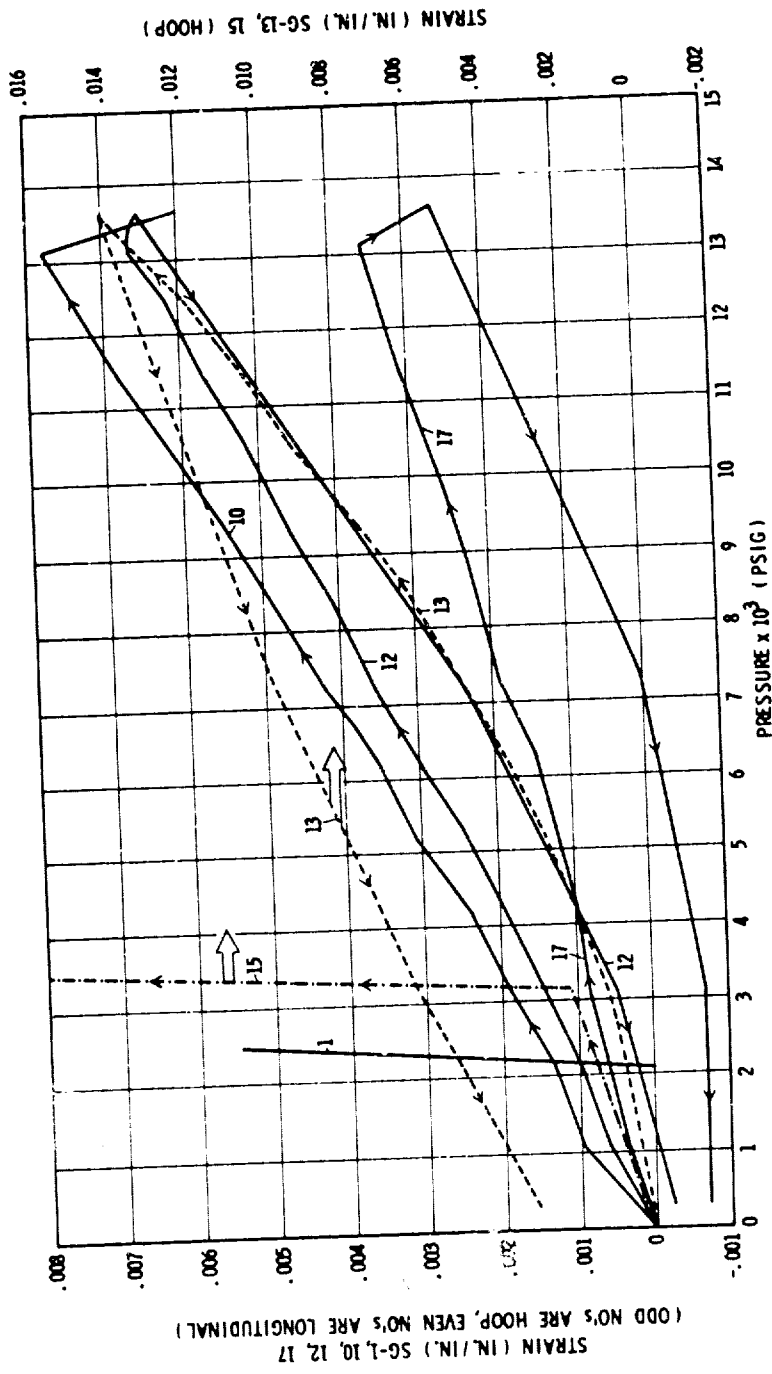


Figure 48. Sectioned Container TW-1 After Hydrotest



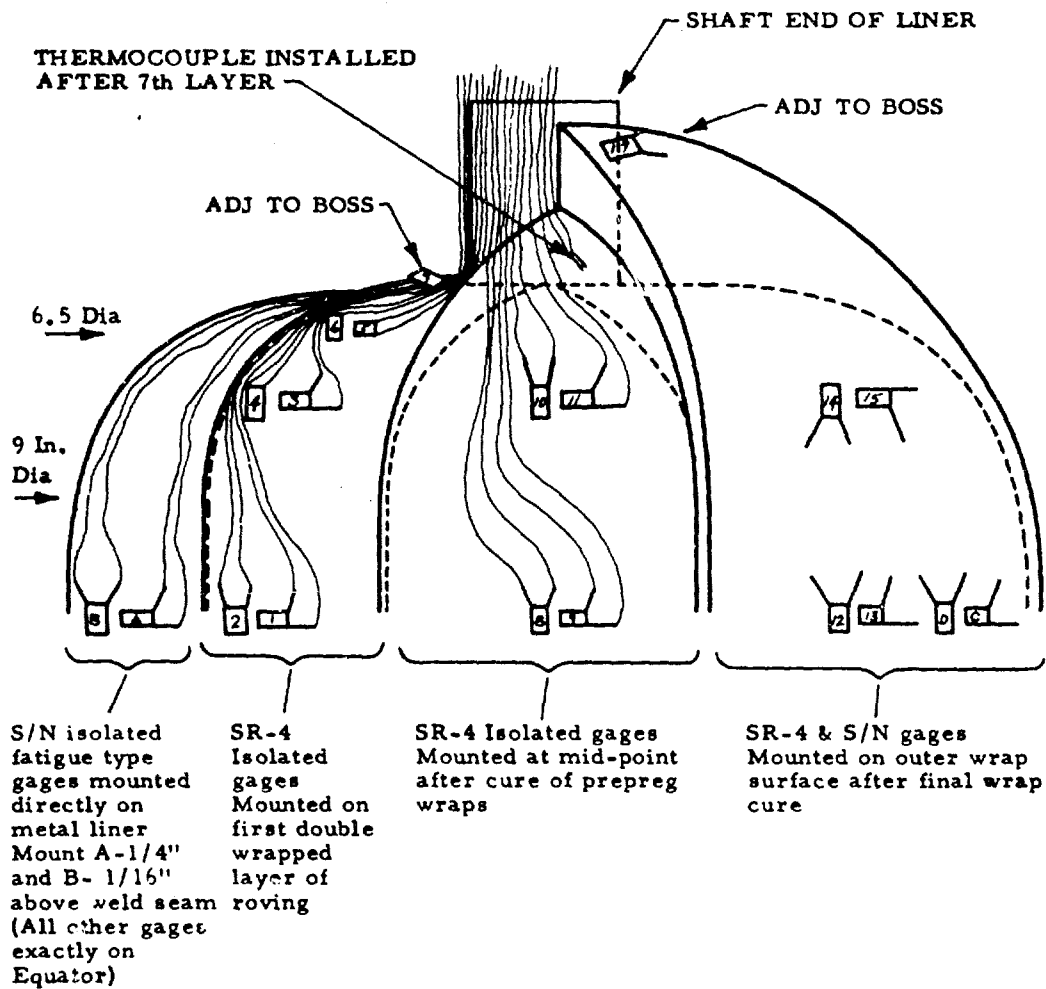
AEROJET GENERAL CORPORATION - VON KARMAN CENTER - THICK-WALL HIGH-PRESSURE CONTAINERS S/N TW-1  
HYDROTEST PRESSURE VS STRAIN TEST - 1st CYCLE MAXIMUM PRESSURE 14,082 PSI

Figure 49. Strain-Gage Curves for Container TW-1 (First Cycle)



AEROJET GENERAL CORPORATION - VON KARMAN CENTER - THICK-WALL HIGH-PRESSURE CONTAINERS SN TW-1  
 HYDROTEST PRESSURE VS STRAIN TEST - 2nd CYCLE - MAXIMUM PRESSURE ..... PSI

Figure 50. Strain-Gage Curves for Container TW-2 (Second Cycle)



**NOTES:**

SUGGESTED LEAD LENGTH 18-24"

LETTERS INDICATE S/N - FATIGUE TYPE GAGES

NUMBERS INDICATE SR-4 GAGES

DO NOT TWIST LEADS

IDENTIFY EACH PAIR OF LEADS WITH NUMBERED METAL TAB

ODD NUMBERS INDICATE HOOP DIRECTION

EVEN NUMBERS INDICATE LONGITUDINAL DIRECTION

THERE ARE A TOTAL OF (20) GAGES ON EACH CONTAINER (No. 16)

Figure 51. Location of Strain Gages

forward boss for the hydrotest fitting was closed and sealed, and the entire container was soaked overnight in "Zyglo Number ZL-1-C" dye penetrant. The container was then cut in half (approximately 1 in. from the equator), and the liner examined under black light for possible leak paths. Leak paths could not be detected. The container was subsequently X-rayed in the weld areas. Distinct flaws or possible leak paths could not be interpreted from the X-ray photographs.

The laminate was then removed from the liner of Container TW-3 by soaking the sectioned container in a stripper solution for approximately three weeks. Inspection of the stripped liner (Figures 52 and 53) indicated that the liner was deformed in the area adjacent to the liner-to-boss weld. This probably occurred during hydrotest since examination of the interior after mandrel removal did not reveal this condition. The liner has apparently folded back onto the boss in a tight "S" configuration as shown in Figure 54. The top of the "S" was crimped and cracked through at several locations. These crimped areas were the leakage paths through the liner. This area and the potential strain magnification occurring during hydrotest due to the mismatch between the thick boss and thin liner is discussed in detail in Section V,2,b,(3).

d. TW-4

Container TW-4 was tested to 10,800 psig and 7,980 psig in two separate tests which were stopped in each case after leakage exceeding the pump capacity had occurred. A rubber bladder, the design of which is shown in Figure 55, was procured and installed in Container TW-4 in order to retest the vessel a third time. The stem of each neoprene rubber bladder was bonded to the inner diameter of each forward boss using "BOSTIK 7086" A and B primer, "BOSTIK 7070" adhesive, and B-4566 hardener. The vessel was instrumented (Figure 56) and hydrostatically retested to a pressure of 14,100 psig, at which point structural failure of the vessel occurred. Curves of the strain data are presented in Figure 57. This data was replotted using the unstrained vessel contour as the zero reference line in order to observe the relative change in vessel shape during pressurization. The contours are presented in Figure 58 for incremental pressure variations.

e. TW-5

This vessel was hydrostatically tested to 4,520 psig and 5040 psig before leakage occurred. The leakage exceeded the pump capacity of 1 gallon per min on both occasions. The vessel was tested a third time by using an internal rubber bladder system. The vessel was subjected to a pressure of 3,150 psig, at which time leakage again occurred and the test was terminated.

f. TW-6

This vessel was to be overwrapped with filaments and cured using the pressurized mandrel technique. After four revolutions of wet-wound glass roving were applied, a wrinkled (buckled) condition occurred in the liner. Therefore, fabrication was not completed, nor was the vessel tested.



Figure 52. Container TW-3 Liner After Removing Laminate

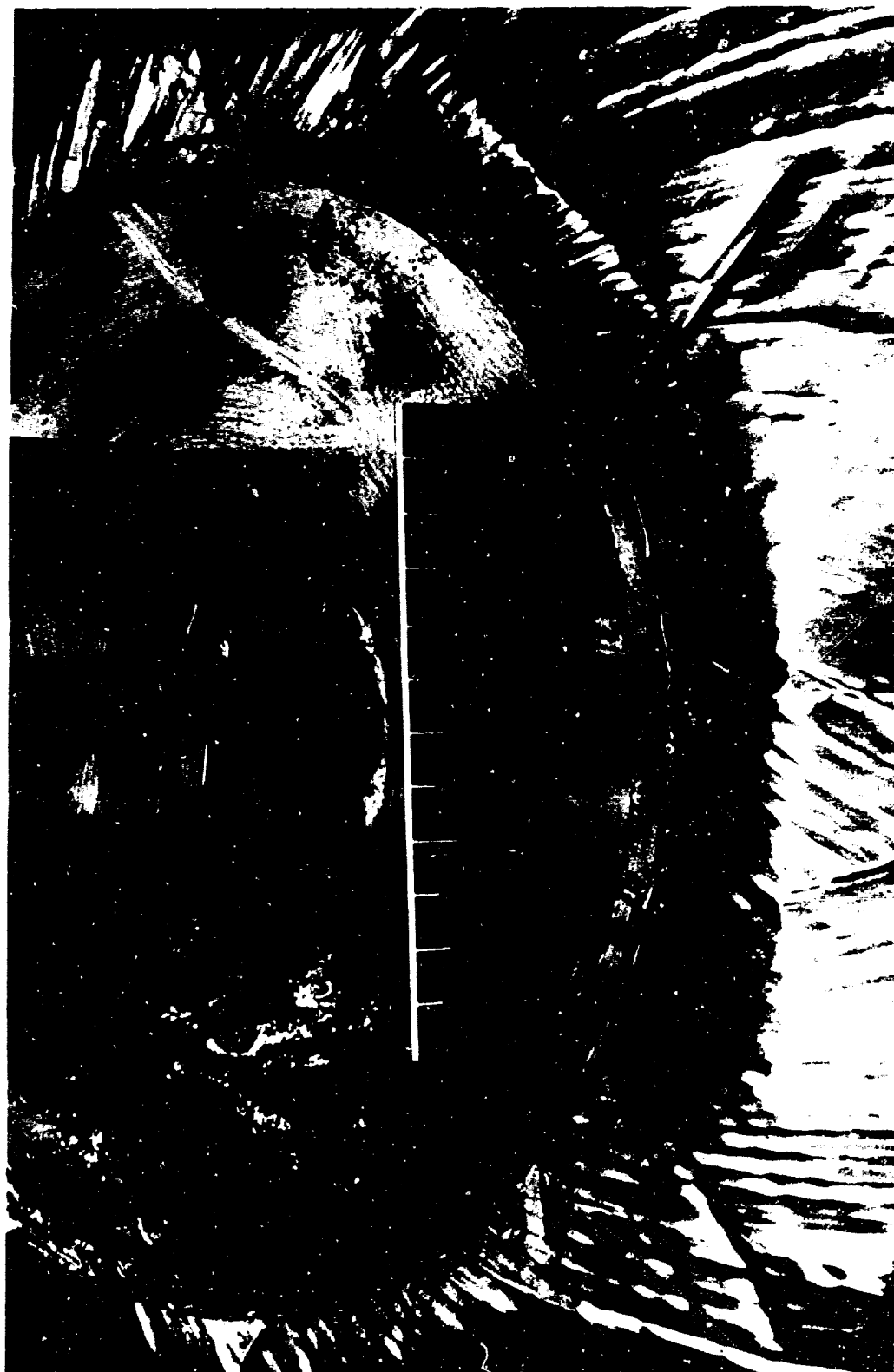


Figure 53. Liner-to-Boss Weld Section of TW-3 Liner After Removing Laminate

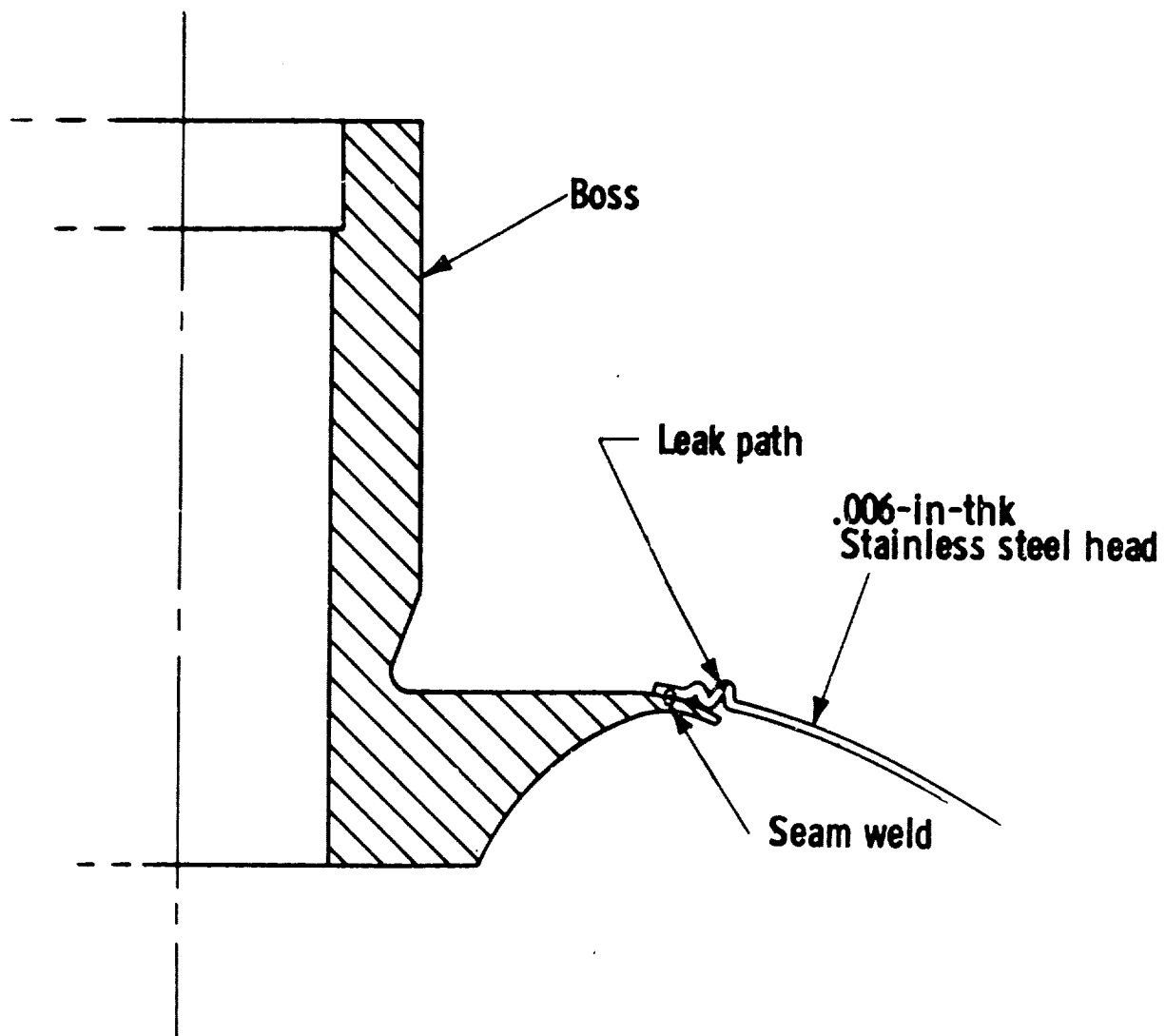
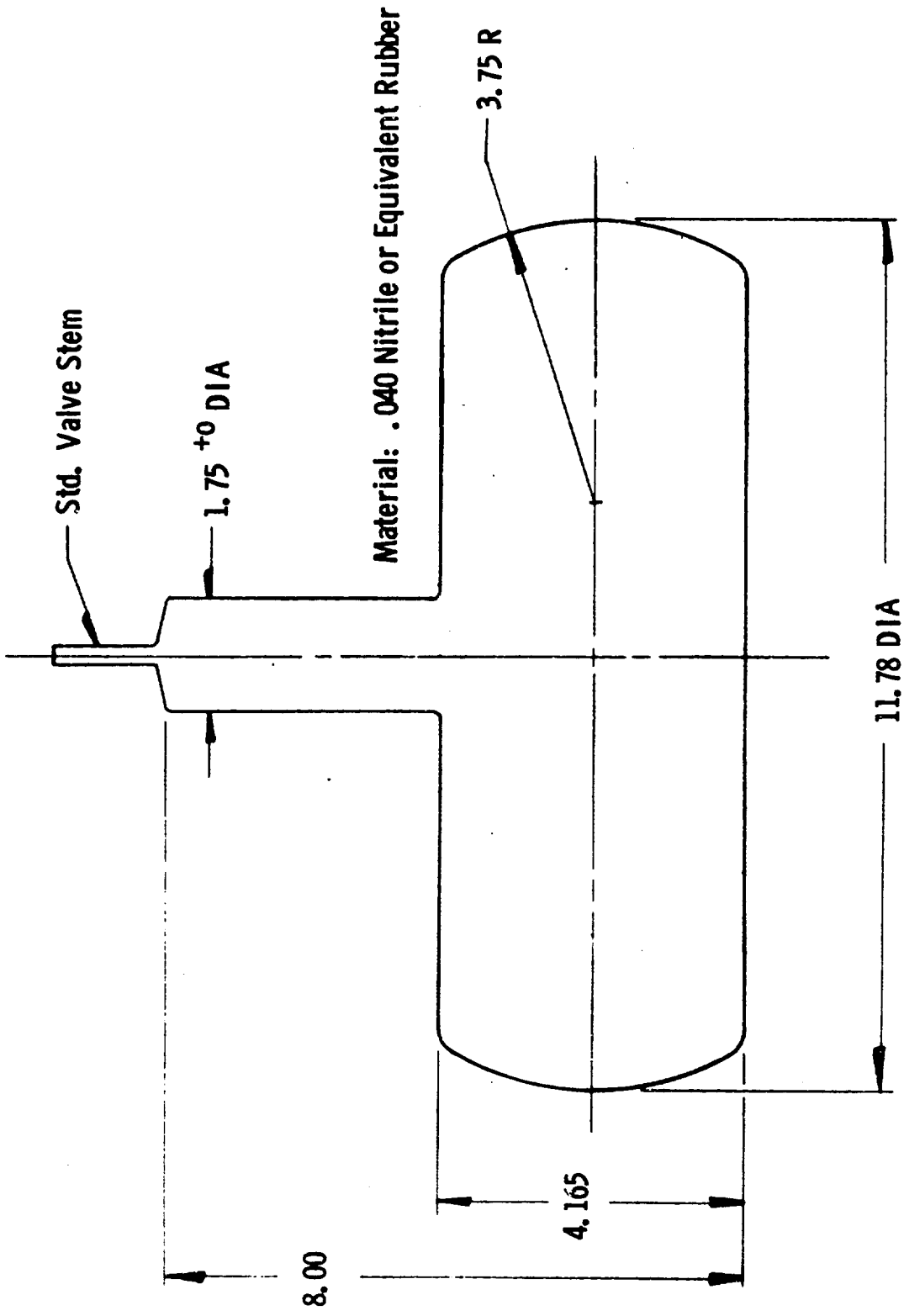


Figure 54. Crimping of Liner Adjacent to the Liner-to-Boss Weld  
(Container TW-3)



**Must Fit Through 1 3/4" Dia.**

Figure 55. Rubber Bladder for Thick-Wall Container

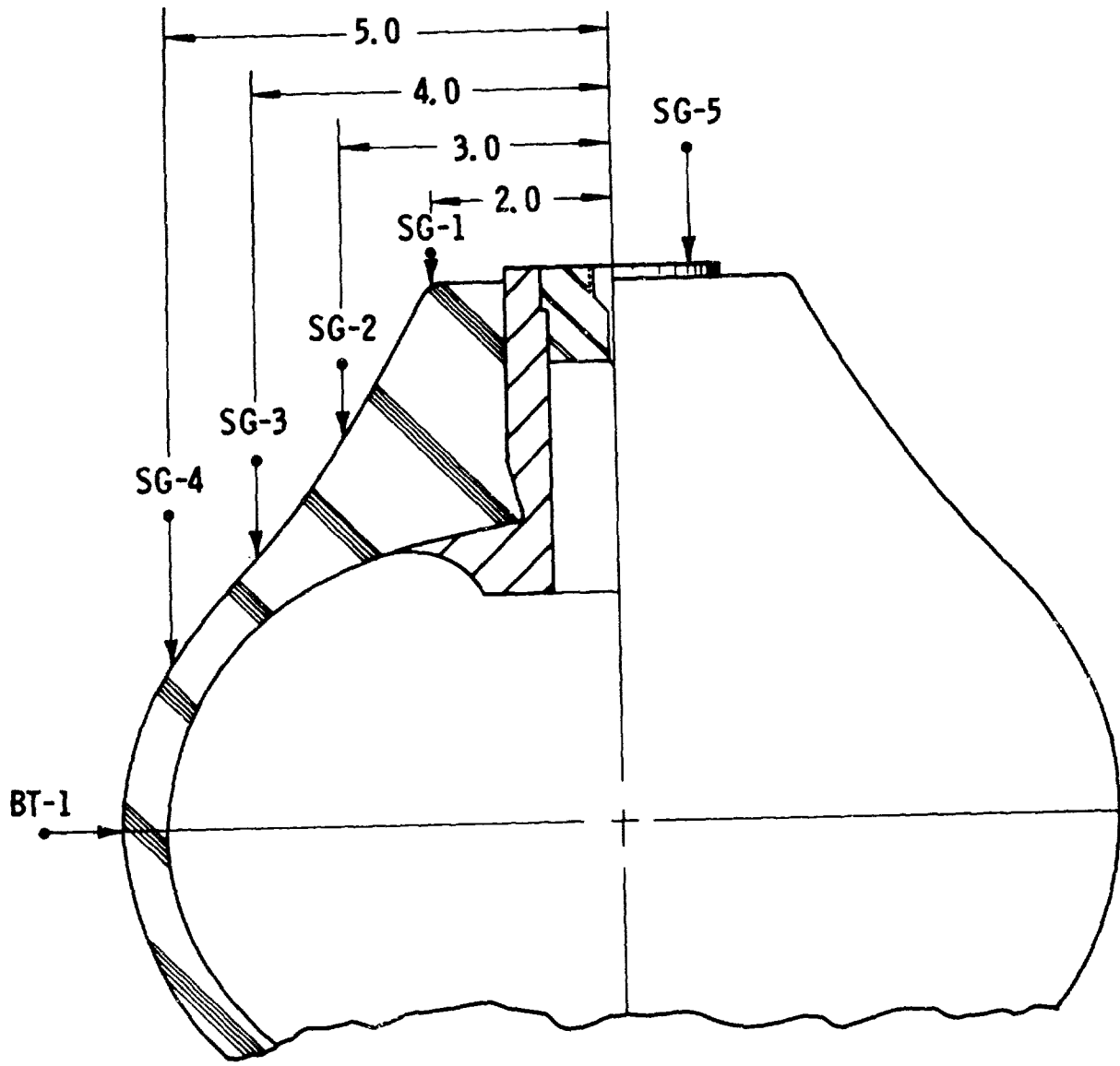


Figure 56. Instrumentation Layout

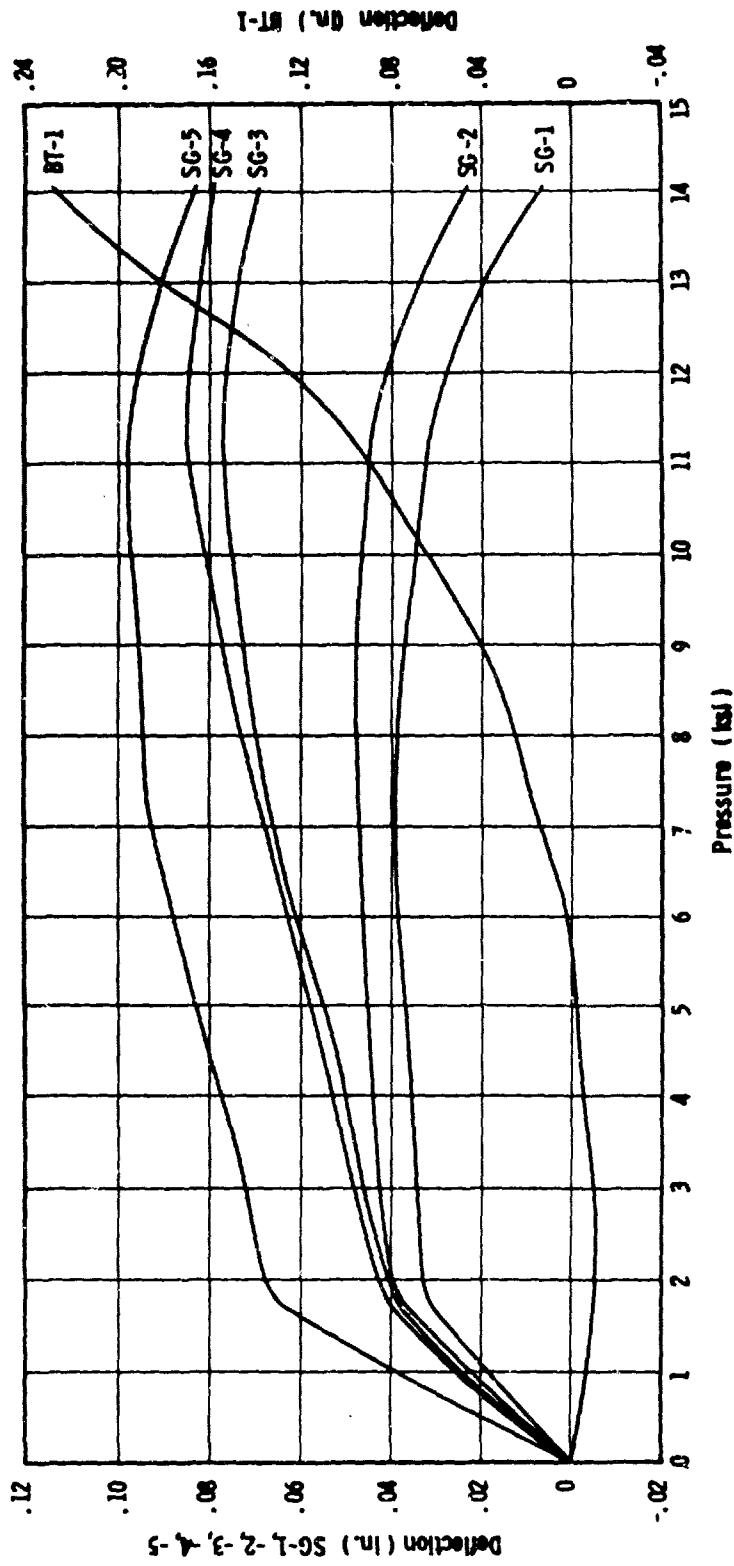


Figure 57. Pressure/Deflection Curves for TW-4

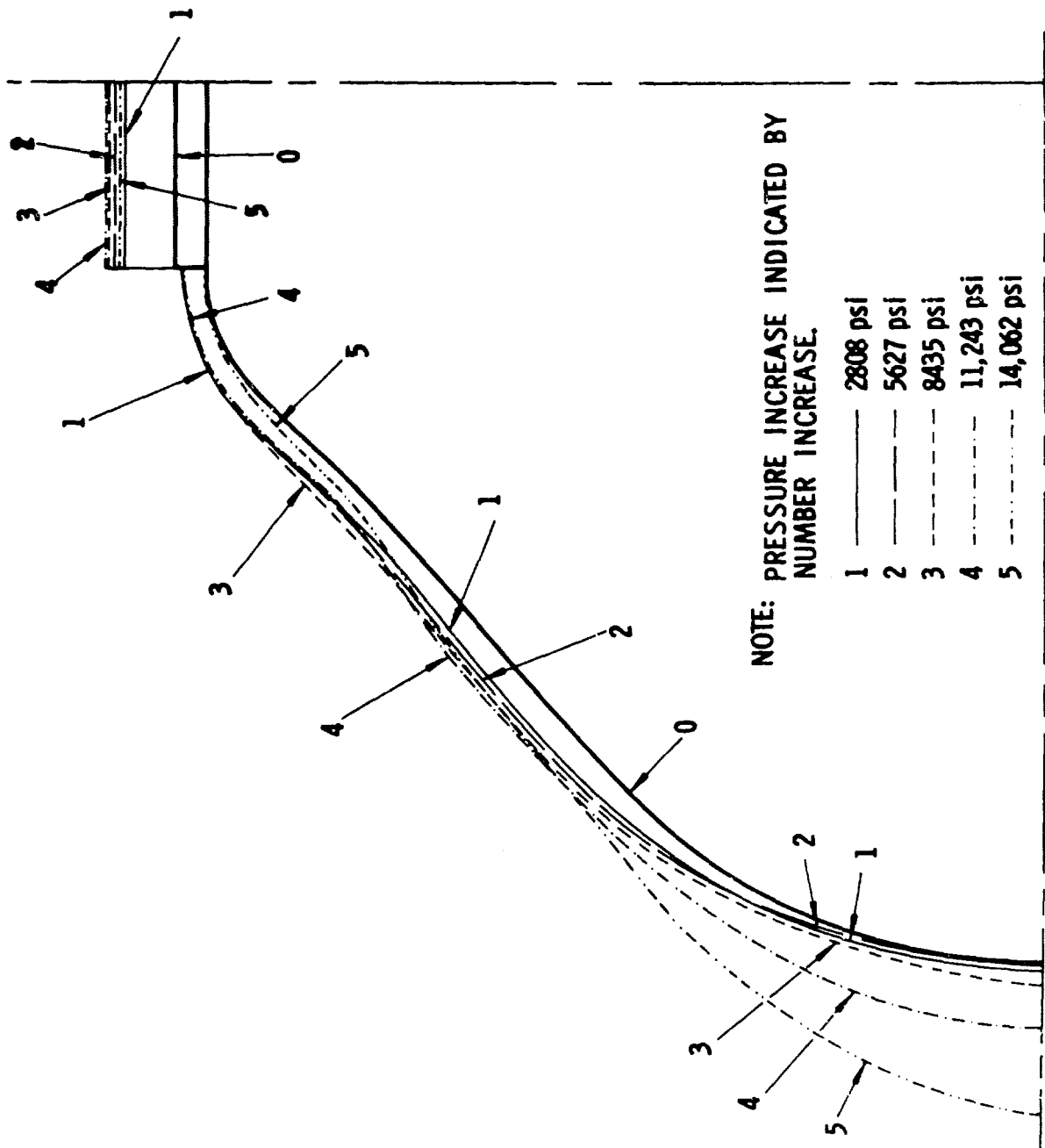


Figure 58. Vessel Growth During Pressurization (TW-4)

g. TW-7

To seal potential leak areas, the interior of this vessel was coated with liquid sealant, "Epon 828"/"LP-3"/"DMP-30" (100/100/10) after mandrel removal. The vessel was hydrostatically tested and attained the highest burst pressure reached to date (19,600 psig). Filament failure occurred at this pressure (Figure 59). Examination of the ruptured vessel, shown in Figure 60, indicates that failure probably initiated in the inner plies between the 6 in. and 9 in. chamber-diameters area. The evaluation suggests that failure may have resulted because of filament bridging in this area.

h. TW-8

The interior of this vessel was also coated with "Epon 828"/"LP-3"/"DMP-30" sealant material prior to hydrotest. This vessel was instrumented with five reed-mounted strain gages and one girth extensometer type of strain gage as shown in Figure 56. The vessel was hydrostatically tested four separate times. During the first three cycles (to 12,900, 12,900 and 12,800 psig, respectively) leakage occurred which exceeded the pump capacity. An oil spray was observed during the third cycle at the upper closure area. An internal rubber bladder was installed. The pressure was applied for the fourth cycle and failure occurred at 9,180 psig in the head area. A curve of the strain gage data during the second cycle is presented in Figure 61. The data was replotted using the unstrained vessel contour as the zero reference line, so that the relative change in vessel shape during pressurization could be evaluated. These contour plots are presented in Figure 62.

i. TW-9

The interior of this vessel was also coated with the "Epon 828"/"LP-3"/"DMP-30" liquid sealant prior to hydrotest. Two separate tests were performed on this vessel. During the first cycle, leakage exceeding the pump capacity occurred at 9,030 psig. After installation of an internal rubber bladder, the vessel was retested and excessive leakage occurred during this cycle at 8,670 psig.

j. TW-10

This vessel was the first in the second iterative design series (TW-10 through TW-12). As previously outlined, principal process changes included: (1) increased winding tensions, (2) wider payoff tape width, and (3) use of glass-reinforcement-tape dollies between the first three revolutions. Inspection of the interior of this vessel after mandrel removal indicated slight wrinkling had occurred. Crimping of the metal around the boss-to-liner weld area was also noticed. The vessel was tested to 16,700 psig, at which time a sharp sound, similar to a metal tensile specimen failing, was heard. Excessive leakage exceeding the pump capacity was encountered at this time and the test was terminated. Visual examination of the composite structure did not reveal failed areas. With slight internal pressure on the vessel, a leakage path was noticed between the boss and adjacent composite structure. This leakage would tend to indicate a liner failure, probably at the boss-to-liner weld with the fluid following the least-resistance path in emerging.



Figure 59. Container TW-7 After Burst

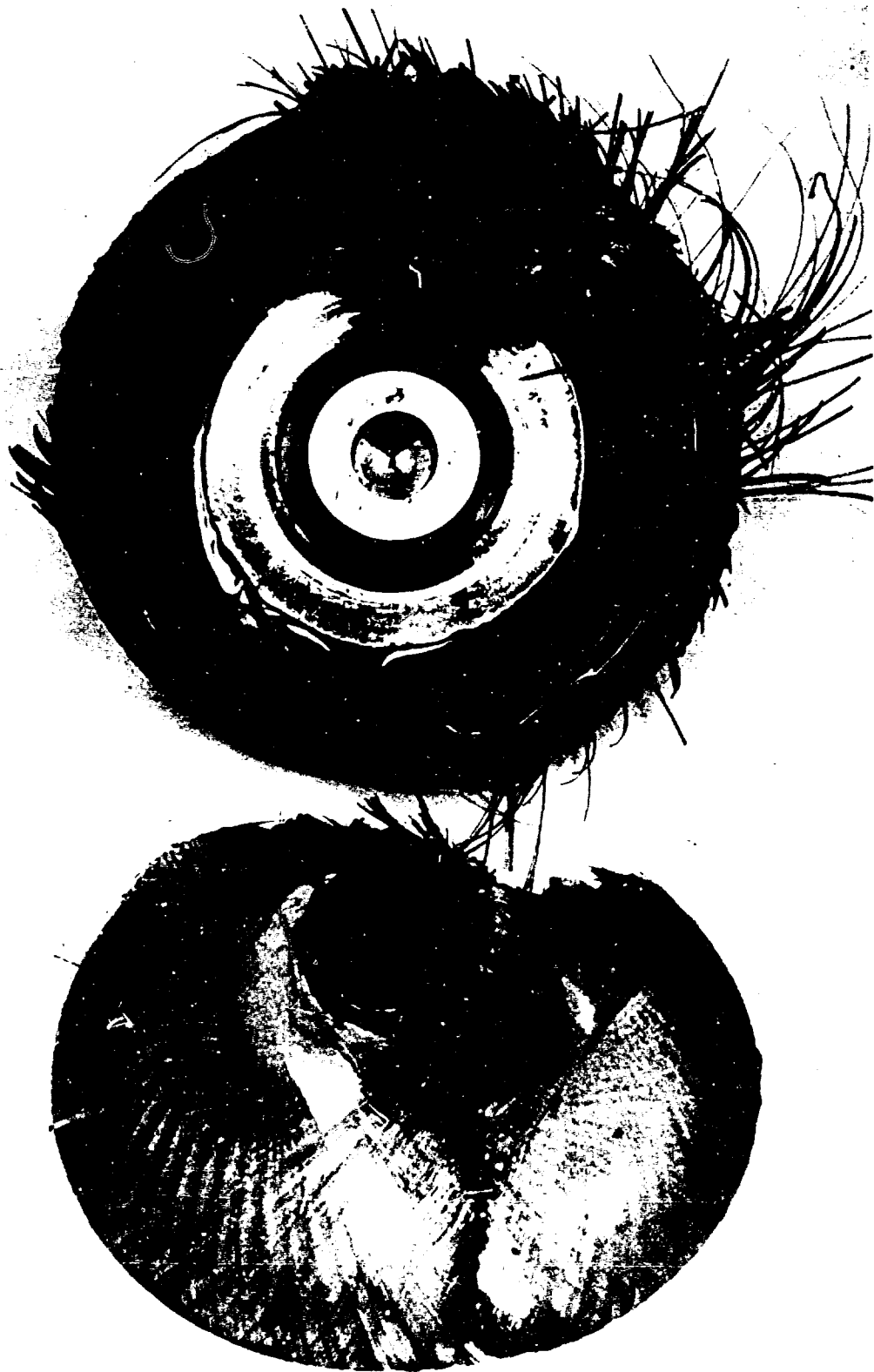


Figure 60. Container TW-7 After Sectioning

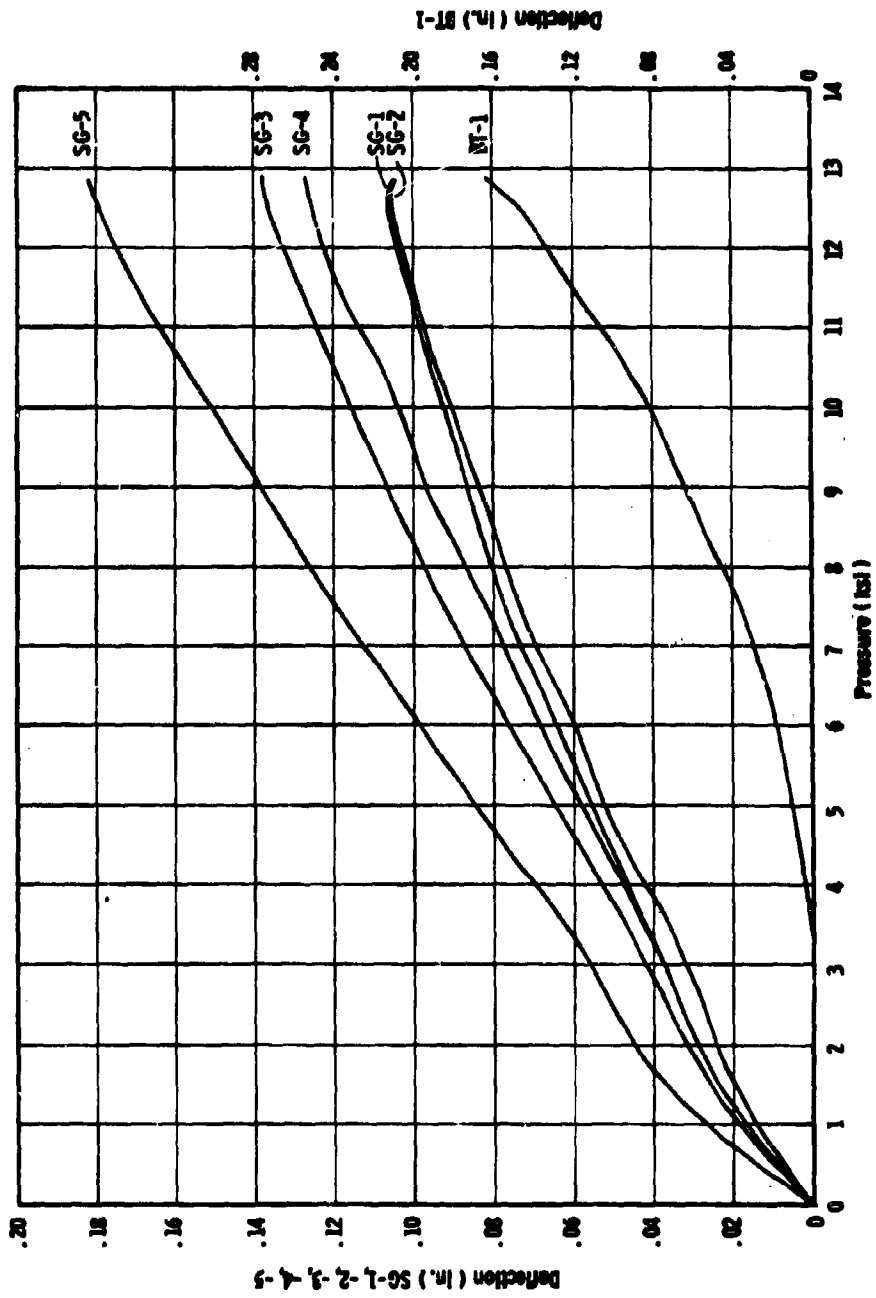


Figure 61. Pressure/Deflection Curves for TW-8

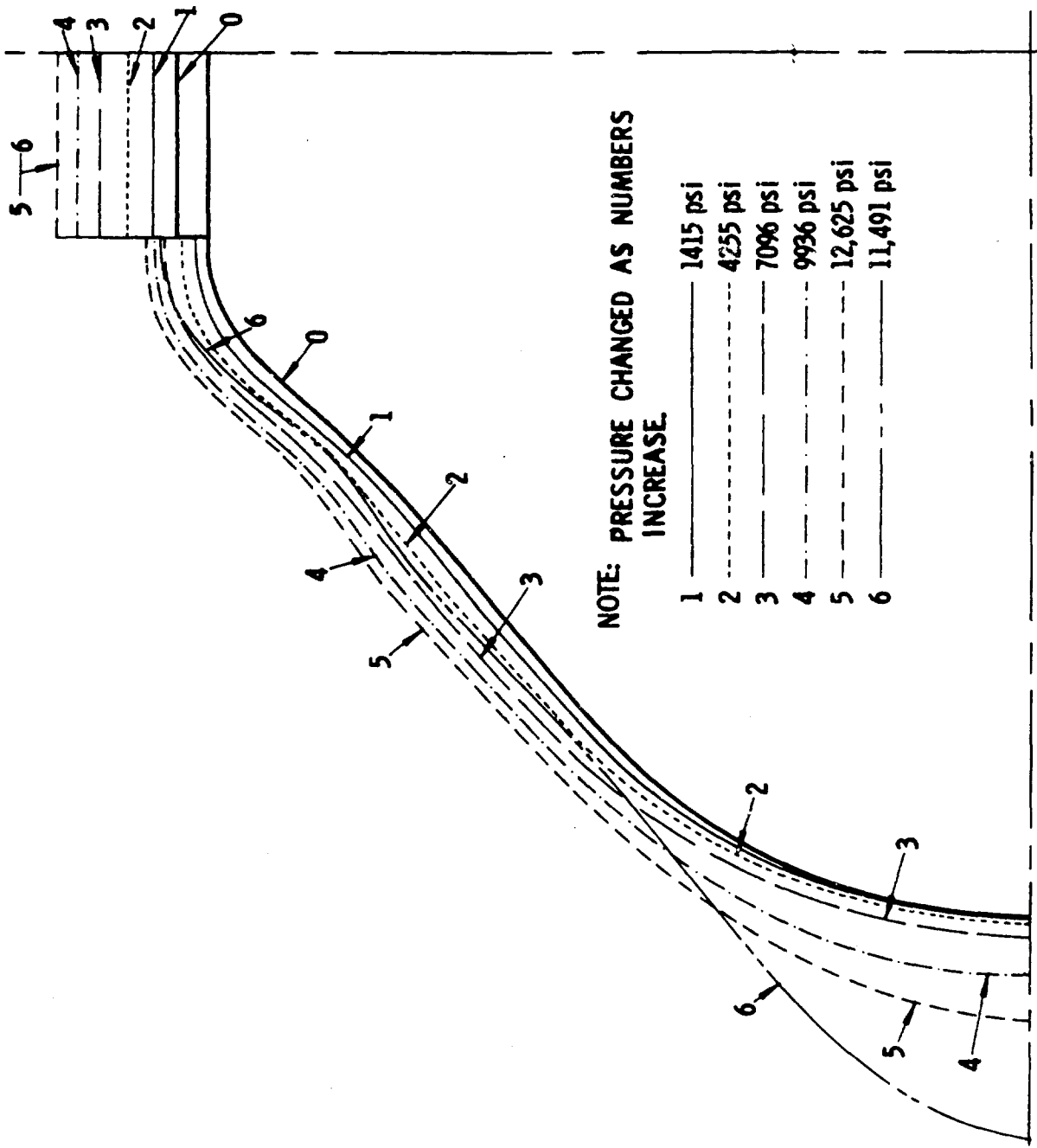


Figure 62. Vessel Growth During Pressurization (TW-8)

k. TW-11

This vessel was tested to 23,700 psig at which time filament failure occurred. Failure appeared to be initiated in the inner filaments adjacent to the aft boss and to propagate to the outer fiber layers and around to the vessel equator (Figure 63). Indications are that higher winding tensions were largely responsible for the increased burst pressure, but that the inner fibers were still supporting the major portion of the load and the outer fibers were not performing as planned.

l. TW-12

Pressurization of the containers had been performed by throttling a check-off valve nearest the test specimen and controlling the pressure rise by means of a by-pass valve in the pump circuit. This rate control restricting technique was used to minimize possible detrimental effects to the specimen from pump-pressure surges. One of the effects from this method was that pressures in the by-pass circuit were higher than desired. During the first cycle of this container, a burst diaphragm failed in the pump circuit at a test specimen pressure of 21,300 psig.

After the diaphragm was replaced, the specimen was repressurized to 20,700 psig at which level the diaphragm burst again. A different type diaphragm was then installed, rate control requirements were removed from the test condition, and the vessel was pressurized for a third cycle. Failure occurred in the filaments at 23,800 psig. The mode of failure was almost identical to that which occurred in TW-11. This pressure was the highest attained to date and was also reached after two cycles to approximately 40% above the vessel operating pressure of 15,000 psig.

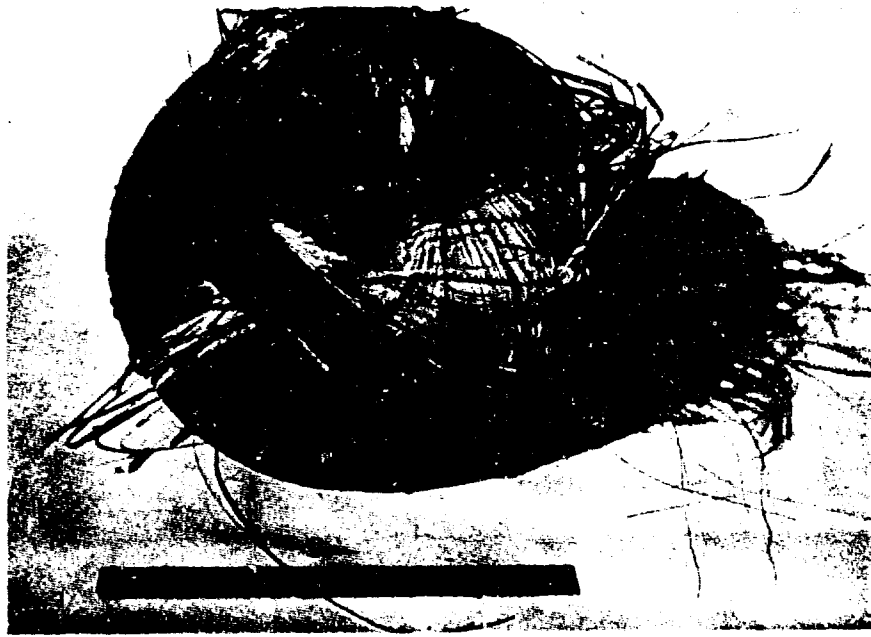
The resultant condition of the failed test specimen is seen in Figure 63. The pressure and strains were recorded on a light beam oscillograph for all three cycles. The tabulated data was plotted in Figure 64 to show the vessel growth during pressurization for the three cycles.

m. TW-13

Visual inspection of the liner interiors of this vessel and TW-15 after mandrel removal revealed negligible wrinkling and only slight crimping of the liner in the boss-to-head areas. Therefore, these two vessels were selected for the fatigue-cycling tests. A good liner-to-composite bond, indicated by the smooth liner, provided the conditions necessary to offset the problem of strain compatibility. The vessel was subjected to 13 pressure cycles from 0 to 15,000 psig. During the 13th cycle, leakage indicating liner failure was noted and the test was terminated.

n. TW-14

The interior of the vessel was examined prior to hydrotest and several wrinkled (buckled) areas were noted. The vessel was filled with water and connected to the pressure line following the hydrotest system checkout. A protective shield was placed over the specimen and pressure was applied at approximately 10,000 psig per minute. Failure occurred at 21,800 psig when



TW - 11



TW - 12

Figure 63. Containers TW-11 and TW-12 After Burst

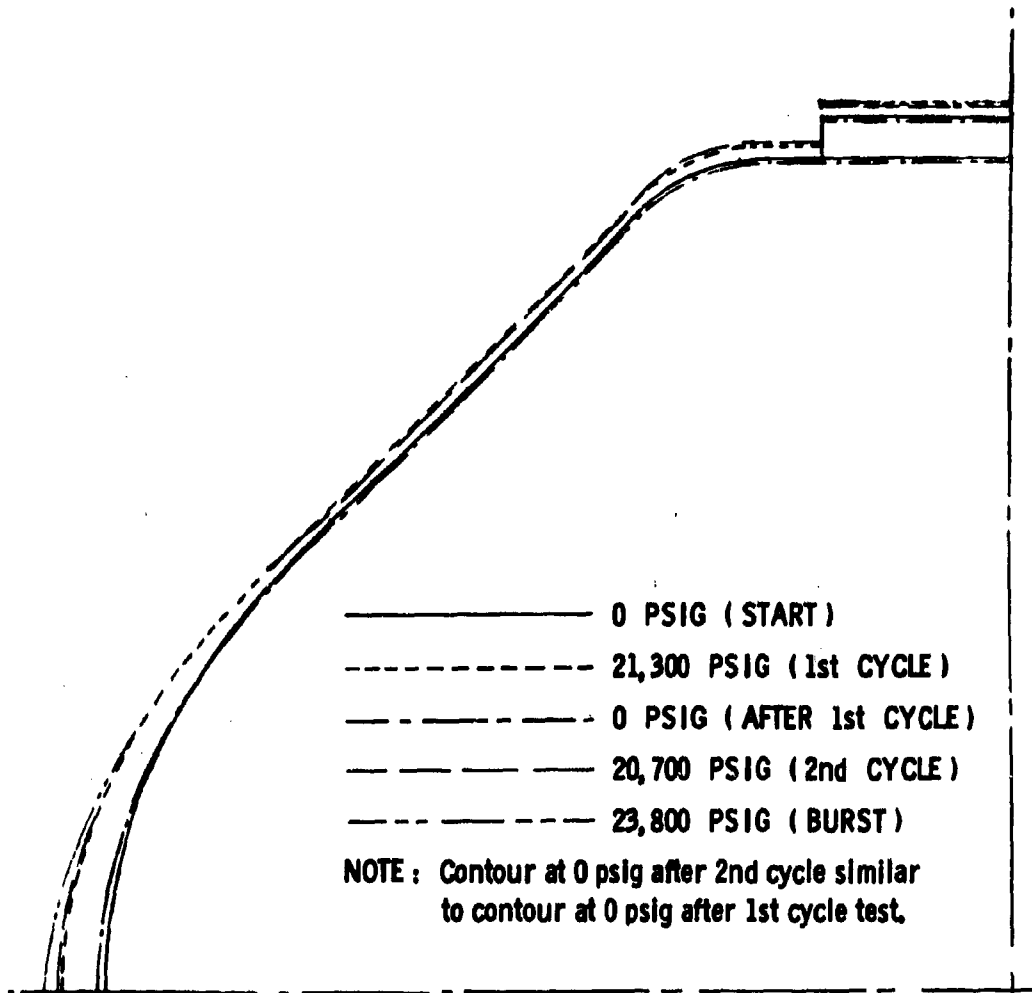


Figure 64. Vessel Growth During Pressurization (TW-12)

the pressure could no longer be increased, and which in fact slowly decayed. The protective shield was removed and it was noticed that the composite structure remained intact. With internal pressure applied to the specimen, fluid was observed to penetrate through the vessel composite wall in several areas, indicating that the liner had developed leaks and was the cause of failure.

o. TW-15

This vessel was subjected to seven pressure cycles from 0 to 15,000 psig. During the 7th cycle, leakage indicating liner failure was noted and the test was terminated.

p. TW-16

This vessel was hydrostatically pressurized in a single-cycle burst test at a rate of approximately 10,000 psig per min. The maximum pressure reached was 15,300 psig, at which point leakage exceeded the pump capacity and the test was terminated. Under slight pressurization, leakage appeared to penetrate through the composite wall. Divergence of the oil through the vessel wall prevented exact identification of the leak area, but since the composite structure remained intact, then leakage was a result of liner failure.

## SECTION VI

### CONCLUSIONS

The principal objectives of this program were to develop the theoretical stress analysis, design, prototype fabrication, and testing of thick-wall, filament-wound, metal-lined high-pressure gas containers. These objectives were all accomplished.

The developed multi-layered thick-wall vessel analysis adapted from thin-wall theory and programmed on the computer appears to satisfy preliminary designs for the thick-wall vessel structure by providing for the variation in fiber properties from layer to layer and defining winding tensions for optimum performance.

The principal design consideration was found to involve boss rigidity compared with extensibility of the filament-wound composite adjacent to the boss. High radial strains in the filaments, combined with the rigidity of the thick-metal boss, led to strain mismatch. As a result, localized strain magnification occurred in the transition area between the thick boss and thin liner to maintain overall strain compatibility. This condition is believed to be the primary contributing factor in premature failure of the single-cycle tested vessels.

The highest single-cycle burst pressures were attained by the three vessels (TW-7, TW-11, and TW-12) which were the only units to fail in the composite structure. Failure in other vessels was due to liner leakage in which the composite shell structure remained intact. The demonstration that significantly higher burst pressures are available with thin-metal liners indicates that further development is warranted, particularly in methods to minimize high radial strains in the filaments adjacent to the thick-metal boss.

Comparisons on the basis of burst pressures indicated that the vessels (TW-10 through TW-12) fabricated after incorporating modifications in processing techniques were clearly superior to preceding units (TW-1 through TW-9). Two of these vessels burst at pressures more than 20% higher than had previously been attained. One of these vessels, TW-12, was cycled twice between zero and 40% above the operating pressure prior to burst. Average burst pressures were 21,400 psi for TW-10 through TW-12 as compared to 11,900 psi for TW-1 through TW-9. This indicated the following modifications were effective in achieving improvements: (a) applying the fibers at higher winding tensions to minimize radial strains, (b) increasing the payoff tape width to reduce filament bridging and excessive filament buildup adjacent to the axial bosses, and (c) using glass-reinforcement doilies to optimize the contour. In addition, it was also felt that machined grooves in the final payoff roller kept the filaments separated and permitted them to be applied as a more uniform band.

The ability of the thin-metal liner to sustain compressive buckling loads after mandrel removal, or after strain cycling, was found to be another significant factor affecting the performance of the thick-wall containers.

In an effort to prevent liner buckling and subsequent premature vessel failure, development work was conducted on (a) a sand-acrylic mandrel material to offer sufficient support for the thin-metal liner during overwrapping and subsequent curing of the composite structure, and (b) a liner cleaning method, followed by an adhesive bonding technique to improve the bond between the metal liner and the composite shell structures.

Only moderate success is attributed to TW-13, which was cycled a total of 13 times between zero psig and the working pressure of 15,000 psig. Liner leakage, which prevented further cycling, was caused by adhesive bond failure, resulting in liner buckling after depressurization and subsequent fatigue failure in the metal.

## SECTION VII

### RECOMMENDATIONS

Additional studies are recommended on glass filament-wound, metal-lined vessels. Further development is required in eliminating compressive buckling of the thin-metal liner by improving or ensuring the integrity of the liner-to-composite shell adhesive bond. These recommended studies include evaluation of adhesives, cleaning processes, application methods, internal mandrel materials, and nondestructive inspection techniques.

Another suggested approach to successful metal-lined glass composite structures would be to utilize a load-bearing, non-buckling metal liner. In this manner the liner would possess sufficient thickness to (a) share the load with the composite structure, (b) work to an efficient filament stress level (requiring the capability to plastically deform and then work in the tensile and compressive elastic regions of the liner), and (c) possess the capability of being cyclically strained on its offset elastic stress-strain curve without incurring buckling under compression loads.

Although vessels with relatively thicker wall liner would not attain performance levels as high as vessels with thin-metal liners, certain advantages would occur. To begin with, adhesive bonding of the liner to the composite structure would not be an area of concern. By maintaining a careful balance between the liner compressive strength and the compressive stresses caused by the overwrapped fibers, the internal mandrel could be eliminated. Intermittent periods during which the composite structure would be cured would be required for thick-wall vessels. Thus, the applied composite structure and metal liner would serve to support the pressures from subsequent windings.

From the fabrication standpoint, the use of the thicker, non-buckling, load-bearing metal liner would offer certain advantages. For example, (a) standard metal fabrication, welding, and inspection procedures would be used in constructing the liners, (b) special handling precautions would not be necessary as with thin-metal foil liners, (c) tooling costs would be minimized since an internal mandrel material would not be required to support the compression loads.

Future investigations should also include the use of higher modulus filaments (graphite, boron, high-modulus glass, etc.) in order to lower strains and thereby improve performance levels.

## APPENDIX I

### THICK-WALL, FILAMENT-WOUND, PRESSURE-VESSEL ANALYSIS

#### I. GENERAL DISCUSSION

This appendix provides an analysis of thick-wall, filament-wound, pressure vessels. The equations are arranged to adapt the analysis to existing high-speed digital-computer programs for thin-wall pressure vessels. The analysis provides for the introduction of different materials in individual layers of the wall, in addition to the computation of winding tensions required for optimum performance. Each layer can be assigned an individual volume percentage of fiber, tensile modulus, thickness, and either fiber winding stress or design-allowable fiber stress.

The major differences between the analysis in this appendix and thin-wall analyses are (a) radius-of-curvature variations from layer to layer are taken into account, (b) each layer has a different length for a given element of the shell, and (c) thickness of a layer changes with the applied load because of the radial stress (pressure) and Poisson's effect from fiber strains within the layer.

The following basic assumptions are made in this analysis:

- A. The pressure-vessel liner is not a load-carrying member.
- B. A netting analysis can be used.
- C. The changes in the hoop and longitudinal strains between the winding and design conditions are equal.
- D. A rigid mandrel is used.
- E. The fiber stresses at the wrapping and design conditions are known for the first layer.
- F. Either the wrap or the design stress is known for all layers other than the first.
- G. The wrap angle is the same for all layers.
- H. Displacements of points within the shell are perpendicular to the surface.
- I. Bending stresses are negligible.

The basic nomenclature is illustrated in Figure 65, which shows the general shell of revolution. Symbols are defined in a list at the end of this appendix.

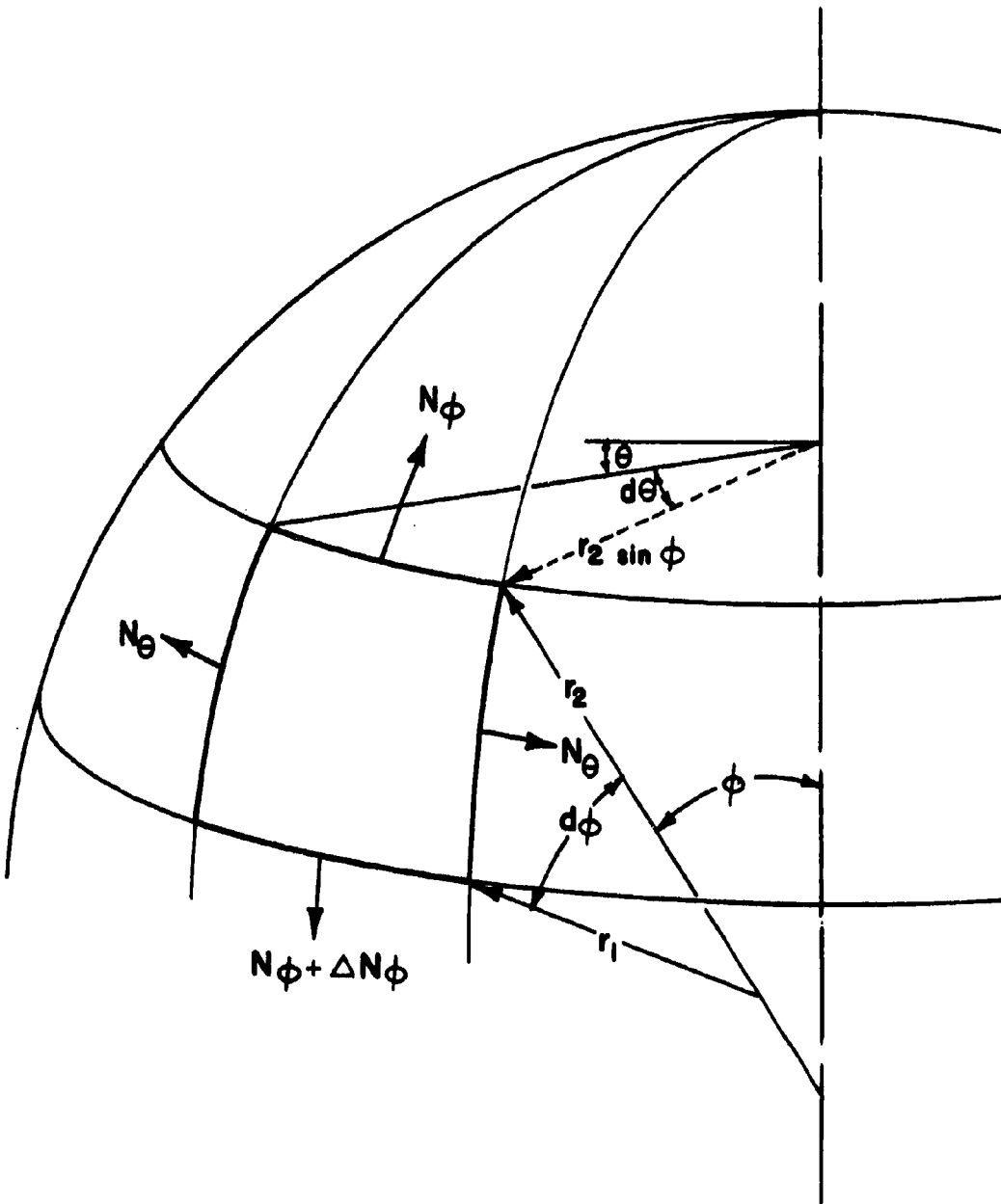


Figure 65. Element of Shell of Revolution

## II. DESIGN OF HEAD

### A. EQUATOR

It is assumed that the changes in the hoop and longitudinal strains between the winding and design conditions are equal. The changes in strain in all directions are therefore equal and can be equated to the change in filament strain. This assumption requires that only one strain-compatibility equation be used.

The presence of equal strains in all directions at all points within the shell results in movement at all points in a direction perpendicular to the shell with changes in the applied load (pressure). This radial movement, shown in Figure 66 for Layers  $i$  and  $i-1$ , establishes the following equation of compatibility:

$$r_{1i}(1+\epsilon_{mi})d\phi = r_{1,i-1}(1+\epsilon_{m,i-1})d\phi + \frac{1}{2} \left[ t_i(1+\epsilon_{ri}) + t_{i-1}(1+\epsilon_{r,i-1}) \right] d\phi$$

where

$$r_{1i} - r_{1,i-1} = \frac{1}{2} (t_i + t_{i-1})$$

Thus,

$$(r_1 \Delta \epsilon_m)_i = (r_1 \Delta \epsilon_m)_{i-1} + t_{i-1} \epsilon_{r,i-1} \quad (1)$$

where

$$(r_1 \Delta \epsilon_m)_i = r_{1i} \epsilon_{mi} - \frac{1}{2} t_i \epsilon_{ri} \quad (2)$$

and

$$(r_1 \Delta \epsilon_m)_{i-1} = r_{1,i-1} \epsilon_{m,i-1} - \frac{1}{2} t_{i-1} \epsilon_{r,i-1} \quad (3)$$

The strain in the meridional direction is equal to the strain in the fibers:

$$\epsilon_{mi} = \left[ (\sigma_d - \sigma_w) / E \right]_i \quad (4)$$

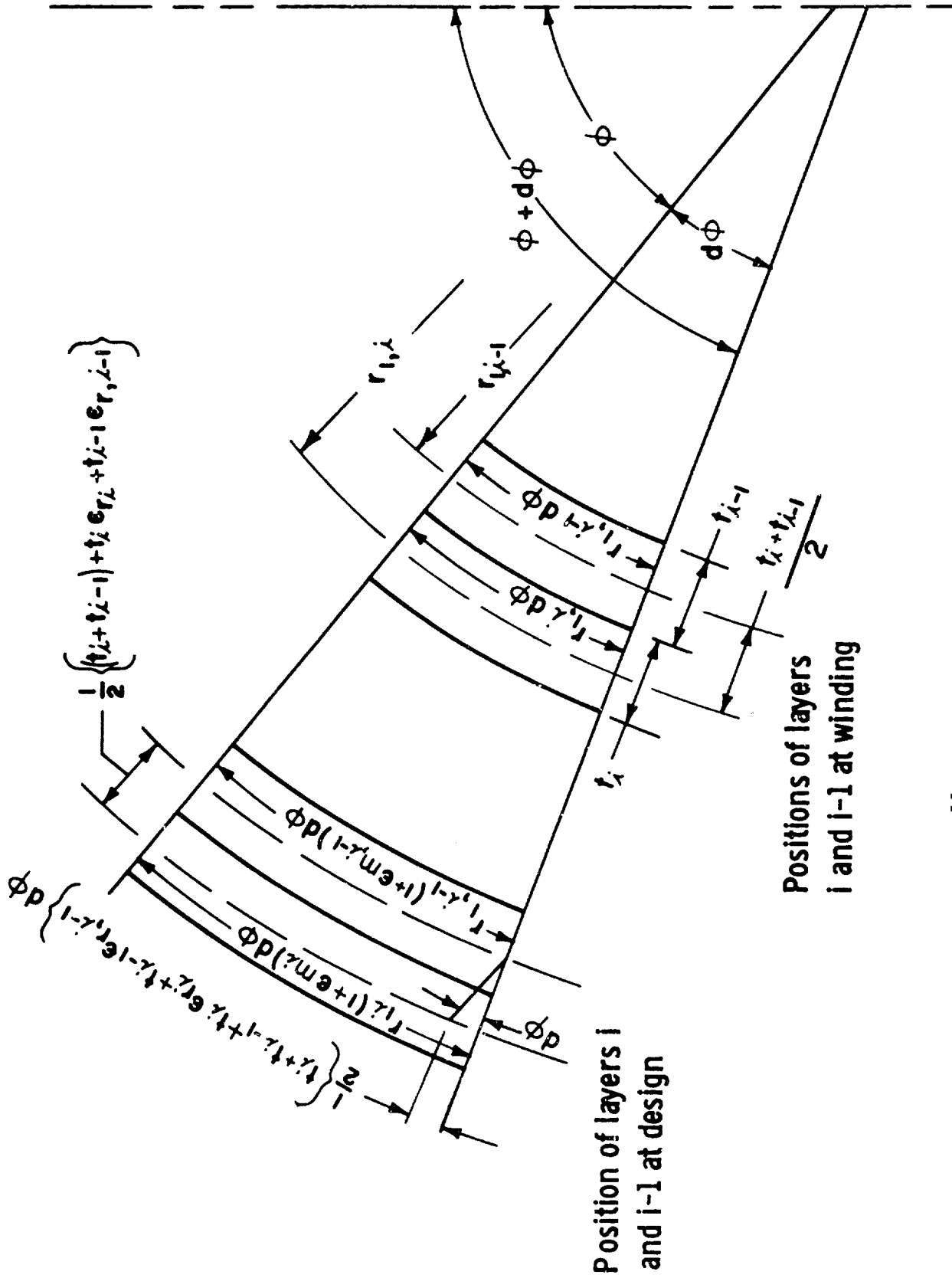


Figure 66. Diagram of Strain Compatibility

and

$$\epsilon_{m,i-1} = \left[ (\sigma_d - \sigma_w) / E \right]_{i-1} \quad (1a)$$

Therefore,

$$(r_1 \Delta \epsilon_m)_i = r_{1i} \left[ (\sigma_d - \sigma_w) / E \right]_i - \frac{1}{2} t_i \epsilon_{ri} \quad (2a)$$

The radial strain,  $\epsilon_{ri}$ , at Layer 1 is computed assuming that the radial stress is the average pressure applied across the layer:

$$\epsilon_{ri} = (-P_{A1}) \frac{1}{E_1 K_1} - \frac{v_1 \sigma_{di}}{E_1} \quad (5)$$

where

$$P_{A1} = P_{A,i-1} - (\Delta p_{i-1} / 2) - (\Delta p_i / 2)$$

Because  $\Delta p_i$  is the portion of the design pressure resisted by Layer 1, this term can be calculated with the aid of a force balance in the axial direction.

$$\text{Applied force} = \pi r_2^2 p_d$$

$$\text{Reacting force} = 2\pi \cos^2 \alpha \sum_{i=1}^n r_{2i} K_i t_i \sigma_{di}$$

Therefore,

$$p_d = \frac{2 \cos^2 \alpha}{r_2^2} \sum_{i=1}^n r_{2i} K_i t_i \sigma_{di} = \sum_{i=1}^n \Delta p_i$$

and

$$\Delta p_i = \frac{K_i t_i \sigma_{di}}{r_{A1}}$$

where

$$\frac{1}{r_{A1}} = \frac{2r_{2i} \cos^2 \alpha}{r_2^2}$$

Assuming  $\sigma_{wi}$  and  $p_{wi}$  are small compared to  $\sigma_{di}$  and  $p_{A1}$ , respectively, the radial strain is

$$\begin{aligned} \epsilon_{r1} &= -p_{A1} \frac{1}{E_1 K_1} - \frac{\nu_1 \sigma_{di}}{E_1} \\ &= \left[ -p_{A,1-1} + (\Delta p_{1-1}/2) \right] \frac{1}{E_1 K_1} + \frac{t_1 \sigma_{di}}{2r_{A1} E_1} - \nu_1 \frac{\sigma_{di}}{E_1} \\ &= \frac{\left[ -p_{A,1-1} + (\Delta p_{1-1}/2) \right]}{E_1 K_1} + \frac{\sigma_{di}}{E_1} \left[ \frac{t_1}{2r_{A1}} - \nu_1 \right] \end{aligned} \quad (5a)$$

From Equations (2a) and (5a),

$$\begin{aligned} (r_1 \Delta \epsilon_m)_1 &= r_{11} \left[ (\sigma_d - \sigma_w)/E \right]_1 - \frac{1}{2} t_1 \frac{\left[ -p_{A,1-1} + (\Delta p_{1-1}/2) \right]}{E_1 K_1} \\ &\quad - \frac{t_1}{2} \frac{\sigma_{di}}{E_1} \left[ \frac{t_1}{2r_{A1}} - \nu_1 \right] \\ &= \frac{\sigma_{di}}{E_1} \left[ r_{11} - \frac{t_1}{2} \left( \frac{t_1}{2r_{A1}} - \nu_1 \right) \right] - \frac{\sigma_{wi} r_{11}}{E_1} \\ &\quad - \frac{t_1}{2} \frac{\left[ -p_{A,1-1} + (\Delta p_{1-1}/2) \right]}{E_1 K_1} \end{aligned} \quad (2b)$$

At the equator,  $r_1 = r_{10}$ ,  $r_2 = a$ , and  $\alpha = \alpha_0$ .

$$r_{10l} \Delta \epsilon_{m1} = \frac{\sigma_{d1}}{E_1} \left[ r_{10l} - \frac{t_1}{2} \left( \frac{t_1}{2r_{A1}} - \nu_1 \right) \right] - \frac{\sigma_{w1} r_{10l}}{E_1} - \frac{t_1}{2} \frac{[-p_{A,i-1} + (\Delta p_{i-1}/2)]}{E_1 K_1} \quad (2c)$$

For the first layer,  $\sigma_{d1}$  and  $\sigma_{w1}$  are known and  $p_{A,i-1} = (\Delta p_{i-1}/2)$   
 $= p_d$ :

$$r_{10l} \Delta \epsilon_{m1} = \frac{\sigma_{d1}}{E_1} \left[ r_{10l} - \frac{t_1}{2} \left( \frac{t_1}{2r_{A1}} - \nu_1 \right) \right] - \frac{\sigma_{w1} r_{10l}}{E_1} + \frac{t_1 p_d}{2E_1 K_1} \quad (2d)$$

where

$$r_{10l} = r_{10} + (t_1/2)$$

$$a_1 = a + (t_1/2)$$

and

$$r_{A1} = \frac{a^2}{2a_1 \cos^2 \alpha_0}$$

Combining Equation (2c) and Equation (1) adjusted for the equator,

$$r_{1,0,i-1} \Delta \epsilon_{m,i-1} + t_{i-1} \epsilon_{r,i-1} = \frac{\sigma_{d1}}{E_1} \left[ r_{10l} - \frac{t_1}{2} \left( \frac{t_1}{2r_{A1}} - \nu_1 \right) \right] - \frac{\sigma_{w1}}{E_1} r_{10l} - \frac{t_1}{2} \frac{[-p_{A,i-1} + (\Delta p_{i-1}/2)]}{E_1 K_1}$$

When  $\sigma_{di}$  is known,

$$\sigma_{wi} = \frac{E_i}{r_{loi}} \left\{ -r_{1,0,i-1} \Delta \epsilon_{m,i-1} - t_{i-1} \epsilon_{r,i-1} - \frac{t_i}{2} \frac{[-p_{A,i-1} + (\Delta p_{i-1}/2)]}{E_i K_i} \right\} + \sigma_{di} \left[ 1 - \frac{t_i}{2r_{loi}} \left( \frac{t_i}{2r_{Ai}} - \nu_i \right) \right] \quad (6)$$

When  $\sigma_w$  is known,

$$\sigma_{di} = \frac{E_i}{r_{loi} - \frac{t_i}{2} \left( \frac{t_i}{2r_{Ai}} - \nu_i \right)} \left\{ r_{1,0,i-1} \Delta \epsilon_{m,i-1} + \epsilon_{r,i-1} t_{i-1} + \frac{\sigma_{wi} r_{loi}}{E_i} + \frac{t_i}{2} \frac{[-p_{A,i-1} + (\Delta p_{i-1}/2)]}{E_i K_i} \right\} \quad (7)$$

The radii of curvature of the positions of neutral stresses at the equator are calculated as follows:

$$a_c = a + \Delta t$$

$$r_{loc} = r_{lo} + \Delta t$$

where

$$\Delta t = \frac{\sum_{i=1}^n \sigma_{di} K_i t_i \left[ (t_i/2) + \sum_{j=1}^{i-1} t_j \right]}{\sum_{i=1}^n \sigma_{di} K_i t_i}$$

B. HEAD CONTOUR

For the applied force in the axial direction (see Figure 65),

$$\text{Applied force} = \pi p_d (r_2 \sin \phi)^2$$

$$\text{Reacting force} = 2\pi r_{2c} \sin \phi N_\phi \sin \phi$$

$$N_\phi = \frac{p_d r_2^2}{2r_{2c}}$$

For the force in the hoop direction, the equilibrium equation (neglecting second-order terms) is obtained from Figure 65:

$$2N_\phi r_{2c} \sin \phi d\theta \frac{d\phi}{2} + 2N_\theta r_{1c} d\phi \sin \phi \frac{d\theta}{2} = p_d r_1 r_2 \sin \phi d\phi d\theta$$

$$N_\theta = \frac{p_d r_1 r_2}{r_{1c}} - N_\phi \frac{r_{2c}}{r_{1c}} = \frac{p_d r_2}{2} \left[ \frac{2r_1}{r_{1c}} - \frac{r_2}{r_{1c}} \right]$$

For proper balance of forces,

$$\frac{N_\theta}{N_\phi} = \tan^2 \alpha = \frac{\frac{p_d r_2}{2} \left[ \frac{2r_1}{r_{1c}} - \frac{r_2}{r_{1c}} \right]}{\frac{p_d r_2^2}{2r_{2c}}}$$

Thus,

$$\tan^2 \alpha = \frac{r_{2c}}{r_2} \left[ 2 \frac{r_1}{r_{1c}} - \frac{r_2}{r_{1c}} \right] = \frac{r_{2c}}{r_2} \frac{r_1}{r_{1c}} \left[ 2 - \frac{r_2}{r_1} \right] \quad (8)$$

$$\tan^2 \alpha = 2 \frac{r_{2c}}{r_2} \frac{r_1}{r_{1c}} - \frac{r_{2c}}{r_{1c}}$$

If it is assumed that the ratios  $r_{2c}/r_2$  and  $r_1/r_{1c}$  remain constant for all points,

$$K_P = \frac{r_{2c}}{r_2} \frac{r_1}{r_{1c}} = \frac{a_c}{a} \frac{r_{1c}}{r_{1oc}}$$

and

$$\tan^2 \alpha = 2K_P - \frac{r_{2c}}{r_{1c}} \quad (8a)$$

The radii of curvature can be expressed as follows in geometric coordinates (Reference 10):

$$\frac{r_{1c}}{a_c} = \frac{- [1 + (u')^2]^{3/2}}{u''} \quad (9)$$

and

$$\frac{r_{2c}}{a_c} = \frac{- z [1 + (u')^2]^{1/2}}{u'} \quad (10)$$

where

$$u = \frac{y}{a_c} \quad (11)$$

and

$$z = \frac{x}{a_c} \quad (12)$$

For a geodesic isotensoid (Reference 11) of  $D = x_0/a_c$ ,

$$\sin \alpha = \frac{x_0}{x} = \frac{D}{z} \quad (13)$$

$$\tan^2 \alpha = \frac{\sin^2 \alpha}{\cos^2 \alpha} = \frac{\sin^2 \alpha}{1 - \sin^2 \alpha} = \frac{D^2}{z^2 - D^2} \quad (14)$$

For in-plane patterns (Reference 12),

$$\tan \alpha = \frac{\tan \gamma \sin \phi + \cos \phi \cos \theta}{\sin \theta} \quad (15)$$

From Equation (10),

$$r_{2c} = \frac{-za_c}{u'} \left[ 1 + (u')^2 \right]^{1/2} \quad (10a)$$

From Figure 67,

$$\sin \phi = -\frac{x}{r_{2c}} = \frac{x u'}{z a_c \left[ 1 + (u')^2 \right]^{1/2}} = \frac{u'}{\left[ 1 + (u')^2 \right]^{1/2}} \quad (16)$$

$$\tan \phi = \frac{dy}{dx} = \frac{du}{dz} = u' \quad (17)$$

$$\cos \phi = \frac{\sin \phi}{\tan \phi} = \frac{1}{\left[ 1 + (u')^2 \right]^{1/2}} \quad (18)$$

Thus, Equation (15) becomes

$$\tan \alpha = \frac{(\tan \gamma) (u') + \cos \theta}{\sin \theta \left[ 1 + (u')^2 \right]^{1/2}} \quad (15a)$$

$$\tan^2 \alpha = \frac{\left[ (\tan \gamma) (u') + \cos \theta \right]^2}{\sin^2 \theta \left[ 1 + (u')^2 \right]} \quad (19)$$

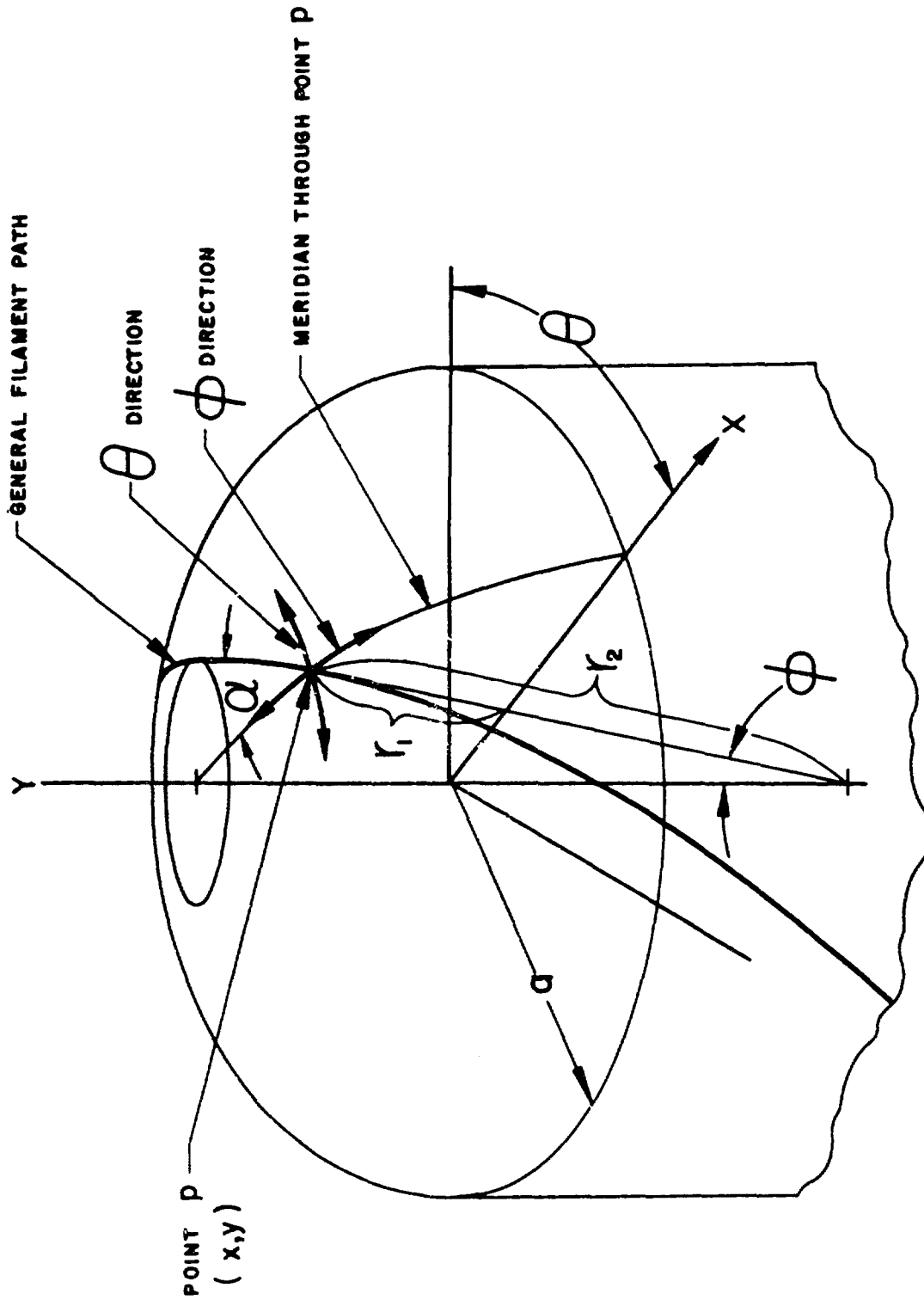


Figure 67. Geometry of General Winding Pattern

From Figure 6A,

$$\cos \theta = \frac{y \tan \gamma + Ca}{x} = \frac{u \tan \gamma + C}{z} \quad (20)$$

$$\sin \theta = \frac{[x^2 - (y \tan \gamma + Ca)^2]^{1/2}}{x} = \frac{[z^2 - (u \tan \gamma + C)^2]^{1/2}}{z} \quad (21)$$

With  $u' = 1/Q$ ,

$$\tan^2 \alpha = \frac{\left[ \frac{z}{Q} \tan \gamma + u \tan \gamma + C \right]^2}{\left[ z^2 - (u \tan \gamma + C)^2 \right] \left[ 1 + \left( \frac{1}{Q} \right)^2 \right]} = \frac{\left[ z \tan \gamma + (u \tan \gamma + C) Q \right]^2}{(1 + Q^2) \left[ z^2 - (u \tan \gamma + C)^2 \right]} \quad (22)$$

Substituting Equations (9) and (10) into Equation (8), the differential equation becomes

$$\tan^2 \alpha = 2K_P - \frac{zu''}{u' \left[ 1 + (u')^2 \right]} \quad (8b)$$

Setting  $Q = k/u'$ ,

$$u' = \frac{du}{dz} = \frac{1}{Q}$$

and

$$u'' = \frac{d(u')}{dz} = \frac{d}{du} \left( \frac{1}{Q} \right) \frac{du}{dz} = -\frac{1}{Q^3} \frac{dQ}{du}$$

$$\tan^2 \alpha = 2K_P - \frac{-\frac{z}{Q^3} \frac{dQ}{du}}{\frac{1}{Q} \left[ 1 + \left( \frac{1}{Q} \right)^2 \right]} \quad (8c)$$

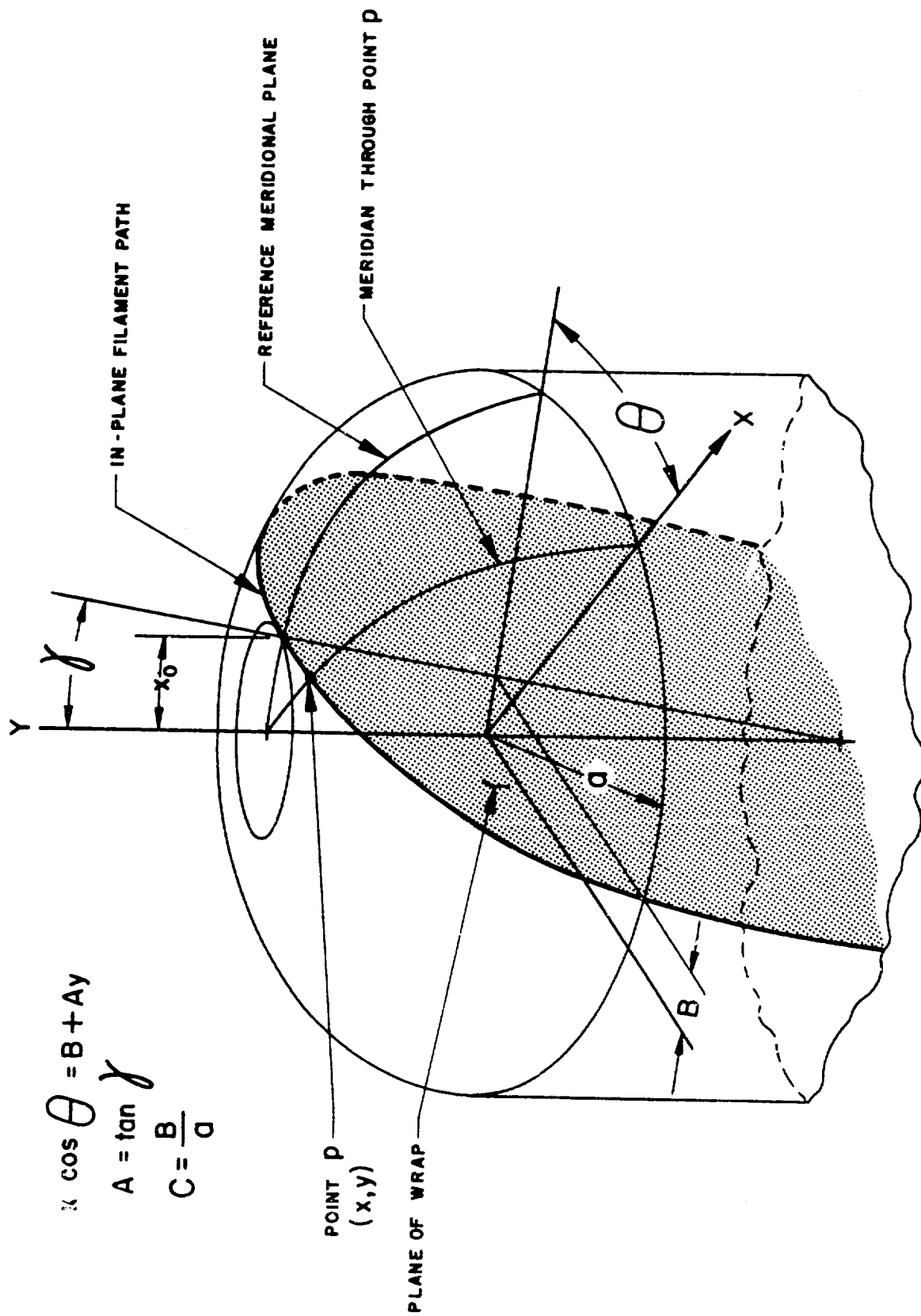


Figure 68. Geometry of In-Plane Winding Pattern

Solving for  $\frac{dQ}{du}$ ,

$$\frac{dQ}{du} = \frac{Q^2 + 1}{z} \left[ \tan^2 \alpha - 2K_P \right] \quad (23)$$

where  $\tan^2 \alpha$  is defined by Equations (14) and (22) for the geodesic-isotensoid and in-plane patterns, respectively.

Equation (23) is solved, by Runge-Kutta integration, with a high-speed digital computer and noting the following boundary conditions at the equator of the head:  $Z = 1$ ,  $u = 0$ , and  $Q = 0$ .

Filament-wound pressure vessels contain an inflection point that occurs at  $\alpha = \tan^{-1} \sqrt{2}$  when Equation (23) changes sign. To close off the contour, it is assumed that the shell is a sphere with a radius of curvature equivalent to  $r_2$  at the inflection point. For the geodesic isotensoid,  $z_L$  and  $u_L$  are obtained as indicated below. The circular arc is

$$z^2 + (u - s)^2 = \left( \frac{r}{2} \right)^2 \quad (24)$$

where

$$r = r_{1c} = r_{2c}$$

Thus, at the next-to-last point,

$$s + u_p - \sqrt{\left( \frac{r}{a} \right)^2 - (z_p)^2} \quad (25)$$

The derivative of Equation (24) is

$$2z dz + 2(u - s) dy = 0 \quad (26)$$

Because  $Q = dz/du$ ,

$$Q = - \frac{u - s}{z} \quad (27)$$

and

$$Q_L = \frac{s - u_L}{z_L} \quad (27a)$$

where

$$z_L = u_L \tan \gamma + C \quad (28)$$

For the geodesic isotenoid,  $z_L = D$ . Thus,

$$u_L \tan \gamma + C = D \quad (28a)$$

and

$$Q_L = \frac{s - u_L}{D}$$

where

$$s = u_p - \left[ \left( \frac{r}{a_c} \right)^2 - (z_p)^2 \right]^{1/2} \quad (29)$$

The head contour in a filament-wound pressure vessel is determined by application of the previously derived equations in an order defined by the specific input to a computer.

### III. ANALYSIS OF HEAD STRESSES

The stresses in the different layers of the head are calculated using the contour developed in Section II,B of this appendix and the stress-distribution equation of Section II,A. In this case, however, the winding stress in the fibers will always be known. The stress in Layer  $i$  at point  $x$  is therefore

$$\begin{aligned} \sigma_{dix} = & \frac{E_i}{r_{lix} - \frac{t_{ix}}{2} \left( \frac{t_{ix}}{2r_{A1}} - \nu_1 \right)} \left\{ r_{1,i-1,x} \Delta \epsilon_{m,i-1,x} \right. \\ & + \epsilon_{r,i-1,x} t_{i-1,x} + \frac{\sigma_{w1}}{E_1} \left[ r_{lix} - \frac{t_{ix} \nu_1}{2} \right] \\ & \left. + \frac{t_{ix}}{2} \frac{[p_{w1} - p_{A,i-1,x} + (\Delta p_{i-1,x}/2)]}{E_1 K_1} \right\} \quad (7a) \end{aligned}$$

where

$$t_{ix} = t_i \left( \frac{r_c}{r_{2c} \sin \phi} \right) \frac{\cos \alpha_o}{\cos \alpha_x}$$

and  $r_{1,i-1,x}$ ,  $\Delta \epsilon_{m,i-1,x}$ ,  $\epsilon_{r,i-1,x}$ ,  $P_{A,i-1,x}$ , and  $\Delta p_{i-1,x}$  are computed as in Section II,A, with the wrap condition pressure and stress terms included.

SYMBOLS

	Definition	Units
a	Internal radius at equator	in.
$a_c$	Mean radius of composite at equator	in.
$a_i$	Mean radius of Layer i at equator	in.
$a_{i-1}$	Mean radius of Layer i-1 at equator	in.
C	Distance from vessel axis to intersection of wrap plane with equator, divided by $a_c$	--
D	Boss radius divided by $a_c$	--
$E_i$	Elastic modulus of fiber in Layer i	psi
$E_{i-1}$	Elastic modulus of fiber in Layer i-1	psi
$K_i$	Filament fraction in Layer i	--
$K_{i-1}$	Filament fraction in Layer i-1	--
$K_p$	Ratio of $a_c$ to a times ratio of $r_{lo}$ to $r_{loc}$	--
$N_\phi$	Meridional force per unit width	lb/in.
$N_\theta$	Circumferential force per unit width	lb/in.
$P_{Ai}$	Pressure applied to Layer i	psi
$P_{A,i-1}$	Pressure applied to Layer i-1	psi
$P_d$	Design pressure	psi
$\Delta p_i$	Internal pressure resisted by Layer i	psi
$\Delta p_{i-1}$	Internal pressure resisted by Layer i-1	psi
Q	Inverse derivative of u with respect to z	--
$Q_L$	Q at $x = x_0$	--
$Q_p$	Q prior to $Q_L$	--
$r_{Ai}$	Radius of Layer i in wrap direction	in.
$r_{A,i-1}$	Radius of Layer i-1 in wrap direction	in.

SYMBOLS (cont.)

	Definition	Units
$r_1$	Internal meridional radius of curvature	in.
$r_{1c}$	Mean composite meridional radius of curvature	in.
$r_{1i}$	Meridional radius of curvature of Layer i	in.
$r_{1,i-1}$	Meridional radius of curvature of Layer i-1	in.
$r_{1o}$	Radius $r_1$ at equator	in.
$r_{1oc}$	Radius $r_{1c}$ at equator	in.
$r_2$	Internal circumferential radius of curvature	in.
$r_{2c}$	Mean composite circumferential radius of curvature	in.
$r_{2i}$	Circumferential radius of curvature of Layer i	in.
$r_{2,i-1}$	Circumferential radius of curvature of Layer i-1	in.
$s$	Normalized distance to center of spherical close-off dome	--
$t_1$	Composite thickness of Layer i at equator	in.
$t_{i-1}$	Composite thickness of Layer i-1 at equator	in.
$\Delta t$	Difference between $a_c$ and $a$	in.
$u$	Axial coordinate, $y/a$	--
$u_L$	Axial coordinate at $x = x_o$	--
$u_p$	Axial coordinate of next-to-last point on head contour	--
$x$	Radial coordinate (used as subscript, indicates evaluated at point x)	in.
$x_o$	Boss radius	in.
$y$	Axial coordinate	in.
$z$	Radial coordinate, $x/a$	--
$z_L$	Radial coordinate at $x = x_o$	--
$z_p$	Radial coordinate of next-to-last point on head contour	--

SYMBOLS (cont.)

	<u>Definition</u>	<u>Units</u>
$\alpha$	Angle between meridian and filament	degrees
$\alpha_0$	Angle between meridian and filament at equator	degrees
$\gamma$	Angle between wrap plane and axis of vessel	degrees
$\epsilon_{mi}$	Strain in meridional direction of Layer i	--
$\epsilon_{m,i-1}$	Strain in meridional direction of Layer i-1	--
$\epsilon_{ri}$	Radial strain in Layer i	--
$\epsilon_{r,i-1}$	Radial strain in Layer i-1	--
$\Delta \epsilon_{mi}$	Change in strain in meridional direction between winding and design conditions for Layer i	--
$\Delta \epsilon_{m,i-1}$	Change in strain in meridional direction and design conditions for Layer i-1	--
$\theta$	Polar angle	degrees
$\nu_i$	Poisson's ratio for fibers in Layer i	--
$\nu_{i-1}$	Poisson's ratio for fibers in Layer i-1	--
$\sigma_{di}$	Fiber design stress in Layer i	psi
$\sigma_{d,i-1}$	Fiber design stress in Layer i-1	psi
$\sigma_{wi}$	Fiber winding stress in Layer i	psi
$\sigma_{w,i-1}$	Fiber winding stress in Layer i-1	psi

Note: Subscript x refers to any point on surface. Absence of subscript x implies equator of head.

## APPENDIX II

### STRUCTURAL DESIGN - THICK-WALL, FILAMENT-WOUND, PRESSURE VESSEL

#### I. COMPOSITE

The thickness of the composite at the equator may be estimated as follows, using thin-wall theory, assuming that equal stresses can be obtained for all layers:

$$t = \frac{pD}{4\sigma_c}$$

where

t = Wall thickness, in.

p = Internal pressure, psi

$\sigma_c$  = Composite design stress, psi

D = Vessel diameter, in.

The composite design stress, assuming a fiber stress ( $\sigma_f$ ) of 330,000 psi, a fiber volume percentage (K) of 0.673, and a wrap angle ( $\alpha$ ) of  $24.5^\circ$ , will be

$$\begin{aligned}\sigma_c &= K \sigma_f \cos^2 \alpha \\ &= (0.673)(330,000)(\cos^2 24.5^\circ) \\ &= 184,000 \text{ psi}\end{aligned}$$

If the design burst pressure is 2.2 times the operating pressure of 15,000 psi, the composite thickness of a 12.5-in.-dia vessel is

$$\begin{aligned}t &= \frac{(15,000)(2.2)(12.5)}{(4)(184,000)} \\ &= 0.56 \text{ in.}\end{aligned}$$

#### II. BOSS FLANGE

It is conservative to assume that the flange on the bosses is attached to an infinitely rigid structure and that the shear load is applied at a diameter calculated from

$$D_w = \left(1 + \frac{\sigma_{f,L}}{E_f}\right) D_o + 2.5 W_L$$

where

$D_w$  = Diameter of load application, in.

$\sigma_{f,L}$  = Longitudinal fiber stress, psi

$E_f$  = Fiber tensile modulus, psi

$D_o$  = Inside diameter of boss flange, in.

$W_L$  = Winding tape width, in.

If

$D_o = 2.4$  in.

$\sigma_{f,L} = 330,000$  psi

$E_f = 12.4 \times 10^6$  psi

$W_L = 0.45$  in.

then

$$\begin{aligned} D_w &= \left(1 + \frac{330,000}{12.4 \times 10^6}\right) (2.4) + 2.5 (0.45) \\ &= 3.5 \text{ in.} \end{aligned}$$

The thickness of the flange is calculated (Reference 13) from

$$t = \left(\frac{\beta W}{\sigma}\right)^{1/2}$$

where

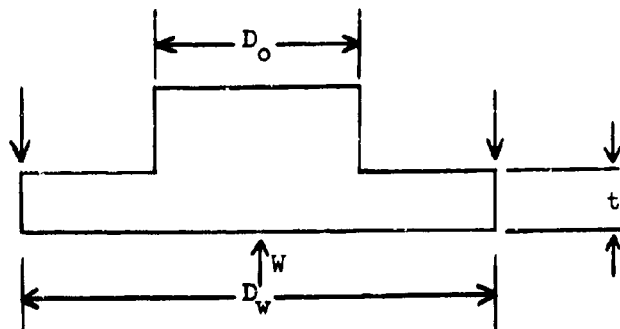
$t$  = Flange thickness, in.

$\beta$  = Coefficient

$W$  = Total axial load, lb

$\sigma$  = Ultimate stress, psi

Assuming the following configuration,



$$\begin{aligned}
 W &= \frac{\pi}{4} D_w^2 p \\
 &= \left(\frac{\pi}{4}\right) (3.5)^2 (15,000)(2.2) \\
 &= 318,000 \text{ lb}
 \end{aligned}$$

The allowable stress is assumed to be 80% of the ultimate strength. For an ultimate strength of 190,000 psi,

$$\begin{aligned}
 \sigma &= (0.8)(190,000) \\
 &= 152,000 \text{ psi}
 \end{aligned}$$

$\beta$  is approximated by  $(D_w/D_o) - 1$ . Thus,

$$\beta = \frac{3.5}{2.4} - 1 = 0.46$$

and

$$\begin{aligned}
 t &= \left[ \frac{(0.46)(318,000)}{152,000} \right]^{1/2} \\
 &= (0.962)^{1/2} \\
 &= 0.982 \text{ in.}
 \end{aligned}$$

APPENDIX III

FABRICATION PROCEDURE FOR 12-IN.-DIA THICK-WALL,  
FILAMENT-WOUND, HIGH-PRESSURE CONTAINERS

Part Title: Container - High-Pressure, Thick-wall, Filament-Wound  
Part Number: 1268893

I. GENERAL INSTRUCTIONS

A. This fabrication procedure is intended as a guide to ensure that the best results are obtained on these developmental, 12-in.-dia thick-wall, high-pressure (33,000 psi) containers. Any deviation in parts, materials, handling, or processes shall be recorded. Comments and suggestions shall also be noted.

B. A total of 16 pressure vessels shall be filament-wound on a 0.006-in.-thick stainless-steel liner and a flexible sand mandrel using either prepreg of in-process impregnated S-901 20-end roving, or both. Vessels shall be fabricated in lots of 9, 3, and 4 units each.

C. A prime coat consisting of an adhesive film and resin adhesive shall be applied to the liner which has been cleaned and pickled.

D. Initially, the first 50% (or 100% for some vessels) of each vessel shall be fabricated with S-glass and the standard prepreg resin system 58-68R ("Epon 1031"/"Epon 828"/MNA/BDMA), and cured. The last 50% of each vessel shall be wet-wound with S-glass and the 58-68R resin system, and cured. After vacuum bag cure, a moisture-resistant coating consisting of "2021" nitrile rubber phenolic shall be brush-applied. These vessels are detailed under Aerojet P/N 1268893.

E. The sequence of fabrication operations shall be as follows:

1. Metal liner assembly inspection
2. Metal liner leak test
3. Plaster mandrel fabrication
4. Assembly of winding shaft
5. Cleaning of metal liner surfaces
6. Application of adhesive coating to metal liner
7. Winding machine setup and calibration
8. Positioning of metal shell in winding machine
9. General instructions for handling of glass roving
10. General instructions for overwrapping
11. Fabrication of doily reinforcement
12. Application and cure of prepreg roving
13. Application and cure of wet wound roving
14. Mixing of resin for wet winding
15. Plaster mandrel removal and cleaning
16. Application of moisture-resistant coating
17. Dimensional checking and weighing
18. Electron-beam welding of closure
19. Test.

F. Extreme care shall be exercised in handling the metal liner throughout the fabrication operations because of its thin (0.006-in.) wall. The liner shall be handled using both bosses, since handling by one boss could distort the metal shell.

G. Personnel shall wear clean, white-cotton gloves to handle the metal liner after the outer surfaces of the liner have been cleaned.

H. Record sheets shall accompany the tank through fabrication and be returned to the Composites Engineering Department when the tank fabrication is completed.

## II. METAL LINER ASSEMBLY INSPECTION

The following procedures shall be followed in metal liner assembly inspection:

A. Handle metal shell wearing only clean, white cotton gloves. Caution: When lifting or handling metal shell assembly, use both bosses.

B. Remove metal shell from protective plastic bag and handling box.

C. Serially mark each welded metal liner (P/N 1268891) with numbers (-1, -2, -3, etc.) in the ID of the aft boss extension.

D. Measure length, diameter, and weight and record.

E. Replace metal shell in plastic bag and handling box.

F. Deliver metal liners to Test Operations for mass spectrometer leak test.

## III. METAL LINER LEAK TEST

A. Each metal liner shall be leak tested to verify the impermeability of the metal-shell structure.

B. The leak test shall consist basically of installing each liner with leak test plug T-120614 into a tank and pressurizing the liner to 5 to 10 psi. A vacuum shall then be drawn on a tank. The total leakage rate of helium from the liner shall not exceed  $2 \times 10^{-5}$  cu cm/sec. Note: Pressure differential across liner shall not exceed 20 psi.

C. The tested metal liners shall be delivered to the Plaster Shop for pouring and curing of the sand mandrel.

## IV. SAND MANDREL FABRICATION

A. A sand mandrel inside the metal-liner assembly shall be used to provide a firm support for the applied windings of glass filaments.

B. Mandrel shaft T-120594 and sand casting spool T-120595 shall be used to establish and hold the correct liner boss-to-boss length during sand casting.

C. Sand casting shaft T-120615, and anti-seize compound shall be used to cover the aft-boss spud during the sand casting.

D. Slush coat of the sand mandrel material shall be prepared and poured into the metal liner.

E. The thickness of the sand casting shall be at least 2.0 in.

F. The metal liner/sand mandrel assembly shall be adequately supported and placed in circulating oven.

G. The sand shall be cured for a minimum of 8 hours at 250°F.

H. After curing, the metal liner/sand mandrel assembly shall be delivered for cleaning of the metal outer surfaces.

#### V. ASSEMBLY OF WINDING SHAFT

The following procedures shall be followed in assembly of the winding shaft:

A. Handle metal shell only with clean, white cotton gloves.

B. Remove metal shell from plastic bag and place it on shop aid stand on foam pad covered with clean, lint-free cheesecloth.

C. Obtain one winding shaft T-120594. Apply anti-seize compound to the threads on the mandrel shaft. Install shaft in metal shell by threading shaft onto internal spud of aft boss. Finger-tighten shaft (6-in.-lb torque maximum) while holding aft boss with spanner wrench T-120607.

D. Align the six holes of the shaft collar with the boss holes. Install six 8-32 UNF by 7/8-in. long socket head cap screws and lock washers. Finger-tighten, and cross-torque all screws to 40-in.-lb.

E. To protect metal shell boss face and bolt holes from resin spillage, apply "Teflon" tape to cover 1/4 in. of side of boss and shaft collar so that resin will not migrate to boss face area.

F. Cover metal shell/winding shaft assembly with plastic bag if the next operation is not going to be performed immediately.

#### VI. CLEANING OF METAL LINER SURFACES

A. The outer surface of the metal liner shall be cleaned to remove contaminants and thus provide a good bonding surface for adhesive application.

B. The outer metal liner surfaces shall be cleaned with Ex-B727-6 paste cleaner.

C. Each cleaned metal liner shall be placed in a plastic bag and protective handling box, and delivered to the Filament Winding Laboratory.

#### VII. APPLICATION OF ADHESIVE COATING TO METAL LINER

A. One coat of FM123-2 (0.3 lb/sq ft) film shall be applied to the outer surfaces of the metal liner in order to obtain a structural bond between the metal-foil liner and the glass-filament case.

B. Liner shall be handled with clean, white cotton gloves, and protected with a plastic sheet prior to applying the adhesive.

C. An adhesive resin shall be applied to the outer surfaces of the FM123-2 only. The resin shall be a mixture of the following constituents and quantities: 828/MNA/BDMA/C-O-S (100/90/0.5/10). The ingredients shall not be weighed out until just prior to application.

D. The FM123-2 shall be precut in accordance with Pie Section Layout SK-20083.

E. The film shall be applied to the liner and all wrinkles and bubbles smoothed. Joints should butt. No gaps shall be permitted although a slight overlap can be allowed, if necessary.

F. The 828/MNA/BDMA/C-O-S resin shall be brushed onto the FM123-2.

#### VIII. WINDING MACHINE SETUP AND CALIBRATION

The following procedures shall be followed in the winding and machine setup and calibration:

A. Install eleven rolls of S-901 20-end preimpregnated roving into the tension devices.

B. Install roving guide rollers T-120600 on sphere winding machine E-100413.

C. Install resin impregnation pot T-120601.

D. Crank machine mount for winding shaft to six o'clock position.

E. Secure "dummy" metal shell/shaft assembly in the threaded mount. Then thread the shaft into the mount until the shaft flange rests against the mount.

F. Crank the winding shaft mount to the setting which gives the required longitudinal winding angle (approximately 25.5°).

G. Tighten the bolt on the backside of the winding machine mount to securely lock the winding shaft into position.

H. Dry-run the winding arm (without paying off roving) and adjust machine settings to obtain the required +5 winding arm turns per mandrel revolution of 360°. Record the machine setting after the turns are obtained.

I. Thread the eleven 20-end rovings through the guide rollers and through the payoff roller. Secure the ends of the roving and set the tension at approximately 4 lb for each 20-end spool.

J. Adjust rollers as required to give the uniform thickness 0.88-in.-wide tape.

K. If possible, make the 0.88-in.-wide tape pass tangent to each boss, with a maximum permissible distance between the boss and tape edge of 0.020 in.

L. Make a few winding arm turns to assure that the tape is passing tangent to the boss. Adjust winding shaft mount setting as required to give proper winding angle.

M. Adjust the tension devices to give 4  $\pm$  1 lb/20-end roving at the roving payoff.

#### IX. POSITIONING OF METAL SHELL IN WINDING MACHINE E-100413

Prior to this operation, machine settings for the winding pattern, winding angle, payoff roller adjustments, resin impregnation pot adjustments, etc. shall have been established or made using a "dummy" unit, or during the winding of the preceding metal shell. The following procedures shall be followed:

A. Handle metal shell only with clean, white cotton gloves.

B. Crank machine mount for winding shaft to six o'clock position.

C. Assemble the adhesive-coated metal shell to the winding machine by securing the shaft in the threaded mount. Thread the shaft into the mount until the shaft flange rests against the mount. Place one dolly reinforcement through shaft and on machine in order that it can be applied after first revolution without removing shaft from machine.

D. Crank the winding shaft mount to the predetermined setting which gives the required longitudinal winding angle.

E. Tighten the bolt on the backside of winding shaft mount to securely lock the winding shaft into position.

F. If the metal shell is not to be overwrapped with filaments immediately, protect with plastic sheet.

#### X. GENERAL INSTRUCTIONS FOR HANDLING OF GLASS ROVING

A. Each roll of S-901 20-end glass filament roving shall be kept in its protective plastic bag, with end plates in place, in its individual box in cold storage at 0°F, or below, except when being used for overwinding one or more metal shells on a given day.

B. At the completion of winding on each day, each roll of roving shall be immediately removed from the tension devices, repackaged with end plates in its plastic bag and box, and returned to 0°F, or below, cold storage.

#### XI. GENERAL INSTRUCTIONS FOR OVERWRAPPING

If any of the following should occur, the overwrapping process shall be halted and the project engineer or laboratory supervisor contacted before the process is restarted:

- A. Filament breakage
- B. Loss of end(s) on guide rollers
- C. Loss of tension on roving
- D. Lack of resin impregnation in roving
- E. Winding pattern gapping
- F. Excessive variation of filament tape width.

#### XII. FABRICATION OF DOLLY REINFORCEMENTS

A. Preimpregnated, unidirectional glass tapes, 1.0-in.-wide (3M 1009-26) shall be used to fabricate dolly reinforcements.

B. The reinforcements shall be flat with a 3.00-in. inside diameter and a 7.00-in. outside diameter. The cognizant engineer shall specify the dolly pattern.

C. Four reinforcements shall be required for each tank, with one reinforcement placed against the windings after the first and second filament winding revolutions are completed.

#### XIII. APPLICATION AND CURE OF PREPREG ROVING

The following procedures shall be followed in application and cure of prepreg roving:

- A. Obtain 11 rolls of S-901 20-end prepreg roving and place on tension device spindles.
- B. Thread roving through guide rollers and payoff head tangent to metal shell boss, and secure in place.
- C. Set machine turn counter to zero.
- D. Identify starting position of winding shaft mount in relation to stationary point on machine immediately adjacent to mount.
- E. Start the longitudinal filament-winding.

F. At completion of first mandrel revolution (approximately 40 turns), stop winding. Maintain tension on roving. Enter number of turns required to complete one revolution.

G. Apply doily reinforcement (one to each head).

H. Locate any required instrumentation "thumbtacks" in accordance with instructions of cognizant engineer.

I. Continue with longitudinal filament winding until second mandrel revolution is completed. Apply doily reinforcement (one to each head). Continue winding until 17 double layers have been wound, adjusting number of turns and tension. Adjust winding angle every third revolution or sooner so that tape is tangent to metal boss.

J. Record total number of turns applied to tank.

K. Remove eleven spools of roving from tension devices.

L. The prepreg wound tank shall be vacuum-bagged cured. Use one layer of "2353 Dacron" cloth for release and two layers of glass contour tape for bleeder. Bag with 0.006-in.-thick PVA sheet tailored to avoid excess wrinkles. Seal bag with zinc chromate putty. Install a vacuum valve other "Dacron" padding on head. Draw 20 in. Hg or better, and check for leaks. Use corks over any instrumentation tacks.

M. Transfer the vacuum-bagged unit to the curing oven.

N. Mount winding shaft on continuous rotation fixture to support container. (Do not rotate during cure.)

O. Check vacuum for 20 in. Hg or better.

P. Cure 2 hours at 150°F, 2 hours at 250°F, and 4 hours at 325°F as indicated by thermocouple probe within the laminate.

Q. Reduce the oven temperature to 100°F at a rate not to exceed 100°F/hour.

R. Remove cured tank from oven, and strip off vacuum bag.

#### XIV. APPLICATION AND CURE OF WET-WOUND ROVINGS

The following procedures shall be followed in application and cure of wet-wound rovings.

A. Wipe wrapped shell with MEK.

B. Obtain 11 rolls of S-901 20-end roving; weigh each roll, record weight, and place on tension device spindles.

C. Thread roving through guide rollers and payoff head tangent to metal shell boss, and secure in place.

D. Four mixed resin (see Section XV) in impregnation pot. Brush impregnate roving between impregnation pot and metal shell. Maintain resin temperature at 85 to 100°F.

E. Set machine turn counter to zero.

F. Identify starting position of winding shaft mount in relation to stationary point on machine immediately adjacent to mount.

G. Start the longitudinal filament winding. If required, brush on extra resin or remove excess resin on filaments.

H. At completion of first mandrel revolution (should be 40 turns), stop winding. Maintain tension on roving. Enter number of turns required to complete one revolution.

I. Locate any required instrumentation "thumbtacks" in accordance with instructions of cognizant engineer.

J. Continue with longitudinal filament winding until second mandrel revolution is completed (should be 41 turns). Continue until a total of 17 double layers are applied.

K. Continually wipe dry to remove excess resin.

L. Record total number of turns applied to tank.

M. Vacuum-bag and cure wound tank. Use one layer of "2353 Dacron" cloth for release and two layers of glass contour tape for bleeder. Bag with 0.006-in. PVA sheet tailored to avoid excess wrinkles. Seal bag with zinc chromate putty. Install a vacuum valve over "Dacron" padding on head. Draw 20 in. Hg or better, and check for leaks. Use corks over any instrumentation tacks.

N. Transfer the vacuum-bagged unit to the curing oven.

O. Mount winding shaft on continuous rotation fixture to support container. (Do not rotate during cure.)

P. Check vacuum for 20 in. Hg or better.

Q. Cure for 2 hours at 150°F, 2 hours at 250°F, and 4 hours at 325°F, as determined by thermocouple probe within the laminate.

R. Reduce the oven temperature to 100°F at a rate not to exceed 100°F/hour.

#### XV. MIXING OF RESIN FOR WET WINDING

A. <sup>(3)</sup>The resin for wet winding shall be a mixture of the following constituents: <sup>(3)</sup>"Epon 828"/"Epon 1031"/BDMA/MNA (50/50/0.5/90).

<sup>(3)</sup>The exact weight of resin proportions is critical.

B. A total mixture of 1000 g shall be mixed at one time, just prior to application, for each six double layers.<sup>(4)</sup> Rollers shall be wiped clean after each mixture ratio is used, and shall be thoroughly solvent-cleaned immediately upon completion of winding.

#### XVI. SAND MANDREL REMOVAL AND CLEANING

The following procedures shall apply in sand mandrel removal and cleaning:

A. Remove T-12059<sup>4</sup> mandrel shaft by first removing the six 8-32 socket head cap screws, then unscrewing the shaft from the aft boss internal spud while holding the aft boss using T-120607 spanner wrench. The spud is designed to fail at a torque exceeding 128 in.-oz, in case of undue binding of the mandrel shaft.

B. Remove the sand using hot water.

C. Clean the pressure vessel interior with hot water (150°F maximum). Do not use wire brushes or metal scraping tools on the interior of the vessel. Wash the vessel with hot water until all foreign matter has been removed, and air-dry at room temperature.

#### XVII. APPLICATION OF MOISTURE-RESISTANT COATING

A. Surface of container shall be cleaned with MEK or trichlorethylene and allowed to dry completely.

B. A 0.010-in. coating of "2021" nitrile rubber phenolic shall be brush-applied. Masking tape shall be applied at any exterior strain gage points.

C. Coating shall be air-dried for 1 hour. It shall then be force-dried for 30 min at 170°F, and 1 hour at 325°F.

#### XVIII. DIMENSIONAL CHECKING AND WEIGHING

A. The diameter at the equator shall be measured and recorded (inches).

B. The composite length adjacent to the bosses shall be measured and recorded (inches), as shall the total length of boss face to boss face.

C. The weight of the container shall be determined and recorded (grams).

D. After cleaning, the wound assembly shall be installed in a handling box and then delivered to the Welding Shop for electron-beam welding of the closure.

#### XIX. ELECTRON-BEAM WELDING OF CLOSURE

A. The closure P/N 1268922 shall be electron-beam welded into the forward boss after winding.

<sup>(4)</sup> Estimated pot life of the mixture is 2 hours.

B. As noted on Container Assembly Drawing 1268893, a minimum 1/2-in. depth of weld penetration shall be required.

C. After welding, the container assembly shall be installed in a handling box and then be delivered to Test Operations for hydrotest.

XX. TEST

A. Design burst shall be 33,000 psi (15,000 psi working x 2.2 safety factor SF).

B. Data shall be reduced and curves shall be supplied by Test Operations for all strain gage data.

C. For the burst tests, the strain rate shall be approximately 1%/min (estimated burst at 3% strain).

D. Fatigue tests shall consist of cycling at 100% of the working stress (15,000 psi), with a strain rate of 1%/min, up and down, and a 2 sec dwell period.

XXI. DATA SHEETS

Care shall be exercised in completing and recording all data, as well as any variation in the fabrication process or any other unusual occurrence concerning each container, to ensure that adequate information is available for substantiating or investigating test data.

## APPENDIX IV

### TEST PROCEDURE FOR 12-IN.-DIA THICK-WALL, FILAMENT-WOUND, HIGH-PRESSURE CONTAINERS

#### I. PURPOSE

This procedure outlines the requirements for the performance of hydraulic-burst testing of thick-wall, filament-wound pressure vessels at the Super Pressure Test Facility.

#### II. APPLICABLE DOCUMENTS

Applicable documents are AGC Specification 13954 (Calibration of Instrumentation) and Drawing No. 1268893 (Thick Wall Pressure Vessel).

#### III. TEST CONDITIONS

Unless otherwise stated, the burst test will be conducted under standard ambient conditions.

#### IV. VESSEL DESIGN PRESSURE RATING

The thick-wall pressure vessel is designed to withstand 33,000 psig without evidence of leakage or failure.

#### V. FACILITY DESIGN & PROVISIONS

The hydraulic test facility (Figure 69) is capable of delivering 1 gpm at 35,000 psi.

The super pressure hydraulic circuit, including the Kobe pump, all valves, Sprague pump, and tubing, has a design working pressure minimum value of 10,000 psi and has been hydrostatically proofed to 36,000 psi.

#### VI. SAFETY REQUIREMENTS

When a tank is under test, the test bay may not be entered under the following conditions:

- When the blast shield is removed and the specimen pressure exceeds 100 psig.
- When the blast shield is in place and the test pressure exceeds one-half the previously verified specimen pressure, or 10,000 psig.

Safety glasses must be worn by all personnel entering the test bay while the test vessel is pressurized.

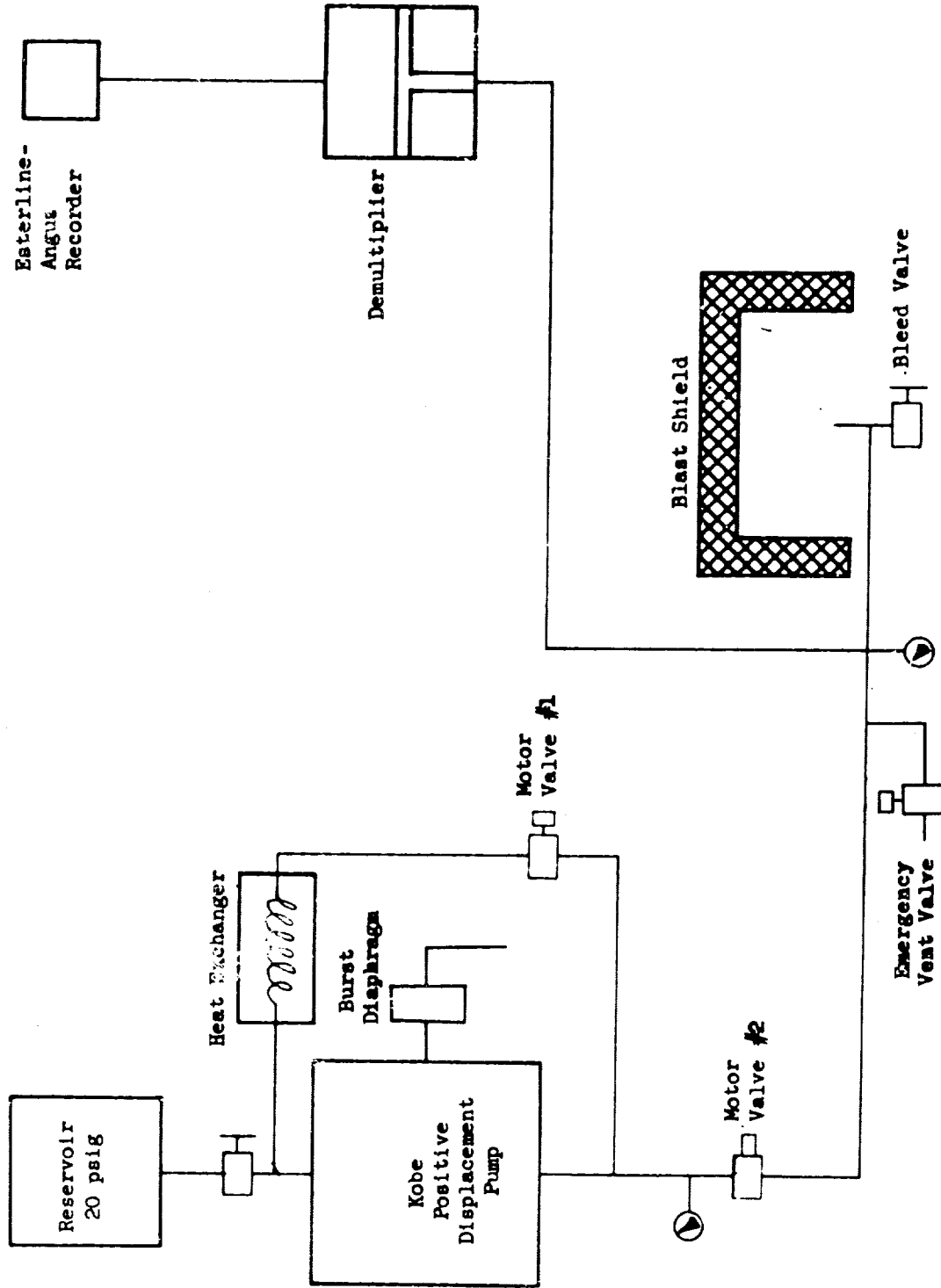


Figure 69. Hydraulic Test Facility Schematic

## VII. LEAK TEST PROCEDURE

### A. GAS LEAK SETUP

Set up the pressurization system in accordance with the schematic illustrated in Figure 70.

### B. LEAK TEST

1. Connect 1/4 in. flex line to the end plug and attach pressure gage on the specimen.
2. Slowly and remotely pressurize the vessel with air to 200 psig, and hold for 2 min.
3. After 2 min, vent the specimen to 100 psig and spray the external surface with leak detector solution.
4. When the leak test has been completed, vent the unit to 0 psig, disconnect the flex lines, and report test results on data sheet.

## VIII. BURST TEST PROCEDURE

### A. BURST TEST SETUP

1. Install the tank assembly on the holding stand located underneath the lifting hoist.
2. Set up pressurization system in accordance with the burst pressure schematic (Figure 69).

### B. BURST TEST SYSTEM PREPARATION

1. Verify that 20 psig pump inlet pressure is supplied to the reservoir, and complete the following tasks in preparation for the specimen setup:
  - Insert the power key in test console.
  - Bleed "in" demultiplier circuit from pressure recorder to demultiplier.
  - Energize motorized bypass valve No. 1 (open position) for 10 sec.
  - Energize motorized throttle valve No. 2 (open position) for 10 sec.
  - Cap the specimen pressure line attached to the shield.
2. Turn on the cooling water to the heat exchanger and verify that the overflow lines are connected to the drain.

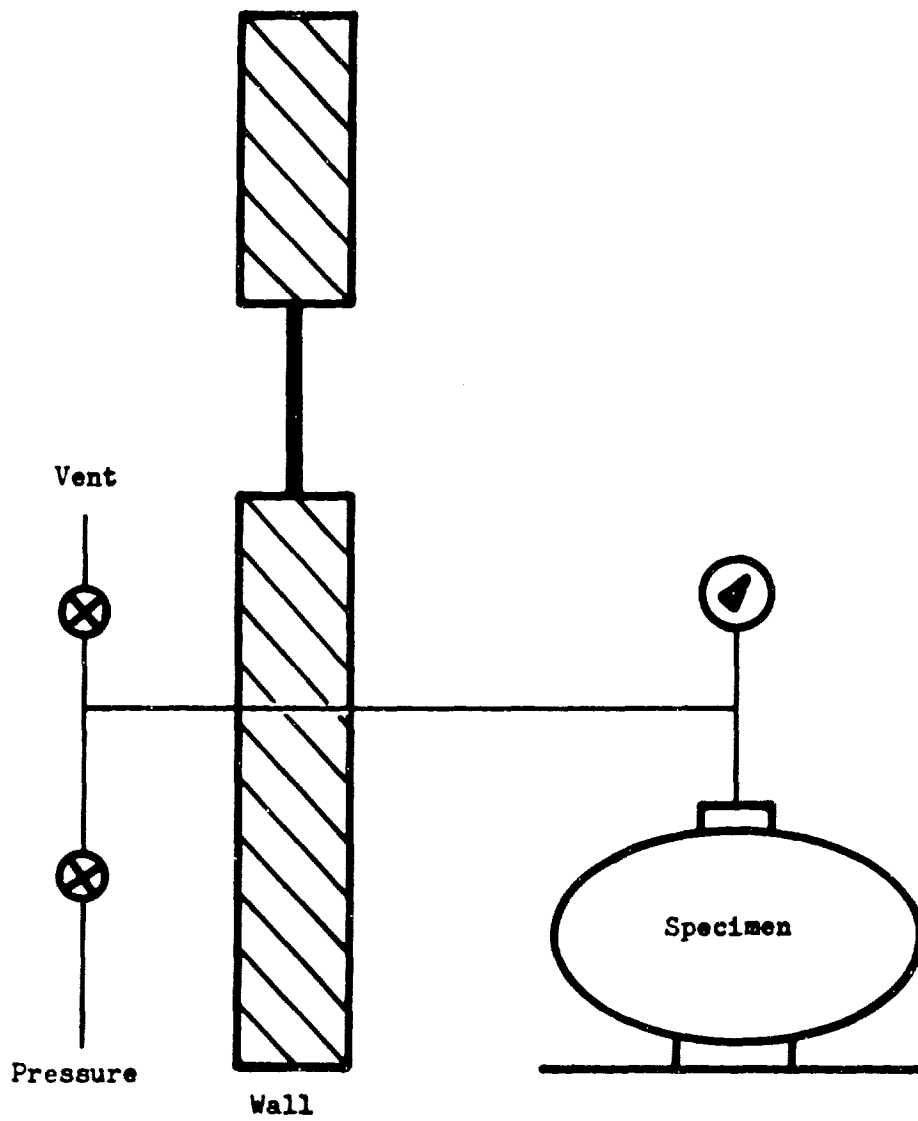


Figure 70. Burst Pressurization Schematic

3. With the bleed throttle valve closed, place the 1/16 in. "bleed" hose through top fitting of the specimen and energize the Kobe pump start button.

4. Adjust the bypass electric valve No. 1 until 3000 psig discharge is observed on the visual gage.

5. Slowly open the "bleed" throttle valve (manual) and completely fill the vessel with oil. To obtain a very good bleed it may be necessary to roll the specimen to remove air ullage.

6. When the vessel has been completely filled with oil, conduct the following tasks:

- Cap the specimen inlet line and close the bleed valve.
- Inside the control room, energize the throttle valve and remove hydraulic pulsations from the test gage by slowly closing the motorized valve No. 2.
- Slowly energize the bypass motor valve No. 1 and increase the discharge pressure to approximately 7000 psig.
- De-energize the Kobe pump start button, after which the hydraulic pressure will drop to 20 psig.

7. Connect the specimen pressure line to the test vessel and cover the vessel with the protective shield.

8. After inserting and tightening two holding bolts in the protective shield, vacate operating bay and turn on the warning bells.

Note: Although the specimen is completely shielded, all personnel must remain inside the control room during the pressurization. All valve changes and adjustments must be conducted remotely during the performance of a burst pressure test.

#### C. BURST TEST

1. Place the restricting chains in the proper places and secure the area for specimen burst test.

2. Turn on the pressure recorder.

3. Energize the Kobe start switch and pressurize the test vessel at a rate of approximately 10,000 psi/min until failure occurs.

4. De-energize the Kobe pump switch, close throttle valve No. 2, and shut off the warning bells.

5. Strip the chart records and identify with date, serial number, test title, and function.

REFERENCES

1. R. W. Buxton, R. N. Hanson, and D. Fernandez, Design Improvements in Liners for Glass-Fiber, Filament-Wound Tanks to Contain Cryogenic Fluids, NASA CR 54-854 (Aerojet-General Report 3141), January 1966.
2. M. J. Sanger, R. Molho, and W. W. Howard, Exploratory Evaluation of Filament-Wound Composites for Tankage of Rocket Oxidizers and Fuels, Air Force Materials Laboratory Technical Report AFML-TR-65-381 (Aerojet-General Report 3078), January 1966.
3. M. J. Sanger, R. Molho, and E. E. Morris, Stainless-Steel-Lined, Glass-Filament-Wound Tanks for Propellant Storage, Air Force Materials Laboratory Technical Report AFML-TR-66-264 (Aerojet-General Report 3243), December 1966.
4. R. Molho, Boron, Graphite, and Glass Filament-Wound Pressure Vessels with Load-Bearing, Non-Buckling Metal Liners, Prepared under an Aerojet Independent Research and Development Program on Advanced Composites, November 1967.
5. E. E. Morris, F. J. Darms, R. E. Landes, and J. W. Campbell, Parametric Study of Glass-Filament-Reinforced Metal Pressure Vessels, NASA Report No. CR 54-855 (Aerojet Report No. 3184), April 1966.
6. A. E. H. Love, A Treatise on the Mathematical Theory of Elasticity, 4th Ed., New York, Dover, 1944, pp. 272-276.
7. F. J. Darms, R. Molho, and B. E. Chester, Improved Filament-Wound Construction for Cylindrical Pressure Vessels, Air Force Materials Laboratory Report ML-TDR-64-43 (Aerojet Report No. 2784), March 1964.
8. L. M. Soffer and R. Molho, Cryogenic Resins for Glass-Filament-Wound Composites, NASA CR-72114 (Aerojet-General Report 3343), January 1967.
9. A. Lewis and G. E. Bush, Improved Cryogenic Resin/Glass-Filament-Wound Composites, NASA CR-72163 (Aerojet-General Report No. 3392), April 1967.
10. Improved Filament-Wound Construction for Cylindrical Pressure Vessels, Technical Documentary Report ML-TDR-64-43, Vol. I prepared by Aerojet-General under Contract AF 33(616)-8442, March 1964, p. 13.
11. Ibid., p. 14.
12. Ibid., p. 16.
13. R. J. Roark, Formulas for Stress and Strain, Fourth Edition, New York, McGraw-Hill, 1965, p. 223 (Case 22).

UNCLASSIFIED

Security Classification

DOCUMENT CONTROL DATA - R&D		
<i>(Security classification of title, body of abstract and indexing annotation must be entered when the overall report is classified)</i>		
1. ORIGINATING ACTIVITY (Corporate author) Aerojet-General Corporation 1100 West Hollyvale Street Azusa, California 91702		2a. REPORT SECURITY CLASSIFICATION Unclassified
		2b. GROUP
3. REPORT TITLE  DEVELOPMENT OF THICK-WALL, FILAMENT-WOUND, HIGH-PRESSURE CONTAINERS		
4. DESCRIPTIVE NOTES (Type of report and inclusive dates) Final Technical Report June 1966 - March 1968		
5. AUTHOR(S) (Last name, first name, initial)  Molho, Ralph Landes, Robert E.		
6. REPORT DATE May 1968	7a. TOTAL NO. OF PAGES 153	7b. NO. OF REFS 13
8a. CONTRACT OR GRANT NO. AF 33(615)-3995	9a. ORIGINATOR'S REPORT NUMBER(S) Aerojet-General Report No. 3532	
b. PROJECT NO. 7381		
c. 738101	9b. OTHER REPORT NO(S) (Any other numbers that may be assigned this report) AFML-TR-68-126	
10. AVAILABILITY/LIMITATION NOTICES This document is subject to special export controls and each transmittal to foreign governments or foreign nationals may be made only with prior approval of the Air Force Materials Laboratory (MAAE), Wright-Patterson Air Force Base, Ohio 45433.		
11. SUPPLEMENTARY NOTES	12. SPONSORING MILITARY ACTIVITY  Air Force Materials Laboratory Wright-Patterson Air Force Base, Ohio	
13. ABSTRACT Thick-wall, glass-filament-wound, high-pressure containers with thin-metal liners were investigated analytically and experimentally. An analysis adapting thin-wall theory to a multilayered thick-wall vessel was developed and programed on the computer. Comparisons to select the most efficient configuration, and evaluation of materials and processing techniques preceded the sequential fabrication and testing of sixteen 12-in.-dia prototype vessels designed to operate at a working pressure of 15,000 psi. Results indicate that mismatch of strains, and relative movement between the rigid thick-metal boss and the overwrapped composite, caused strain magnification in the transition area between the boss and liner. This condition developed because of the need to maintain overall strain compatibility between the filaments and metal structure and was the principal factor contributing to premature vessel failure. Tests indicated that improvements in the structure could be achieved by (a) applying the fibers at high winding tensions, (b) increasing the payoff tape width, and (c) using glass-reinforcement tapes to optimize the contour. Studies were also conducted on improving the internal supporting mandrel material and increasing the adhesive bond strength between the liner and composite structure. Continued studies are recommended in these areas and in thick-wall composite structures with load-bearing, non-buckling liners.		

DD FORM 1473 0101-807-8800

UNCLASSIFIED  
Security Classification

UNCLASSIFIED

Security Classification

14. KEY WORDS	LINK A		LINK B		LINK C	
	ROLE	WT	ROLE	WT	ROLE	WT
Filament tensioning Filament-winding technology High-pressure containers Liner-to-composite adhesive bond Metal-liner mandrel support Multi-layered, thick-wall vessels Thick-wall composite structures Thin metal-lined tankage Strain magnification						

INSTRUCTIONS

1. ORIGINATING ACTIVITY: Enter the name and address of the contractor, subcontractor, grantee, Department of Defense activity or other organization (corporate author) issuing the report.

2a. REPORT SECURITY CLASSIFICATION: Enter the overall security classification of the report. Indicate whether "Restricted Data" is included. Marking is to be in accordance with appropriate security regulations.

2b. GROUP: Automatic downgrading is specified in DoD Directive 5200.10 and Armed Forces Industrial Manual. Enter the group number. Also, when applicable, show that optional markings have been used for Group 3 and Group 4 as authorized.

3. REPORT TITLE: Enter the complete report title in all capital letters. Titles in all cases should be unclassified. If a meaningful title cannot be selected without classification, show title classification in all capitals in parenthesis immediately following the title.

4. DESCRIPTIVE NOTES: If appropriate, enter the type of report, e.g., interim, progress, summary, annual, or final. Give the inclusive dates when a specific reporting period is covered.

5. AUTHOR(S): Enter the name(s) of author(s) as shown on or in the report. Enter: last name, first name, middle initial. If military, show rank and branch of service. The name of the principal author is an absolute minimum requirement.

6. REPORT DATE: Enter the date of the report as day, month, year, or month, year. If more than one date appears on the report, use date of publication.

7a. TOTAL NUMBER OF PAGES: The total page count should follow normal pagination procedures, i.e., enter the number of pages containing information.

7b. NUMBER OF REFERENCES: Enter the total number of references cited in the report.

8a. CONTRACT OR GRANT NUMBER: If appropriate, enter the applicable number of the contract or grant under which the report was written.

8b, 8c, & 8d. PROJECT NUMBER: Enter the appropriate military department identification, such as project number, subproject number, system numbers, task number, etc.

9a. ORIGINATOR'S REPORT NUMBER(S): Enter the official report number by which the document will be identified and controlled by the originating activity. This number must be unique to this report.

9b. OTHER REPORT NUMBER(S): If the report has been assigned any other report numbers (either by the originator or by the sponsor), also enter this number(s).

10. AVAILABILITY/LIMITATION NOTICES: Enter any limitations on further dissemination of the report, other than those

imposed by security classification, using standard statements such as:

- (1) "Qualified requesters may obtain copies of this report from DDC."
- (2) "Foreign announcement and dissemination of this report by DDC is not authorized."
- (3) "U. S. Government agencies may obtain copies of this report directly from DDC. Other qualified DDC users shall request through \_\_\_\_\_."
- (4) "U. S. military agencies may obtain copies of this report directly from DDC. Other qualified users shall request through \_\_\_\_\_."
- (5) "All distribution of this report is controlled. Qualified DDC users shall request through \_\_\_\_\_."

If the report has been furnished to the Office of Technical Services, Department of Commerce, for sale to the public, indicate this fact and enter the price, if known.

11. SUPPLEMENTARY NOTES: Use for additional explanatory notes.

12. SPONSORING MILITARY ACTIVITY: Enter the name of the departmental project office or laboratory sponsoring (paying for) the research and development. Include address.

13. ABSTRACT: Enter an abstract giving a brief and factual summary of the document indicative of the report, even though it may also appear elsewhere in the body of the technical report. If additional space is required, a continuation sheet shall be attached.

It is highly desirable that the abstract of classified reports be unclassified. Each paragraph of the abstract shall end with an indication of the military security classification of the information in the paragraph, represented as (TS), (S), (C), or (U).

There is no limitation on the length of the abstract. However, the suggested length is from 150 to 225 words.

14. KEY WORDS: Key words are technically meaningful terms or short phrases that characterize a report and may be used as index entries for cataloging the report. Key words must be selected so that no security classification is required. Identifiers, such as equipment model designation, trade name, military project code name, geographic location, may be used as key words but will be followed by an indication of technical context. The assignment of links, roles, and weights is optional.

UNCLASSIFIED

Security Classification